Impact of Surface Texture on Entropy Generation in Viscous Flows

By:

Sajid Khan
Reg. No. 45-FBAS/PHDMA/F14

Department of Mathematics and Statistics
Faculty of Basic and Applied Sciences
International Islamic University, Islamabad
Pakistan
2022

Impact of Surface Texture on Entropy Generation in Viscous Flows

By:

Sajid Khan
Reg. No. 45-FBAS/PHDMA/F14

Supervised By:

Dr. Ahmer Mehmood

Department of Mathematics and Statistics
Faculty of Basic and Applied Sciences
International Islamic University, Islamabad
Pakistan
2022

Impact of Surface Texture on Entropy Generation in Viscous Flows

By:

Sajid Khan
Reg. No. 45-FBAS/PHDMA/F14

A DISSERTATION
SUBMITTED IN THE PARTIAL FULFILLMENT
OF THE REQUIREMENTS FOR THE DEGREE
OF
DOCTOR OF PHILOSOPHY
IN
MATHEMATICS

Supervised By:

Dr. Ahmer Mehmood

Department of Mathematics and Statistics
Faculty of Basic and Applied Sciences
International Islamic University, Islamabad
Pakistan
2022

Author's Declaration

I, **Sajid Khan** Reg. No. **45-FBAS/PHDMA/F14** hereby state that my Ph.D. thesis titled: **Impact of Surface Texture on Entropy Generation in Viscous Flows** is my own work and has not been submitted previously by me for taking any degree from this university, **International Islamic University, Sector H-10, Islamabad, Pakistan** or anywhere else in the country/world.

At any time if my statement is found to be incorrect even after my Graduation the university has the right to withdraw my Ph.D. degree.

Name of Student: ***(Sajid Khan)***
Reg. No. **45-FBAS/PHDMA/F14**
Dated: **27/01/2022**

Plagiarism Undertaking

I solemnly declare that research work presented in the thesis titled: **Impact of Surface Texture on Entropy Generation in Viscous Flows** is solely my research work with no significant contribution from any other person. Small contribution/help wherever taken has been duly acknowledged and that complete thesis has been written by me.

I understand the zero tolerance policy of the HEC and University, **International Islamic University, Sector H-10, Islamabad, Pakistan** towards plagiarism. Therefore, I as an Author of the above titled thesis declare that no portion of my thesis has been plagiarized and any material used as reference is properly referred/cited.

I undertake that if I am found guilty of any formal plagiarism in the above titled thesis even after award of Ph.D. degree, the university reserves the rights to withdraw/revoke my Ph.D. degree and that HEC and the University has the right to publish my name on the HEC/University Website on which names of students are placed who submitted plagiarized thesis.

Student/Author Signature: 

Name: **(Sajid Khan)**

Certificate of Approval

This is to certify that the research work presented in this thesis, entitled: **Impact of Surface Texture on Entropy Generation in Viscous Flows** was conducted by **Mr. Sajid Khan,** Reg. No. **45-FBAS/PHDMA/F14** under the supervision of **Dr. Ahmer Mehmood** no part of this thesis has been submitted anywhere else for any other degree. This thesis is submitted to the **Department of Mathematics & Statistics, FBAS, IIU, Islamabad** in partial fulfillment of the requirements for the degree of **Doctor of Philosophy in Mathematics, Department of Mathematics & Statistics, Faculty of Basic & Applied Science, International Islamic University, Sector H-10, Islamabad, Pakistan.**

Student Name: Sajid Khan **Signature:** _____

Examination Committee:

a) **External Examiner 1:**
Name/Designation/Office Address **Signature:** _____
Prof. Dr. Mazhar Hussain
Professor of Mathematics,
National University of Computer & Emerging Sciences,
Lahore, Pakistan.

b) **External Examiner 2:**
Name/Designation/Office Address) **Signature:** _____
Prof. Dr. Muhammad Afzal Rana
Professor of Mathematics,
Ripha International University,
Islamabad/Pakistan Atomic Energy Commission Islamabad,
Pakistan.

c) **Internal Examiner:**
Name/Designation/Office Address) **Signature:** _____
Prof. Dr. Muhammad Sajid T.I
Professor

Supervisor Name:
Dr. Ahmer Mehmood **Signature:** _____

Name of HOD:
Prof. Dr. Tariq Javed **Signature:** _____ 16/02/22

Name of Dean:
Prof. Dr. Muhammad Irfan Khan **Signature:** _____

Dedicated

To

My Beloved Parents

Wife

&

Kind Supervisor Dr. Ahmer Mehmood

who have been supportive and encouraging

in my accomplishments

Acknowledgement

Praise to the **Allah** Almighty, the Cherisher and the most Gracious and the most merciful. I am grateful to Almighty Allah for enabling me to complete the research presented in this thesis. It is his unending mercy that the task has moved to a success. I offer my humblest and sincerest thanks to the Holy Prophet Hazrat **Muhammad** Mustafa (SAW) who is forever a torch of guidance and knowledge for humanity.

I express my humble gratitude to my kind nature and devoted supervisor **Dr. Ahmer Mehmood** for his kind and valuable guidance and assistance to complete this task. His sincere efforts, support, motivation and valuable contribution has a major part in the completion of my thesis. I would appreciate the painstaking attitude of my supervisor. He is one of the best teacher and researcher in his field because he is hard worker and involve with the research students till the completion of the task.

Thanks are due to **Prof. Dr. Tariq Javed** Chairperson Department of Mathematics for his motivation and administrative support. I express my sincere thanks to external examiners **Prof. Dr. Muhammad Afzal Rana** and **Prof. Dr. Mazhar Hussain** for valuable comments and encouragement.

I am grateful to the faculty and staff of Mathematics Department especially **Prof. Dr. Muhammad Sajid (T.I)** and **Prof. Dr. Nasir Ali** for their cooperation and moral support throughout my study. Acknowledgement is also gratefully extended to **Dr. Muhammad Saleem Iqbal** and **Dr. Muhammad Usman** for their kind help, guidance, and cooperation.

I would like to express my thanks to my colleagues especially **Dr. Muhammad Ashraf** for his motivation and encouragement. I am grateful to all my friends **Dr. Amad Zafar, Dr. Umair Ali, Ghulam Dastgir Tabassum, Tariq Hussain, Babar shah, Muhammad Usman Javed, Manzar Masud,** for their encouragement and moral support. Special thanks to **Mr. Iqrar Raza,** and **Mr. Muhammad Awais,** for their extraordinary support in all affairs throughout my research work.

In the end, I am extremely grateful to my beloved parents, brother, sister, and my wife for their extra care, sacrifices and patience throughout my study. The completion of my education was not possible without their prayers and supports. I am also thankful to my little princess **Abeeha** and my cute nephew **Ayaan Khan** for their love and sacrifices.

Preface

In recent decades, the scientists and engineers have focused on the efficiency of the system by reducing the loss of useful energies. The efficiency of any engineering system is primarily affected due to the existence of thermal irreversibility which is inherently present in all real devices. Such an irreversibility of these processes can be measured through the calculation of entropy. Also, entropy is a tool which can be utilized to judge the performance of engineering devices such as heat engine, refrigerators, turbines, compressors and nozzles etc. In fluid motion there are two primary sources (viscous dissipation and heat transfer) that cause the production of entropy. Literature survey reveals that in many engineering devices the surfaces are intentionally made rough for the improvement in heat transfer rate. Thus, the analysis of entropy generation in heat and fluid flow problems over such kind of surfaces is quite obvious. Being motivated with this fact the current research is aimed to investigate the role of surface texture in the generation of entropy during a convective transport process. Though the study of entropy generation in viscous transport processes is a topic of great interest but the impact of surface texture on entropy generation has not been investigated so for. Based on this fact the current study considers a variety of flow situations involving non-flat surfaces to study the generation of entropy due to the ongoing viscous transport process.

Chapter two includes entropy generation analysis in a viscous flow along a moving wavy surface at a constant temperature. Keller Box scheme has been utilized to calculate entropy generation phenomenon. The obtained results reveal that the surface roughness plays a vital role towards the minimization of entropy production. Moreover, interesting results are found due to the longitudinally wavy surface of the plate. The contents of this chapter are published in **Thermal Science: Year 2019, Vol. 23, No. 1,**

pp. 233-241. Another way of enhancing the thermal conductivity and heat transfer rate of viscous fluid is the mixing of nanometer-sized material particles in the based fluid. Several empirical models of nanofluids are available in literature however, Tiwari and Das model and Buongiorno model are widely being used for the analysis of heat transfer process. In **Chapter three** analysis has been done for entropy generation in a viscous flow of nanofluid along horizontally moving wavy surface by considering Tiwari and Das model. To see the overall behavior of irreversibility, average entropy number and average Bejan number have been calculated. The material of this chapter is published in **Thermal Science: Year 2021, Vol. 25, No. 2A, pp. 1171-1180.**

Chapter four covers the analysis of entropy generation phenomenon of nanofluid along a moving wavy boundary. The transport equations have been modeled with the utilization of Buongiorno model. The impact of Brownian motion and thermophoresis upon entropy generation and Bejan number have been examined in detail through various graphs. The contents of the current chapter are published in **International Journal of Exergy: Year 2019, Vol. 28, No. 4, pp. 317-332.** Irreversibility analysis of mixed convection flow along vertical wavy wall has been discussed through **Chapter five.** How does the mixed convection parameter alter the entropy generation and Bejan number is the question investigated in the current chapter. Also, it has been investigated that how entropy production rate can be minimized in the natural convection phenomenon. The contents of the current chapter are published in **The European Physical Journal Plus: Year 2020, 135:111.** In further proceedings the analysis of entropy production of mixed convection flow along an inclined wavy plate has been investigated numerically in **Chapter six**. The findings have been reported in detail with the help of graphs plotted against dimensionless variables ξ and η. The analysis of non-similar flow and entropy generation along the vertical wavy cone has been reported in

Chapter seven and published in **Journal of Thermal Analysis and Calorimetry: Year 2021, https://doi.org/10.1007/s10973-021-10979-w.** A numerical scheme commonly known as Keller Box scheme has been used for the numerical integration of non-similar equations. In this study the role of cone half angle towards the minimization of entropy production has been reported. Also, the contribution of viscosity of the fluid particles and heat transfer rate in entropy production have been deliberated. In **Chapter eight,** the problem of entropy analysis of three-dimensional viscous flow over a wavy rotating disk has been discussed. Analysis for entropy generation have been performed subject to constant wall temperature and constant heat flux cases. For clear picture of the impact of the physical parameters upon entropy generation and Bejan number, average values of entropy and Bejan number have been discussed through graphs.

Contents

List of Symbols

Be	Bejan number
$\overline{Be}$	Average Bejan number
Br, Br^*, Br^{**}	Brinkman number
C	Concentration function
c_p	Specific heat at constant pressure
C_f	Skin friction coefficient
D_B	Brownian diffusion coefficient
D_m	Mass diffusivity
D_T	Thermophoretic diffusion coefficient
d, d_1, d_2	Material parameters
Ec	Eckert number
f	Dimensionless stream function
g	Acceleration due to gravity
l	Reference length
Le	Lewis number
N_S	Dimensionless entropy generation
$\overline{N_S}$	Average entropy generation
N_b	Brownian motion parameter
N_t	Thermophoresis parameter
$\hat{n}$	Unit normal to the wavy surface
Nu	Nusselt number
p	Pressure
Pr	Prandtl number
q	Constant heat flux
q_w	Surface heat flux
r	Radius of the cone
Re	Reynolds number
Ri	Richardson number

S	Sinusoidal wavy function
Sh	Sherwood number
S_G	Volumetric entropy generation rate
$S_{G_0}, S^*_{G_0}, S^{**}_{G_0}$	Characteristic entropy generation rate
T	Fluid temperature
T_w	Temperature at the surface
T_∞	Ambient temperature
u	Velocity component along x-direction
U	Free stream velocity
v	Velocity component along y-direction
$\boldsymbol{V}$	Velocity vector

Greek symbols

$\bar{\alpha}$	Amplitude
α	Amplitude to wavelength ratio
α^*_f	Thermal diffusivity of regular fluid
α^*_{nf}	Thermal diffusivity of nanofluid
β	Thermal expansion coefficient
γ	Cone half angle
$\dot{\gamma}$	Shear rate
η, ξ, ζ	Dimensionless variables
θ	Dimensionless temperature
κ	Thermal conductivity of fluid
μ	Dynamic viscosity
ν	Kinematic viscosity
Ω_T	Dimensionless temperature difference
Ω^*	Rotation rate
Ω_c	Dimensionless concentration difference
ω	Group parameter
Λ	Dimensionless heat flux

ρ	Density
σ	Sinusoidal wavy surface
τ_w	Surface shear stress
Φ	Viscous dissipation
φ	Dimensionless concentration
ϕ	Uniform concentration of nanoparticles
ψ	Stream function

Subscripts

f	Base fluid
nf	Nanofluid
p	Nanoparticle
w	Condition at the surface
∞	Condition at the Infinity
η, ξ, ζ	Partial derivatives
x	Local quantity

Superscript

$'$	Ordinary derivative w.r.t η

Chapter 1

Introduction and preliminaries

The material of this chapter comprises of two major parts. First part represents the background of the research debated in this thesis. Second part possesses some basics of fluid mechanics, its fundamental laws and related dimensionless numbers for the facility of the reader. Non-similar flow and the concept of entropy generation which is the primary objective of this thesis are also included.

1.1 Introduction

Since last many decades or so, much of the research has been focused on how to enhance the efficiency of thermal engineering systems. If the loss of useful energy is reduced, efficiency of the engineering systems can be upgraded. So far, no mechanical device has been invented which can completely convert the supplied energy into useful work. The heat losses are always tried to be minimized by utilizing various techniques. The situation becomes more uneconomical when the useful energy is destroyed and results in reducing thermal and mechanical efficiency. This becomes a major reason in the disorder of a system which is called the entropy of the system. Thermodynamic irreversibility is linked with entropy generation and it exists in all types of heat transfer phenomenon. The influence of entropy generation over flow/heat transfer phenomenon is of great interest due to its vast application in combustion engines, heat exchangers, turbo-machinery, cooling of nuclear reactors, transport phenomena and heat exchangers etc. Characteristics of convective heat transfer, viscous dissipation effect, and finite temperature gradient are the main causes of irreversibility and are accountable for

entropy generation. Non-equilibrium state of fluid due to the presence of thermal gradient between the two media causes the entropy generation. Since the primary objective of thermodynamic analysis of flow and heat transfer phenomenon is to investigate the situations for the full use of the energy resources by reducing energy losses and improving the thermal systems. For analyzing the efficiency of the engineering processes, we use second law of thermodynamics because second law examines the irreversibility in the system through entropy generation rate. The entropy generation rate is important for enhancing work capacity and reducing loss of available energy of the system. Therefore, using the information and guidelines obtained from theories of thermodynamics, one can construct an efficient thermal system in respect of minimizing cost, effective design and reducing the loss of available power. The pioneer work towards the analysis of entropy generation was done by Bejan [1-4] where he analyze the entropy generation phenomenon in convective heat transfer phenomenon through some physical parameters, like entropy generation number, Bejan number, and irreversibility rate.

San et al. [5] examined the irreversibility process through an isothermal medium. Arpaci and Selamet [6] discussed entropy generation in boundary layer flows and concluded that temperature gradient and viscosity effects cause entropy generation. Carrington and Sun [7] established entropy generation equation by applying Second law analysis on internal and external flows and discussed its applications. Mahmood and Fraser [8] examined the forced convection flow through a channel. They derived analytic expression for entropy generation and Bejan number. Odat et al. [9] investigated the influence of joule heating on entropy generation rate. They observed that, entropy generation increases as the joule heating strengthens. Makinde [10] discussed the variable viscosity effects on entropy generation using second law of

thermodynamics in the presence of thermal radiation. The entropy generation rate was shown to be increasing near the surface as thermal radiation increases. Butt and Ali [11] examined that the magnetic field is a strong source of causing thermal irreversibility in fluid flow along radially stretching surface. Rashidi et al. [12] investigated the entropy production of nanofluid for stagnation point flow past a permeable stretching surface. Falade et al. [13] examined that the entropy generation rate augments for the large temperature difference. Butt et al. [14] investigated that in Blasius flow viscous dissipation increases the entropy generation.

The study of convective heat transfer along irregular surface is of fundamental importance because of their frequent occurrence in several practical applications. To enhance the convection phenomenon, the subject bodies are intentionally roughened because the roughening elements disturb the flow, consequently, the convection strengthens and hence heat transfer rate is increased. Yao [15] investigated the natural convective heat transfer phenomenon over vertical sinusoidal wavy surface in a viscous fluid. Yao et al. [16] discussed the influence of surface undulations on natural convection flow. Rees and Pop [17] analyzed natural convective flow along vertical wavy surface in porous media. Rees and Pop [18] analyzed free convective and heat transfer along wavy horizontal plate. Hossain and Pop [19] inspected the contribution of magnetic field in the non-similar flow of viscous fluid.

Molla et al. [20] discussed the thermal transport phenomenon for free convection boundary layer flow. They found that, the heat generation increases the thermal state of the fluid and opposite result is obtained for heat absorption. Molla et al. [21] inspected the free convection phenomenon over the complex boundary which consists of fundamental wave and its harmonics. They found that the boundary layer thickness due to a complex boundary is greater as compared to the simple sinusoidal surface. Alim et

al. [22] conceived that the local skin friction coefficient increases but heat transfer rate decreases as the value of heat generation rises. Narayana et al. [23] investigated effects of double diffusive on a horizontal wavy plate in porous medium. Based upon this importance of wavy texture **Chapter 2** includes the entropy generation analysis over the moving wavy surface.

Another way to enhance the heat transfer rate is the selection of nanofluid instead of pure fluid. Due to their higher thermal properties in comparison to liquids, the material particles present in the base fluid do increase the thermal conductivity and the density of the resulting nanofluid. In this regard, Choi [24] developed, experimentally, the nano-fluids by considering the material particles of size having diameter less than 100 nm in Argonne National Lab. After the experimental work, for theoretical discussion, the development of mathematical model of nanofluid was essential. In the literature there are two types of theoretical models available, namely, single-phase (homogeneous) and two-phase (non-homogenous). Single phase models got much attention due to their simple nature. The most famous models which are extensively used in the theoretical analysis of nanofluids are Tiwari and Das [25] and Buongiorno [26] models. The model of Tiwari and Das emphases upon the material properties of the nanoparticles whereas thermophoresis and Brownian motion are also included in Buongiorno model. According to Buongiorno model thermophoresis and Brownian motion are very important because due to thermophoresis phenomenon, the particles move from high temperature to low temperature region while due to the Brownian motion the particles travel from higher concentration region to lower concentration region. Thus, the study of nanofluids has a great importance in present years because of its wide applications in different areas like raw oil extraction, losses of heat from piping, nuclear power plants, drilling technology, cooling of microchips, optical

devices etc. The heat transfer properties of thermal system, radiators, engines, and air conditioning devices can be enhanced by the addition of nanoparticles [27]. Khanafer and Vafai [28] discussed the influence of nanoparticles on dynamic viscosity. They observed that the presence of nanoparticles does also enhance the dynamic viscosity. Many authors, [29-37] have perceived that heat transfer rate of nanofluids depends on size, type of nanoparticle, shape, and working temperature of regular fluid. The analysis of natural convection flow of nanofluid along a vertical wavy boundary was done by Gorla and Kumari [38]. Natural convection flow along the wavy surface by assuming local thermal non-equilibrium condition was discussed by Ahmed et al. [39]. They observed that surface undulations increase heat transfer rate without enhancing the overall volume of the equipment. Mehmood el al. [40] discussed MHD nanofluid flow along a moving wavy surface. Nanoparticles of different metals have been used for the analysis of cooling of wavy surface. Later on, Mehmood and Iqbal [41-42] studied natural convection flow of nanofluid along sinusoidal surface. Mustafa et al. [43] examined heat generation effect on free convection flow of nanofluid along wavy surface. Furthermore, Mustafa and Javed [44] extended the analysis for variable heat flux. The analysis of entropy generation for turbulent and laminar flows in channels was conducted by Singh et al. [45]. They observed that consideration of nanoparticles in base fluid augments entropy ratio. Lie and Kleinstreuer [46] studied entropy generation in nanofluid filled in trapezoidal microchannel and observed that entropy generation minimizes because of concentration of nanoparticles. Bianco et al. [47] discussed entropy phenomenon for turbulent flow in a square conduit by applying control volume method. Karami et al. [48] inspected entropy generation phenomenon for fluid having alumina particles in a tube. Falahat and Vosough [49] studied laminar and turbulent flow in a coiled tube. They observed that in the case of laminar flow an

increase of 1% volume fraction of nanoparticles results in 3% decrease of entropy. Rashidi et al. [50] discussed the irreversibility phenomenon for the flow past a rotating disk under the influence of magnetic force. They observed that average rate of entropy increases with the increase of magnetic parameter. Mahmoudi et al. [51] applied finite volume method to explore the impact of physical parameters upon free convection flow through a cavity. They found that best configuration of the flow can be selected on the base of entropy generation results. Malvandi et al. [52] determined the self-similar solution of entropy generation over a flat plate in the presence of nanoparticles. Noghrehabadi et al. [53] considered the Boungiorno model of nanofluid over the stretching surface and examined the entropy generation phenomenon. Abolbashari et al. [54] investigated unsteady MHD flow over stretching boundary in the presence of nanoparticles and observed the influence of nanoparticles upon entropy of the system. Das et al. [55] inspected the entropy analysis for magneto-nanofluid over accelerating sheet. They observed that more entropy generates due to the presence of metallic nanoparticles as compared to regular fluid. A rich material is available in the literature regarding entropy generation analysis of nanofluid for self-similar flows only few of them are discussed above. It is revealed from this fact that there is a huge gap in literature and reflects the lack of understanding of irreversibility process in the non-similar boundary layer flows for nanofluids. Due to importance of convective heat transfer with nanofluids for non-similar flows **Chapter 3** includes entropy generation in the non-similar flow governed by the uniform motion of a uniformly heated non-flat surface by considering Tiwari and Das [25] model. In **Chapter 4** Buongiorno [26] model has been considered for the analysis of entropy generation by taking the same geometry and flow configuration as given in previous chapter.

Mixed convection phenomenon of convective heat transfer is widely used in a variety of engineering processes. Some important engineering applications include heat exchangers, oil separation, solar collectors, cooling process of electronic devices, and thermal insulation systems etc. In numerous applied problems, one can find noticeable temperature gradients between a free stream and the hot surface. Hence the density is changed due to such temperature differences. When gravitational force is also taken into consideration, the intensity of the free convection effects is increased significantly. The two-dimensional flow of mixed convection along a vertical flat boundary is an obvious physical model. In a boundary layer flow, Sparrow [56] discussed the mixed convection phenomenon along a vertical and an inclined non-isothermal flat surface. He determined a criterion for the classification of forced, free, and mixed convection by considering a range of convection parameter. Merkin [57] analyzed the influence of buoyancy force on boundary layer flow along a vertical isothermal flat surface. He calculated the solution of his problem for two cases: first, when the flow is opposed by a buoyancy force and the other, when buoyancy force acts in the direction of flow. Lloyd and Sparrow [58] examined the convection phenomenon over a vertical plate by taking various Prandtl numbers. The graphical results for mixed convection flow were discussed in detail for liquid metals, gases, and ordinary liquids. Combined free and forced convection flow along a vertical plate with constant heat flux was investigated by Wilks [59]. His numerical results depict that, with the augmentation of mixed convection parameter the velocity profile enhances. Moulic and Yao [60] examined a forced flow past a vertical wavy plate and found that a forced convection transport exists at the leading edge. They also explored that total heat flux over sinusoidal boundary was smaller as compared to flat plate. Considering a uniform surface temperature of an impermeable surface, Hossain and Takhar [61] observed the radiative

effects on heat transfer rate by considering three types of convection. It was seen that the heat transfer rate enhances by decreasing radiation parameter for all three cases. Hady et al. [62] examined the variable viscosity effects on the flow of boundary layer type along a flat boundary. They observed that, the variable viscosity has a substantial impact on Nusselt number and wall-skin friction. Combined buoyancy effects on mass and thermal diffusion in a force convection flow were observed by Hossain and Rees [63]. They found that the concentration profile increases with a variation in Schmidt number. Jang and Yan [64] inspected a mixed convection flow over a vertical wavy surface for diffusion of heat and mass. The influence of mixed convection parameter and amplitude to wavelength ratio on velocity, temperature, and concentration profiles were discussed in detail. Molla and Hossain [65] employed the Keller-Box method and a straight forward finite difference method to obtain a numerical solution of mixed convection phenomenon over a sinusoidal boundary. Their numerical results illustrate that boundary layer thickness was enhanced by incrementing the radiation parameter. Siddiqa and Hossain [66] discussed a radiative flow over a flat boundary by considering the mixed convection phenomenon. They developed a relationship between convection and thermal radiation. Siddiqa et al. [67] analyzed the radiating flow phenomenon past a vertical wavy surface. They found that the wavy amplitude decreases with increasing value of radiation parameter. Parveen et al. [68] discussed the impact of viscosity in natural convective flow over a sinusoidal boundary and showed that the thickness of boundary layer becomes prominent with respect to viscous dissipation parameter. Siddiqa et al. [69] inspected free convection flow along the wavy surface having triangular geometry. Srinivasacharya et al. [70] discussed the radiative mixed convective flow past a vertical sheet by considering the flow through porous medium. They also utilized the thermal conductivity and viscosity (as temperature dependent)

and highlighted the variations in velocity, temperature, and concentration profiles with respect to these variable properties.

Selamet and Arpaci [71] examined the irreversibility phenomenon in the boundary layer region by considering thermal radiation effect. They observed that due to nonlinearity of temperature distribution within the boundary layer the entropy production increases. Hijleh and Heilen [72] conducted the irreversibility analysis for natural convection phenomenon over an isothermal rotating cylinder. Haddad et al. [73] explored that the thermal entropy increases by incrementing the temperature gradient in an axi-symmetric flow around a cylinder. They also observed that during the entropy production the contribution of thermal irreversibility is prominent as compared to viscous irreversibility. Narusawa [74] examined entropy production for fully developed flow in a rectangular duct and determined the cross-sectional rate of irreversibility under a fully-developed condition for forced convection and mixed convection flow. Tasnim and Mahmud [75] examined the nature of irreversibility in a mixed convective phenomenon along a vertical annulus. They found that, the temperature profiles are linear for small radius ratio and nonlinear for large radius ratio. Mahmud and Fraser [76] examined, analytically, the influence of radiation on mixed convection phenomenon through a vertical channel by implementing the thermodynamics laws. They observed that the involvement of mixed convection parameter in the production of entropy is significant as compared to Hartman number (first introduced by Hartman, it gives the relative importance of magnetic force and viscous force). Odat et al. [77] inspected irreversibility analysis of forced convection flow in the presence of magnetic force. They analyzed that the entropy production minimizes due to an increase in the free stream temperature. Laminar forced convection flow is inspected by Haddad et al. [78-79] through microchannel and gave a detailed discussion on the dependence of

irreversibility phenomenon on various controlling parameters. Chen et al. [80] examined mixed convection flow along wavy surface in the presence of thermal radiation. They concluded that increase in radiation parameter augments the entropy. Butt et al. [81] discussed a mixed convection flow along a stretching surface and determined an average entropy generation rate for a fully developed flow. They analyzed that the entropy production increases for a larger mixed convection parameter. Butt et al. [82] analyzed boundary layer flow over a stretching sheet in porous medium and discussed the effects of viscoelasticity on entropy production. Morsli and Bendehina [83] inspected the entropy generation in a free convection flow occurring in a square cavity having one wavy wall. They observed that a considerable variation in the entropy generation exists due to the surface undulations. Keeping in view this momentous considerations, entropy generation analysis of mixed convection flow along vertical wavy surface has been explored through **Chapter 5**.

Mixed convection boundary layer flows over non-vertical inclined surfaces are of great interest in various fields of science and engineering. Some important engineering applications include solar energy plants, thermal insulation systems, oil separation, heat exchangers, steam generators, etc. Kierkus [84] discussed the natural convection flow along an isothermal plate and calculated the perturbation solution for various values of inclination angle of the surface. Pera and Gebhart [85] explored the influence of inclination angle on heat transfer in natural convection flow. Their results show the enhancement in heat transfer rate because of inclination angle of the boundary as compared to the horizontal surface. Wickern [86] examined a mixed convection flow over an inclined flat surface and discussed the dependence of Nusselt number upon the inclination angle. Lin and Chen [87] discussed the instability of a mixed convection flow along inclined and horizontal boundaries. They found that the flow is more stable

for larger inclination angles. Wang and Chen [88] discussed an MHD flow along an inclined non-flat surface and showed that the flow is accelerated in upstream location while decelerated in downstream location. Varol and Oztop [89] studied the heat transfer phenomenon of free convection flow in an inclined solar collector by considering the flat absorber and wavy absorber. They found that heat transfer rate augments in case of wavy enclosure. Mixed convection flow over an inclined flat surface embedded in porous medium was performed by Rashidi et al. [90]. They determined a series solution by differential transform method and gave a comparison with the numerical method. Uddin et al. [91] studied the impact of MHD on a mixed convection flow over a porous plate. Tian et al. [92] elaborated the phenomenon of combined (free & forced) convection by an experiment done in a narrow-heated channel. The experimental findings ensure that the flow inside a narrow-inclined channel gives remarkable information to improve the engineering design of heat exchangers. Roy [93] discussed a free convection phenomenon of combustible along a thermal surface and presented that increment in inclination angle accelerated the temperature of fluid. Free convection flow in an inclined porous cavity and the associated entropy production was inspected by Baytas [94]. Makinde and Osalusi [95] examined the irreversibility analysis for a liquid film flow over an inclined heated porous plate. They found that production of entropy is reduced with the suction parameter. In another study Makinde [96] performed the second law analysis of a non-Newtonian liquid film over an isothermal plate. Taghizadeh and Asaditaheri [97] analyzed the entropy generation phenomenon for laminar mixed convection flow in an inclined enclosure. They utilized a finite volume method for the solution of their problem. Their numerical results revealed that the inclination angle is an important parameter to control the irreversibility of the system in an enclosure. Fully developed

couple stress flow and entropy generation analysis along an inclined plate was inspected by Adesanya et al. [98]. Couple stress inverse and Newtonian cooling have considerable impact on the production of entropy. Due to this importance **Chapter 6** includes the entropy analysis along inclined wavy surface of mixed convection flow.

In engineering applications mixed convection flow along a conical geometry is applicable in numerous thermal design systems like solar collectors, solar energy plants, heat exchangers, steam generators, etc. The importance of mixed convection flow is more considerable in those situations where the buoyancy force becomes significant due to the presence of temperature gradient. Initially, Merk and Prins [99-100] examined the impact of cone geometry upon free convection flow. They considered the flow for large Prandtl number by neglecting the inertial forces. Consequently, the viscous effects were seen to diffuse quicker than the thermal effects. Hering and Grosh [101] observed that the natural convection flow over the cone geometry possesses a similarity solution and provided a comparison of their solution with the experimental results. Later on, Hering and Grosh [102] extended their problem to a rotating vertical cone by including the forced convection phenomenon to the already happening natural convection flow. They developed the criteria for the flow to be purely forced; free, and combined by subdividing the flow regime. Alamgir [103] discussed heat transfer phenomenon over a heated cone by applying an approximate method. Singh et al. [104] investigated free convection flow along a cone having constant wall temperature and the results were obtained by non-similarity method. Kumari et al. [105] inspected a mixed convective flow along a circular cone and reported the results of Nusselt number and skin-friction for different types of fluids. Heat transfer characteristics for constant wall heat flux along frustum of a cone was reported by Singh et al. [106]. Wang et al. [107] examined a mixed convection flow

along a rotating cone. They discussed the relative importance of free and forced convection in detail. Yih [108] discussed the phenomenon of mixed convection along a cone geometry in the presence of porous medium for both VWT and VHF cases. He found that temperature profile increases with the enhancement of mixed convection parameter. Later on, Yih [109] discussed the impact of radiation on local Nusselt number along an isothermal cone. He found that the surface temperature rapidly reaches to the ambient temperature for small values of radiation parameter. Pop et al. [110] reported the mixed convective flow for the fluids of any Prandtl number along a vertical cone. They obtained the results for opposing flow as well as assisting flow cases. They pointed out that for an opposing flow there also exists a reverse flow for some particular values of the Richardson number. Pop and Na [111] examined a natural convective phenomenon around a cone involving longitudinal wavy configuration. The influence of sinusoidal wave on transport phenomenon was presented graphically. By choosing Darcian fluid, the flow of natural convection about a sinusoidal cone was also reported by Pop and Na [112-113]. Hossain et al. [114] discussed natural convection fluid flow along a sinusoidal surface by considering variable viscosity of the fluid. Since the wavy shaped cone geometry has significant importance in many industrial processes. Therefore, in order to enhance the efficiency of the system it is important to identify the loss of useful energy through irreversibility analysis. Because of this importance, the entropy generation of mixed convection flow over wavy cone has been included in **Chapter 7**.

The flow of viscous fluid over a rotating disk finds important applications in various fields of engineering including turbines, spinning disk reactors, lubrication, oceanography etc. The opening effort upon the analysis of steady flow along an infinite rotating disk was done by von Kármán [115]. For the analysis of axi-symmetric velocity

profile he developed similarity transformations to convert the Navier-Stokes equations to a non-linear system of ordinary differential equations. Later on, Cochran [116] applied the numerical scheme for the solution of von Kármán problem and this solution indicates that a rotating disk works like a centrifugal fan. Bödewadt [117] extended the von Kármán's problem by considering the stationary disk and the fluid rotating over it like a solid body. Batchlor [118] analyzed the class of solutions of Navier-Stokes equations for rotationally symmetric flow which is in fact a generalization of von Kármán solution. Stuart [119] discussed the flow over a porous disk having infinite radius for the case of uniform suction. He found that enhancement in suction parameter reduces the magnitude of radial component of velocity. Rogers and Lance [120] investigated that a physically acceptable solution exists when the outer flow rotates in the same direction as the rotation of the disk. Kelson and Desseaux [121] applied shooting method for the solution of the governing differential equations of rotating porous disk flow. They concluded that the injection phenomenon is the right feature for the existence of axial reverse flow. Turkyilmazoglu [122] computed the solution by homotopy analysis method (HAM) for MHD flow over a rotating disk and gave a comparison with numerical solution. He suggested that HAM solution overcomes the difficulty faced for the higher values of injection parameter. Das [123] also utilized HAM for the conditions of constant and variable angular velocities of the flow. Ibrahim [124] inspected the time dependent flow along the rotating disk. He concluded that temperature profile increases with the increments of heat generation.

Besides several other applications the rotating disk flow finds its important applications in turbomachinery operating at high temperature, a quite specific example can be given of gas turbine in which the rotating cavities operate at extremely high temperatures. In such an extreme thermal conditions efficient heat removing techniques are required all

the time. In such situations passive heat transferring techniques are of quite profit as they not only result in an efficient heat transfer process but also enhance the flow and the power of the machine. The initial work related to convective heat transfer over the disk having non-flat surface texture was done by Lepalec [125]. The results of Lepalec and Lepalec et al. [126] show the influence of surface texture upon heat transfer rate. The findings of [125] depict 15% augmentation in heat transfer rate as compared to the flat disk case. The impact of surface roughness of rotating disk on heat transfer mechanism has been studied by Yoon et al. [127]. They provided enough physical explanation of the enhancement of average Nusselt number due to surface roughness. Later on, Yoon et al. [128] extended the same flow configuration in the presence of magnetic field. Recently, Mehmood et al. [129] examined the heat and mass transfer phenomena over the non-isothermal rotating disk. They found that, the heat transfer rate can further be increased by the consideration of non-uniform temperature distribution over the surface of the disk. Usman et al. [130] inspected the impact of forced flow mechanism along rotating wavy disk with non-uniform temperature. In all these studies significant rise in the heat transfer rate is reported.

As mentioned earlier second law analysis has received much attention from researchers regarding the efficiency of mechanical system. Efficiency measure of an engineering system in the form of entropy generation is more suitable and reliable for practical resolutions. Analysis of entropy production of viscous flow over rotating disk was discussed by Arikoglu at al. [131]. They investigate the slip effect of rotating disk on entropy generation and gave comparison for slip and no slip case. Also, they applied genetic algorithm to optimize the system under minimum entropy. Chen [132] studied convectional flow in which fluid filled in vertical cylinder bounded above by a rotating disk. He analyzed the impact of three modes of convection upon entropy production.

Rashidi et al. [133] inspected the entropy generation in unsteady flow along a rotating disk and introduced the ANN and PSO algorithm to minimize the production of entropy. Butt and Ali [134] examined unsteady flow in a rotating channel and noticed that entropy of the system is enhanced due to rotation parameter. **Chapter 8** includes the study of entropy generation phenomenon of viscous fluid over a rotating disk of sinusoidal wavy texture.

1.2 Preliminaries

The contents of the current section include some basic definitions of fluid mechanics necessary for the subsequent chapters. Dimensionless numbers and the fundamental laws of conservation of mass, linear momentum, and energy are also given.

1.2.1 Fluid

A material that continuously deforms (change its shape) under the application of some external force (regardless how small is it) is known as fluid. Mainly fluids are characterized as liquids and gases. Liquids are the material that are compressed hardly while the gases are compressed easily. Water contains the shape of vessel with free upper surface while the gas is fully expanded to fill the vessel with no free surface. Because of the continuously deformation of fluid under the action of applied shear stress its shape changes continuously unless the force is released. Fluid flow is a fundamental phenomenon which occur commonly in our daily life.

1.2.2 Fluid mechanics

Fluid mechanics is a unique and attractive field of science due to not only its wide applications in nature but also in all branches of engineering. The optimized designs of all means of transportation including aircrafts for both subsonic and supersonic flights, ground effect machines, submarines and automobile etc. can never be obtained without knowledge of fluid mechanics. Moreover, the detailed knowledge of this area is

essential in the constructions of dams, turbines and pumps, canals, airplanes, ships, rivers, windmills, missiles, engines, filters, jets, sprinklers, and highway drainage etc.

1.2.3 Types of fluids

1.2.3.1 Newtonian fluid

A fluid that obeys the Newton's law of viscosity is called a Newtonian fluid. In such kind of fluids shear rate and shear force obey a linear relationship. Consequently, viscosity does not change even how fast to force the flow through a pipe or channel. Some examples are water, organic solvents, gasoline, alcohol etc. Viscosity of such fluids changes only with respect to temperature of the fluid. Mathematically,

$$\tau = \mu\dot{\gamma}, \tag{1.1}$$

where τ, μ, and $\dot{\gamma}$ are shear stress, dynamic viscosity, and shear rate, respectively. Above relation is known as Newton's law of viscosity.

1.2.3.2 Non-Newtonian fluid

A fluid whose viscosity increases or decreases (depending upon nature of the fluid) under the applied shear force is known as non-Newtonian fluid. These fluids do not follow Newtonian's law of viscosity (1.1). There are four different types of these fluids, commonly known as dilatant, pseudoplastic, rheopectic, and thixotropic fluids. In such types of fluids relationship between shear rate and shear force is non-linear. Many fluids such as ketchup, paint, shampoo, cream, glue, gypsum paste, and polymers are non-Newtonian in nature.

1.2.3.3 Nanofluid

The adequate heat transfer performance has been a major issue for long time to improve the efficiency of the thermal system. This issue can be resolved by the enhancement of thermal conductivity of the working fluid. Maxwell [135] in 1881 observed that heat

transfer augment due to the addition of tiny (micro sized) particles in the working (base) fluid. After his analysis, it was seen that although some enhancement in heat transfer rate was gained by the addition of these particles, but there arose some other issues like clogging, rapid sedimentation, erosion, and high pressure drop. Due to these drawbacks, this idea was not implemented practically for the next so many years. After a long time, Choi [24] in 1995 gave an innovative idea about nanofluid. He took the metallic particles of size (1-100nm) in the base fluid. This size of the particles is so much small as compared to the Maxwell's one, so the problems of clogging and pressure drop were automatically resolved. After the implementation of the nanofluid practically, the next task was to explore the mathematical model to explain the further analysis in this field theoretically. Literature survey reveals that there are two types of models, namely, the homogenous model and non-homogeneous model. The most famous homogenous models are due to Tiwari & Das [25] and Buongiorno [26]. The Tiwari and Das model involve the updation of material properties while the Buongiorno model involves the characteristics of thermophoresis and Brownian motion.

1.2.4 Classification of fluid flow

1.2.4.1 Laminar and turbulent flow

In 1883, Reynolds performed an experiment in a glass tube to classify the laminar and turbulent flow. He observed that when a colored liquid was flown through the tube, their path was seen as a piece of string without mingling with outlying water. After reaching a certain value of velocity of water, he saw that colored lines suddenly became turbulent on mingling with the peripheral water. He gave the name laminar flow to the former situation and turbulent to the latter case.

1.2.4.2 Steady and unsteady flow

Steady flow is the type of flow whose velocity and other characteristics at any location of the flow do not depend upon time. On the other way, if these physical quantities at any location of the flow can alter with respect to time, then the flow is known as unsteady flow. As an example, water flow out from a tap, when it is just opened then the flow is unsteady but after some time flow becomes steady.

1.2.4.3 Compressible and incompressible flow

A flow whose density does not alter throughout the course of flow is characterized as incompressible. Therefore, in such kind of flow every portion of the fluid possesses constant volume during its motion. Whereas, if the density of the fluid flow changes with space coordinates or time or both then the flow is compressible. Generally, the liquids are categorized as incompressible fluids and the gases as compressible. However, in the case of highly pressurized liquid, compressibility is taken into account such as oil in a hydraulic machine. Similarly, in low pressure gases compressibility may be omitted.

1.2.4.4 Internal and external flow

Fluid flowing around a solid body which is completely immersed in a fluid is known as external flow. The common examples of such flows are water flow around submarines and fish, air flow around missiles, rockets, and birds etc. On the other hand, the flow which is bounded by a surface is known as internal flow. The flow in ducts, nozzles, and pipes etc. are the internal flows. The same differential equations describe these flows but due to different boundary conditions flows are completely different.

1.2.4.5 Boundary layer flow

Boundary layer theory has proved to be the single most important tool in modern flow analysis especially in the field of aerodynamics, hydrodynamics, wind engineering, and ocean engineering. In 1905 Prandtl was the first who gave the description of the boundary layer concept and explored the two divergent branches of fluid mechanics. He suggested that if the real fluid flows around a solid body, the region of the flow can be classified into two regions. One is the thin layer closed to the solid boundary is known as boundary layer and the flow within this region is called boundary layer flow. In this region the resistance of solid surface is very much important. The other region outside this layer where the resistance is negligible is called inviscid flow region. Prandtl's investigation made it easy to compute the solution of Navier Stokes equations for the viscous flow problem. Thus, the concept of boundary layer contributed remarkably in the modern era of fluid dynamics.

1.2.5 The phenomena of convection

In thermodynamical systems heat can be transferred by means of three fundamental mechanisms. These mechanisms are convection, conduction, and radiation and most of the convective heat transfer problems are governed through convection process. The basic criterion for heat transfer in all these cases is the presence of temperature difference. In fluid flow processes transfer of heat occurs by means of convection phenomenon. In the convection phenomenon the energy of the hot particles of the fluid is transferred to the adjacent cooler fluid particles because of their motion. As an example, the temperature of hot block is reduced by means of fan blowing air over its surface. In mass convection, the fluid particles of high concentration close to the surface leave the place and that place is fill up by the fluid of low concentration.

In natural convection phenomenon, the fluid flow is due to buoyancy force, which establishes itself as the rise of lighter fluid and the fall of denser fluid. Physically, in many devices the phenomenon of natural convection occurs frequently, examples can be given of heat exchanger, combustion modeling, petroleum reservoirs, and nuclear reactor cooling etc. In forced convection, fluid flow occurs over a surface by an external mean such as pump or a fan. The forced convective flow past a moving plate in a moving fluid has numerous applications in engineering including the cooling of polymer sheets. Thermal transport due to a continuously moving plate through quiescent or moving fluid finds applications in processes such as plastic extrusion and continuous casting. The combination of forced convection and natural convection is called as mixed convection. Some examples are the electronic devices cooled by fans and solar receivers exposed to wind currents etc.

1.2.6 Entropy

The loss of useful energy in a mechanical system is measured as the entropy of the system. In 1865 two scientists Clausius and Kelvin gave the concept of entropy production by using the thermodynamics second law. Entropy is a thermodynamic variable which depends only on the state of the system. Whenever heat flows from a higher temperature state to lower temperature state the process is irreversible. In the light of second law of thermodynamics almost all the physical devices possess irreversible process because without expenditure of work heat cannot be transferred from low to the high temperature. The situation becomes more uneconomical when useful energy is destroyed while reducing thermal and mechanical efficiency. This becomes the major reason in the disorder of a system which is called the entropy of the system.

1.2.6.1 Entropy generation

In the previous decade, the influence of entropy on fluid flow phenomenon has been of great interest because of the development of environmental friendly technologies. The recommendations of the entropy analysis find their wider applications in diverse engineering systems such as combustion engines, heat exchangers, turbo-machinery, cooling systems, and transport phenomena etc. In fluid flow phenomenon there are many sources of entropy generation including convective transfer of heat, solar radiation, viscous dissipation, and mass diffusion etc. The volumetric entropy generation as proposed by Bejan [1-4] is measured as

$$S_G = \frac{k}{T_\infty^2}(\nabla T)^2 + \frac{\mu}{T_\infty}\Phi, \tag{1.2}$$

where k and Φ denote the thermal conductivity and viscous dissipation of the fluid. The ambient temperature of the fluid is denoted by T_∞. In the above equation, expression clearly indicates that two factors (thermal conductivity and viscosity) are accountable for the production of entropy in convective heat transfer phenomena. Also, this equation is valid for pure fluid and the nanofluid in which Tiwari and Das model [25] is considered. In case of Buongiorno model [26] Eq. (1.2) is expressed as

$$S_G = \frac{k}{T_\infty^2}(\nabla T)^2 + \frac{\mu}{T_\infty}\Phi + \frac{RD_B}{C_\infty}(\nabla C)^2 + \frac{RD_B}{T_\infty}(\nabla C.\nabla T), \tag{1.3}$$

where R and D_B are the gas constant and Brownian diffusion coefficient, respectively.

1.2.6.2 Bejan number

Entropy number is unable to classify the dominancy of irreversibility mechanism. To overcome this difficulty Bejan number is constructed to analyze the irreversibility mechanism. Bejan number Be is formed by dividing the heat transfer irreversibility to the total entropy production. Generally, Bejan number (Be) have the following form:

$$Be = \frac{entropy\ production\ due\ to\ heat\ transfer}{total\ entropy\ production}. \tag{1.4}$$

The above equation clearly shows that the range of Be is between 0 and 1: when $Be = 1$, the entropy production owing to heat transfer is dominant, when $Be = 1/2$, the involvement in entropy production due to transfer of heat and sum of viscous dissipation and heat and mass diffusion are equal, when $Be = 0$, the irreversibility mechanism due to viscous dissipation and heat and mass diffusion dominate the entropy generation.

1.2.7 Fundamental Equations

1.2.7.1 Equation of continuity

This law describes that, the mass of a closed surface considered in a fluid is conserved. The mathematical form that defines this law is known as equation of continuity. Hence, in the continuous motion of the fluid the mass of any closed region must be constant i.e. the amount of mass that enter into the region is same as the amount that leaves. The mathematical form of this law is as under:

$$\frac{\partial \rho}{\partial t} + \nabla.(\rho \boldsymbol{V}) = 0, \tag{1.5}$$

where ρ is density of the fluid and fluid velocity at any location is represented by the vector $\boldsymbol{V}$. In the case of incompressible fluid, the density is constant due to which the equation of continuity (1.5) simplifies to

$$\nabla.\boldsymbol{V} = 0. \tag{1.6}$$

1.2.7.2 Navier-Stokes equations

Generally, the nonlinear partial differential equation that govern the motion of fluid are known as Navier-Stokes equations. These equations are based on the fundamental law of conservation of linear momentum and are therefore commonly known as the

momentum equations or the law of conservation of linear momentum. Mathematical form of law of conservation of linear momentum reads as

$$\rho\frac{DV}{Dt} = -\nabla p + \nu\nabla^2 \boldsymbol{V} + \rho \boldsymbol{b}, \tag{1.7}$$

where $\boldsymbol{b}$ represent the body force, and ∇ denotes the gradient operator. Body force in the problems reported in this dissertation is the bouncy force. The bouncy force is given by

$$\boldsymbol{b}_{bou}=\boldsymbol{g}\beta(T - T_\infty), \tag{1.8}$$

where $\boldsymbol{g}$ denotes the gravitational acceleration and β described the thermal expansion.

1.2.7.3 Energy equation

For a viscous incompressible fluid having constant thermal conductivity, zero internal heat generation and negligible viscous dissipation effects, the energy equation (law of conservation of energy) is given as

$$\frac{DT}{Dt} = \alpha_f^* \nabla^2 T. \tag{1.9}$$

The Eq. (1.9) is valid for pure fluid, for Tiwari and Das model, α_f^* is replaced by α_{nf}^*. For the Buongiorno model [26] the above energy equation is written as

$$\frac{DT}{Dt} = \alpha_f^* \nabla^2 T + \tau^* \left(D_T \frac{\nabla T . \nabla T}{T_\infty} + D_B \nabla C . \nabla T \right), \tag{1.10}$$

where D_T, D_B and τ^* are the thermophoretic diffusion coefficient, the Brownian diffusion coefficient, and the ratio of heat capacity of a nanoparticle to the base fluid, respectively.

1.2.7.4 Concentration equation

Fick's law usually used to describe the transport phenomenon of any constituents/species in the fluid flow processes. The mathematical form of this phenomenon is written as

$$\frac{DC}{Dt} = D_m \nabla^2 \mathrm{C}, \tag{1.11}$$

and in view of Buongiorno nanofluid model [26], Eq. (1.11) modifies as

$$\frac{DC}{Dt} = D_B \nabla^2 C + \left(\frac{D_T}{T_\infty}\right) \nabla^2 T. \tag{1.12}$$

Equations (1.11) and (1.12) show that the concentration C occupies the place of temperature, while, the mass diffusivity D_m replaces the thermal diffusivity α_f^* in the energy equation. The above equations are in general form where C denotes the mass concentration in the fluid. The subscript ∞ denotes the property at the ambient location.

1.2.8 Wavy texture

In this dissertation our objective is to analyze the boundary layer flows past a non-flat surface. The flow along such wavy texture is interestingly non-similar in nature. Following function illustrates the texture of wavy plate extended in x −direction:

$$\bar{y} = \bar{S}(\bar{x}) = \bar{\alpha} sin\left(\frac{\pi \bar{x}}{l}\right), \tag{1.13}$$

where l is the wave length and $\bar{\alpha}$ is the fixed amplitude . This wavy surface is assumed to be semi-infinite in the xz −plane and is occupied by the ambient fluid. Any non-flat sheet surface can be considered in the analysis of such kind of problems. However, such a consideration must be accompanied by a proper justification in view of technological applications. In practice, a flat heat transferring surface of a heat exchanger can easily be replaced by a periodic wavy surface for the purpose of improvement in the heat transferring capacity of the heat exchanger. Therefore, a sinusoidal wavy surface has been considered in this dissertation. Moreover, a sinusoidal wavy surface is a continuous, smooth, and has no sharp corners like the wavy surface of the triangular and square nature. Because of this reason, its mathematical handling is also quite simple. The geometry of the wavy surfaces considered in the subsequent chapters are given in Figure 1.1.

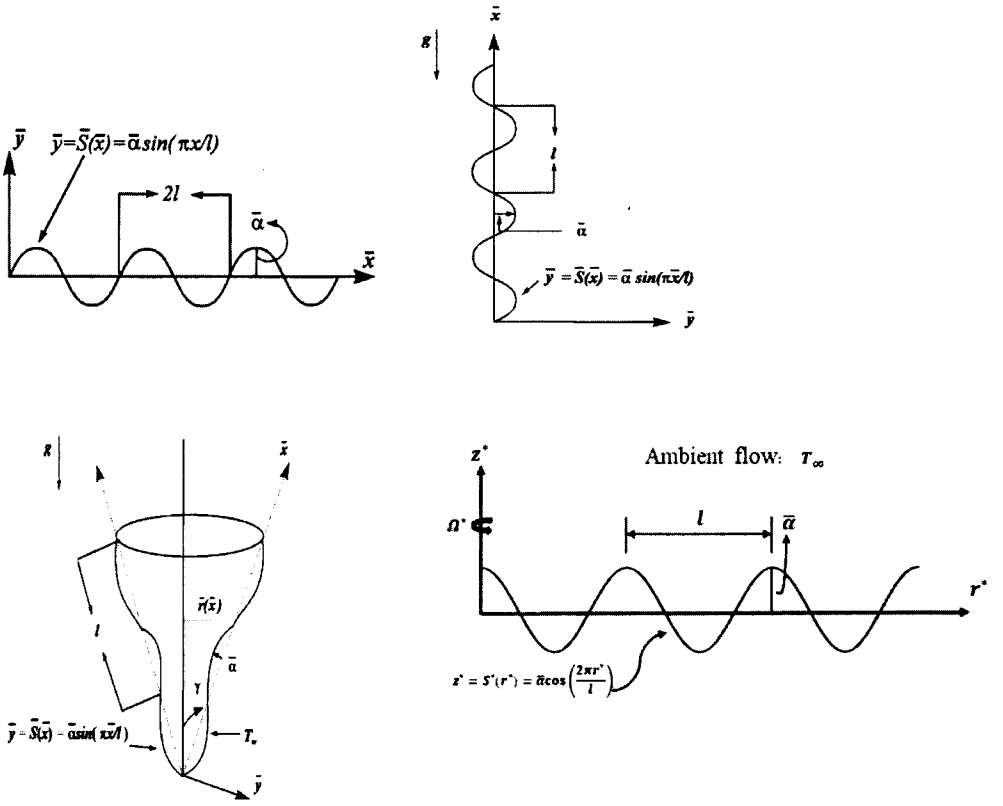

Fig. 1.1: Representation of the wavy surfaces.

1.2.9 Skin-friction coefficient

An important physical quantity that describes the measurement of frictional (drag) force between the fluid and solid boundary. In mathematical form it is given by

$$C_{fx} = \frac{\tau_w}{\rho U^2}, \tag{1.14}$$

where τ_w represents the shear stress at the wall and is defined as

$$\tau_w = \mu(\nabla \bar{u} . \hat{n})_{\bar{y}=0}, \tag{1.15}$$

where $\hat{n} = (n_x, n_y) = (-\frac{\sigma_\xi}{\sigma}, \frac{1}{\sigma})$ signify the unit vector perpendicular to the solid wavy boundary and $\sigma = \sqrt{1 + S_\xi^2}$ describes the waviness of the surface. Reference velocity is denoted by U.

1.2.10 Nusselt number

It is a dimensionless quantity that demonstrates the heat transfer rate at the boundary either heat gets in or out from the wall. Nusselt number is the ratio of convective heat transfer and conductive heat transfer i.e.,

$$Nu_x = \frac{\bar{x}q_w}{\kappa(T_w - T_\infty)}, \tag{1.16}$$

where q_w is the wall heat flux and is calculated as

$$q_w = -\kappa(\nabla T.\hat{n})_{\bar{y}=0}. \tag{1.17}$$

Heat transfer rate can be determined by the value of Nu_x at any specific location at the plate. Because of dependence on a specific location in fact it is a local Nusselt number and usually appears in non-similar flows.

1.2.11 Sherwood number

In the analysis of mass transfer phenomenon Sherwood number is frequently used for the measurement of mass transfer rate at the specific position of the boundary. It is the ratio of convective to diffusive mass transfer and is described as

$$Sh_x = \frac{\bar{x}q_m}{D_B(C_w - C_\infty)}, \tag{1.18}$$

where q_m signifies mass flux at the wall and is written as

$$q_m = -D_B(\nabla C.\hat{n})_{\bar{y}=0}. \tag{1.19}$$

1.2.12 Reynolds number

In 19th century, this dimensionless number was developed by the British scientist Osborne Reynolds which proved to be a significant innovation in the history of fluid mechanics. Reynolds number helps to classify the types of flow pattern in different types of flow problems. Its mathematical form is:

$$Re = \frac{Ul}{\nu}. \tag{1.20}$$

This number is regarded as the ratio of inertial forces to the viscous forces. Reynolds number is used to categorize the flows as laminar or turbulent.

1.2.13 Prandtl number

Ludwig Prandtl, a German scientist, gave the idea about how to classify the nature of fluid. For this motivation he used this dimensionless number. Pr is the ratio of diffusivity due to momentum and diffusivity due to heat, that is

$$Pr = \frac{\nu}{\alpha_f^*} = \frac{\mu c_p}{\kappa}, \tag{1.21}$$

where α_f^* is the thermal diffusivity. For gases $Pr \backsim 0.7$; for liquids such as water, $Pr \backsim 7.0$ and for liquid metals, $Pr << 1$.

1.2.14 Grashof number

This dimensionless number is the ratio of buoyancy forces and viscous forces. Any flow and heat transfer problem which involves the situation of natural convection, Grashof number arises there and is used for the complete analysis of the flow. Mathematically,

$$Gr = \frac{g\beta\Delta T l^3}{\nu^2}. \tag{1.22}$$

1.2.15 Lewis number

Ratio of thermal diffusion rate and mass diffusion rate is known as Lewis number. This number has physical importance in the combined analysis of heat and mass transfer. Mathematical form of Lewis number is written as

$$Le = \frac{\alpha_f^*}{D_m}, \tag{1.23}$$

where D_m is the mass diffusivity.

1.2.16 Brinkman number

It is a dimensionless number that describes the transfer of heat from boundary to the viscous fluid. There are several mathematical forms of Brinkman number, one of which is

$$Br = \frac{\mu U^2}{\kappa \Delta T}. \tag{1.24}$$

1.2.17 Non-similar flows

Non-similar flows are one of the types of boundary layer flows in which similarity solution does not exist. Generally, it is an easy task to solve the momentum and energy equations in the case of similar flows by transforming the original governing system of partial differential equations into ordinary differential equations by the implementation of similarity transformation. But in the non-similar flows such kind of similarity transformation does not exist, so one has to tackle the non-linear partial differential equations with variable coefficients. The essential reason of self-similarity breaking (as reported in this dissertation) is the surface roughness of the solid boundary along which fluid flows. Practically, surfaces are deliberately made rough for the enhancement of heat transfer rate and consequently the flow becomes non-similar in nature.

1.2.18 Solution methodology

Non-linear partial differential equations arise in many fields of engineering and science and the analytical approach towards the solution of most of these equations is not possible. So, it is necessary that the advanced technique may be constructed for the solution of such equations especially in the area of fluid mechanics, aerospace engineering, and control engineering. The pioneer work has been done by Keller [136] in 1970 and the method is commonly known as Keller-box method. This method is

valid for the solution of all non-similar problems and is specially designed for the boundary layer flows. This method is widely used in numerous industrial and physical fluid dynamics problems. This algorithm is mesh independent and has accuracy of the order two. The key points of the algorithm are as follows:

Step I. Differential equations of higher order are converted into differential equations of order one by using new functions.

Step II. The derivative of transformed first order differential equations is replaced by the central difference approximation due to which one can achieve a system of algebraic equations which could be linear or non-linear.

Step III. If non-linear algebraic system of equations is obtained in previous step, then the Newton's method is implemented for linearization.

Step IV. Linearized system of algebraic equations are putt in the form of tri-diagonal matrix and then solved by LU-decomposition or block elimination method.

Chapter 2

Entropy analysis of boundary layer flow past a moving hot wavy surface

Significant enhancement in the rate of heat transfer can be obtained due to the modification of the flat surface texture of the system. Due to mathematical facility, the appropriate modification of the surface texture of the working body is to transform the flat one into the periodic wavy surface. Literature survey reveals that wavy surface of the working body significantly effects the heat transfer phenomenon. In this regard, analysis of entropy generation is quite essential for the flow and heat transfer phenomena over the non-flat boundary. In this chapter analysis is performed to see the effects of surface undulations upon entropy generation. Impact of various other physical parameters upon entropy generation rate is reported.

2.1 Mathematical description

We consider a steady incompressible viscous flow due to a horizontal wavy sheet moving uniformly in x-direction. The surface shape is assumed to be smooth differentiable described by Eq. (1.13). The schematic of the plate geometry and the associated coordinate system is shown in Fig. 2.1. The leading edge of the wavy surface is coinciding with the origin of coordinate system which also serves as the leading edge of the corresponding flat surface. Mathematics of the considered wavy texture is given in Eq. (1.13) and is labelled in Fig. 2.1.

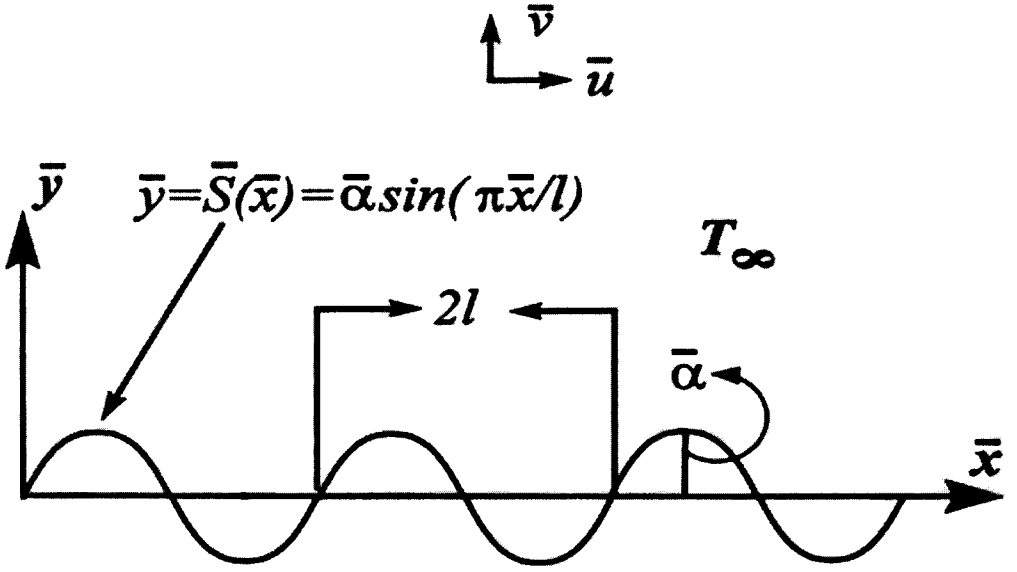

Figure 2.1: Schematic diagram of the flow configuration.

Essentially the flow is two-dimensional and the variation in the velocity of the fluid with the variable $\bar{x}$ occurs continuously due to wavy texture of the boundary and consequently the flow is non-similar in nature. The mass, momentum, and energy conservation laws in component form are described as

$$\frac{\partial \bar{u}}{\partial \bar{x}} + \frac{\partial \bar{v}}{\partial \bar{y}} = 0, \tag{2.1}$$

$$\bar{u}\frac{\partial \bar{u}}{\partial \bar{x}} + \bar{v}\frac{\partial \bar{u}}{\partial \bar{y}} = -\frac{1}{\rho}\frac{\partial \bar{p}}{\partial \bar{x}} + \nu\nabla^2\bar{u}, \tag{2.2}$$

$$\bar{u}\frac{\partial \bar{v}}{\partial \bar{x}} + \bar{v}\frac{\partial \bar{v}}{\partial \bar{y}} = -\frac{1}{\rho}\frac{\partial \bar{p}}{\partial \bar{y}} + \nu\nabla^2\bar{v}, \tag{2.3}$$

$$\bar{u}\frac{\partial T}{\partial \bar{x}} + \bar{v}\frac{\partial T}{\partial \bar{y}} = \alpha_f^*\nabla^2 T, \tag{2.4}$$

where $(\bar{u}, \bar{v})$ are the components of velocity parallel to the dimensional coordinates $(\bar{x}, \bar{y})$, and α_f^* is the thermal diffusivity. The associated boundary conditions are expressed as (see for instance [18]):

$$\begin{aligned} &\bar{y} = \bar{S}(\bar{x}):\ \bar{u}\bar{t}_{\bar{y}} - \bar{v}\bar{t}_{\bar{x}} = 0, \bar{u}\bar{t}_{\bar{y}} + \bar{v}\bar{t}_{\bar{x}} = U, T = T_w \ \text{ for all } \ \bar{x} > 0, \\ &\bar{y} \to \infty:\ \bar{u} = \bar{v} = 0, \bar{p} = p_\infty, T = T_\infty, \ \text{ for all } \ \bar{x} > 0, \end{aligned} \tag{2.5a}$$

where $(t_{\bar{x}}, t_{\bar{y}})$ are the components of the unit tangent vector along the coordinate axes. Since the development of boundary layer starts at $\bar{x} > 0$, therefore the ambient conditions of the flow are considered to be valid at the leading edge $\bar{x} = 0$, which are read as

$$\bar{x} = 0: \bar{p} = p_\infty, T = T_\infty \text{, for all } \bar{y} \neq 0 . \tag{2.5b}$$

Let us consider the following dimensionless quantities

$$\xi = x = \frac{\bar{x}}{l}, u = \frac{\bar{u}}{U}, S = \frac{\bar{S}(\bar{x})}{l}, y = \frac{(\bar{y} - \bar{S}(\bar{x}))}{l}\sqrt{Re}, v\frac{(\bar{v} - S_\xi \bar{u})}{U}\sqrt{Re},$$
$$\alpha = \frac{\bar{\alpha}}{l}, Re = \frac{Ul}{\nu}, \theta(\xi, \eta) = \frac{T - T_\infty}{T_w - T_\infty}, p = \frac{\bar{p}}{\rho_f U^2}. \tag{2.6}$$

The amplitude to wavelength ratio is assumed to be small as compared to boundary layer thickness due to which the variation in pressure $(\partial p/\partial x)$ along x-direction can be neglected. Thus, by the elimination of the term $\partial p/\partial y$ from (2.2)-(2.3), and due to the utilization of Eq. (2.6), the set of equations (2.2)-(2.4) attains the following dimensionless form

$$u\frac{\partial u}{\partial x} + v\frac{\partial u}{\partial y} = (1 + \sigma_\xi^2)\frac{\partial^2 u}{\partial y^2} - \frac{\sigma_\xi}{\sigma}u^2, \tag{2.7}$$

$$u\frac{\partial \theta}{\partial x} + v\frac{\partial \theta}{\partial y} = \frac{1}{Pr}(1 + \sigma_\xi^2)\frac{\partial^2 \theta}{\partial y^2}, \tag{2.8}$$

where Pr is the Prandtl number and the parameter σ and σ_ξ represent the wavy contribution in the governing system. To reduce the governing system in a computationally convenient form, we use the following transformations:

$$\psi(\xi, \eta) = \sqrt{\xi} f(\xi, \eta), \quad \eta = \frac{y}{\sigma\sqrt{\xi}}, \quad \theta = \theta(\xi, \eta), \tag{2.9}$$

in which $f(\xi, \eta)$ is the dimensionless stream function due to which the equation of continuity is satisfied identically. Due to these transformations Eqs. (2.7)-(2.8) transform as

$$f''' + \frac{1}{2}ff'' - \xi\frac{\sigma_\xi}{\sigma}\left[ff'' - f'^2\right] = \xi\left[f'\frac{\partial f'}{\partial \xi} - f''\frac{\partial f}{\partial \xi}\right], \tag{2.10}$$

$$\frac{1}{Pr}\theta'' + \frac{1}{2}f\theta' + \xi\frac{\sigma_\xi}{\sigma}f\theta' = \xi\left[f'\frac{\partial \theta}{\partial \xi} - \theta'\frac{\partial f}{\partial \xi}\right]. \tag{2.11}$$

The boundary conditions (2.5a) in view of Eq. (2.6) and (2.9) also transform to a form

$$\left.\begin{aligned} f(\xi,0)=0,\ f'(\xi,0)=\frac{1}{\sigma},\ \theta(\xi,0)=1,\\ f'(\xi,\infty)=0,\ \theta(\xi,\infty)=0. \end{aligned}\right\} \tag{2.12}$$

The local skin-friction coefficient and the local Nusselt number are given by

$$C_{fx}=\frac{\tau_w}{\rho U^2},\ Nu_x=\frac{\bar{x}q_w}{k(T_w-T_\infty)}, \tag{2.13}$$

where τ_w indicates the shear stress at the wall and heat flux at the boundary is represented by q_w. The expressions of these physical quantities are given by

$$\tau_w=\mu(\nabla\bar{u}\cdot\hat{n})_{y=0},\ q_w=-k(\nabla T\cdot\hat{n})_{y=0}, \tag{2.14}$$

where $\hat{n}$ denotes the unit normal vector on the sinusoidal boundary. After using Eqs. (2.6), (2.9), and (2.14), skin-friction coefficient and Nusselt number have the following expression:

$$\begin{aligned} C_f=C_{fx}(\mathrm{Re}_x)^{1/2}=\frac{1}{\sigma}f''(\xi,0),\ Nu=Nu_x(\mathrm{Re}_x)^{-1/2}\\ =-\theta'(\xi,0). \end{aligned} \tag{2.15}$$

2.2 Entropy generation

For a viscous and incompressible fluid which follows the Fourier law of heat conduction and is in local thermodynamic equilibrium. Expression for entropy production in Cartesian coordinate system is defined due to Bejan [1-4]:

$$\begin{aligned} S_G=\frac{k}{T_\infty^2}\left[\left(\frac{\partial T}{\partial\bar{x}}\right)^2+\left(\frac{\partial T}{\partial\bar{y}}\right)^2\right]\\ +\frac{\mu}{T_\infty}\left[2\left(\frac{\partial\bar{u}}{\partial\bar{x}}\right)^2+2\left(\frac{\partial\bar{v}}{\partial\bar{y}}\right)^2+\left(\frac{\partial\bar{v}}{\partial\bar{x}}+\frac{\partial\bar{u}}{\partial\bar{y}}\right)^2\right]. \end{aligned} \tag{2.16}$$

The above expression shows that the viscosity (μ) and the thermal conductivity (k) are responsible for the generation of irreversibility. Entropy rate is positive and finite only if the gradient of velocity or temperature exist in the medium. The entropy generation

number defined by Bejan [1-4] is the ratio of volumetric entropy generation rate to the characteristic entropy generation rate. Using aforementioned set of dimensional variables listed in Eqs. (2.6) and (2.9) the entropy generation number takes a form

$$\frac{N_s}{Re} = \frac{S_G}{S_{G_0}} = \frac{1}{\xi}\theta'^2 + \frac{\omega(1+\sigma_\xi^2)}{\xi} f''^2, \\ = N_H + N_F, \tag{2.17}$$

where $S_{G_0} = k(\Omega_T/l)^2, \Omega_T = \Delta T/T_\infty$, $T_\infty, \omega = Br/\Omega_T$ and $Br = \mu U_w^2/k\Delta T$ are the characteristic entropy, the dimensionless temperature difference, the reference temperature of the fluid, group parameter, and Brinkman number, respectively. The first term represents the heat transfer irreversibility denoted by N_H and the second term represents fluid friction irreversibility and is denoted by N_F. Ratio of the entropy produced by the heat transfer to the total entropy of the system is known as the Bejan number (as defined in Eq. (1.4)) which is given by

$$Be = \frac{\theta'^2}{\theta'^2 + \omega(1+\sigma_\xi^2)f''^2}. \tag{2.18}$$

Bejan number serves in characterizing the major role of irreversibilities towards the production of entropy. If the value of the Bejan number is near 0 the entropy is dominated by fluid friction effects. However, if Be reaches to 1 then the heat transfer factor is responsible for entropy production. Similarly, the irreversibility due to both factors is equal if Be is 0.5.

2.3 Numerical solution and validation of results

The governing non-similar system of partial differential Eqs. (2.10) - (2.11) appended by the boundary data (2.12) are numerically solved. For doing so Keller-Box method [136-139] is implemented. Using Keller-Box implicit finite difference technique the

system of non-similar partial differential equations is first reduced to first-order differential equations by choosing new variables

$$f' = g, \qquad g' = q, \theta' = p, \tag{2.19}$$

due to which the differential equations (2.10)-(2.11) are re-written as:

$$q' + \frac{1}{2} fq - \xi \frac{\sigma_\xi}{\sigma}(fq - g^2) = \xi \left[g \frac{\partial g}{\partial \xi} - q \frac{\partial f}{\partial \xi} \right], \tag{2.20}$$

$$\frac{1}{Pr} p' + \frac{1}{2} fp + \xi \frac{\sigma_\xi}{\sigma} fp += \xi \left[g \frac{\partial \theta}{\partial \xi} - p \frac{\partial f}{\partial \xi} \right], \tag{2.21}$$

and the boundary conditions also modify as

$$f(0,\xi) = 0,\ g(0,\xi) = 1/\sigma,\ \theta(0,\xi) = 1,\ f(\infty,\xi) = 0,\ \ \theta(\infty,\xi) = 0. \tag{2.22}$$

Defining $\xi\eta$ −net on the plane (ξ, η) in the following way

$$\begin{gathered} \eta_0 = 0, \eta_j = \eta_{j-1} + \Delta\eta, \eta_j = \eta_\infty, j = 1,2, \ldots, J-1, \\ \xi^0 = 0, \xi^n = \xi^{n-1} + \Delta\xi, n = 1,2, \ldots, \end{gathered} \tag{2.23}$$

where $\Delta\eta = h$ and $\Delta\xi = k$ are breadths of the mesh, n and j are positive integers. The partial derivative of the net functions $f, g, q, \theta, p,$ and d at any net point (ξ^n, η_j) are replaced with central difference formula and average centered difference is used for these functions at the point $(\xi^{n-1/2}, \eta_{j-1/2})$ i.e.

$$\frac{\partial}{\partial \xi}(f)\Big|_j^{n-1/2} = \frac{1}{k}(f_j^n - f_j^{n-1}),\ \ \frac{\partial}{\partial \eta}(f)\Big|_{j-1/2}^{n} = \frac{1}{h}(f_j^n - f_{j-1}^n),$$

and

$$f_j^{n-1/2} = \frac{1}{2}(f_j^n + f_j^{n-1}),\ \ f_{j-1/2}^n = \frac{1}{2}(f_j^n + f_{j-1}^n).$$

With the help of above central differences the non-linear system (2.20) and (2.21) are transformed into a system of difference equations by discretization:

$$\left(\frac{1}{2}\right)\left(\frac{q_j^n - q_{j-1}^n}{\mathrm{h}}\right) + \frac{1}{2}\left(\frac{f_j^n + f_{j-1}^n}{2}\right)\left(\frac{q_j^n + q_{j-1}^n}{2}\right) - \xi$$
$$* \left(\frac{\sigma_\xi}{4\sigma}\right)\left[(g_j^n + g_{j-1}^n)^2 - (f_j^n + f_{j-1}^n)(q_j^n + q_{j-1}^n)\right]$$
$$- \left(\frac{\xi^{n-\frac{1}{2}}}{8\mathrm{k}}\right)\left\{(g_j^n + g_{j-1}^n)^2 - (q_j^n + q_{j-1}^n)(f_j^n + f_{j-1}^n)\right. \quad (2.24)$$
$$+ (q_j^n + q_{j-1}^n)(f_j^{n-1} + f_{j-1}^{n-1})$$
$$\left. - (q_j^{n-1} + q_{j-1}^{n-1})(f_j^n + f_{j-1}^n)\right\} = r_{j-\frac{1}{2}}^{n-1},$$

$$\left(\frac{1}{2Pr}\right)\left(\frac{p_j^n - p_{j-1}^n}{h}\right) + \frac{1}{2}\left(\frac{f_j^n + f_{j-1}^n}{2}\right)\left(\frac{p_j^n + p_{j-1}^n}{2}\right)$$
$$+ \left(\frac{\sigma_\xi}{4\sigma}\right)\left[(f_j^n + f_{j-1}^n)(p_j^n + p_{j-1}^n)\right]$$
$$- \frac{\xi^{n-\frac{1}{2}}}{8\mathrm{k}}\left[(g_j^n + g_{j-1}^n + g_j^{n-1} + g_{j-1}^{n-1})(\theta_j^n + \theta_{j-1}^n)\right. \quad (2.25)$$
$$\left. - (p_j^n + p_{j-1}^n)(f_j^n + f_{j-1}^n - f_j^{n-1} - f_{j-1}^{n-1})\right] = m_{j-\frac{1}{2}}^{n-1},$$

$$f_j^n - f_{j-1}^n = \frac{h}{2}(g_j^n + g_{j-1}^n), \quad (2.26)$$

$$g_j^n - g_{j-1}^n = \frac{h}{2}(q_j^n + q_{j-1}^n), \quad (2.27)$$

$$\theta_j^n - \theta_{j-1}^n = \frac{h}{2}(p_j^n + p_{j-1}^n), \quad (2.28)$$

here

$$r_{j-\frac{1}{2}}^{n-1} = -\left(\frac{1}{2h}\right)\left[(q_j^{n-1} - q_{j-1}^{n-1})\right] - \left(\frac{1}{16}\right)\left[(f_j^{n-1} + f_{j-1}^{n-1})(q_j^{n-1} + q_{j-1}^{n-1})\right]$$
$$+\xi * \left(\frac{\sigma_\xi}{4\sigma}\right)\left[(f_j^{n-1} + f_{j-1}^{n-1})(q_j^{n-1} + q_{j-1}^{n-1}) - (g_j^{n-1} + g_{j-1}^{n-1})^2\right] + \quad (2.29)$$
$$\left(\frac{\xi^{n-\frac{1}{2}}}{8k}\right)\left([-(g_j^{n-1} + g_{j-1}^{n-1})^2] + [(q_j^{n-1} - q_{j-1}^{n-1})] * [(f_j^{n-1} + f_{j-1}^{n-1})]\right),$$

$$m_{j-\frac{1}{2}}^{n-1} = -\left(\frac{1}{2Prh}\right)\left[(q_j^{n-1} - q_{j-1}^{n-1})\right] - \left(\frac{1}{16}\right)\left[(f_j^{n-1} + f_{j-1}^{n-1})\right. \quad (2.30)$$
$$\left. * (p_j^{n-1} + p_{j-1}^{n-1})\right]$$

$$+\xi * \left(\frac{\sigma_\xi}{4\sigma}\right)\left[\left(f_j^{n-1} + f_{j-1}^{n-1}\right) * \left(p_j^{n-1} + p_{j-1}^{n-1}\right)\right]$$
$$+ \xi\left(\frac{1}{8k}\right)\left(\left[\left\{\left(g_j^n + g_{j-1}^n\right) + \left(g_j^{n-1} + g_{j-1}^{n-1}\right)\right\}\right.\right.$$
$$* \left\{-\left(\theta_j^{n-1} + \theta_{j-1}^{n-1}\right)\right\}\left.\right] - \left[\left(p_j^{n-1} + p_{j-1}^{n-1}\right)\right.$$
$$\left.\left. * \left\{\left(f_j^n + f_{j-1}^n\right) - \left(f_j^{n-1} + f_{j-1}^{n-1}\right)\right\}\right]\right).$$

The boundary conditions (2.22) take the form

$$f_0^n = 0, g_0^n = 1/\sigma, \theta_0^n = 1, g_j^n = \theta_j^n = 0. \tag{2.31}$$

Introducing $(i+1)^{th}$ iterates on the nonlinear algebraic Eqs. (2.24) & (2.25) by Newton's linearization method as

$$\left(f_j^n\right)^{(i+1)} = \left(f_j^n\right)^{(i)} + \left(\delta f_j^n\right)^{(i)}, \tag{2.32}$$

which equally applies to all other unknown quantities. As an initial guess first term on the RHS is known in the interval $0 < j \leq J$ and second term is unknown. A system of linear algebraic equation is achieved after applying Newton linearization method and omitting higher order terms of $\left(\delta f_j^n\right)^{(i)}, \left(\delta g_j^n\right)^{(i)}, \left(\delta q_j^n\right)^{(i)}, \left(\delta \theta_j^n\right)^{(i)}$ and $\left(\delta p_j^n\right)^{(i)}$:

$$\delta f_j^n - \delta f_{j-1}^n - \frac{\mathrm{h}}{2}\left(\delta g_j^n + \delta g_{j-1}^n\right) = (r_{11})_j,$$

$$(s_{11})_j \delta f_{j-1}^n + (s_{12})_j \delta f_j^n + (s_{13})_j \delta g_{j-1}^n + (s_{14})_j \delta g_j^n + (s_{15})_j \delta q_{j-1}^n + (s_{16})_j \delta q_j^n = (r_{12})_j,$$

$$(s_{21})_j \delta \theta_{j-1}^n + (s_{22})_j \delta \theta_j^n + (s_{23})_j \delta p_{j-1}^n + (s_{24})_j \delta p_j^n = (r_{13})_j,$$

$$\delta g_j^n - \delta g_{j-1}^n - \frac{h}{2}\left(\delta q_j^n + \delta q_{j-1}^n\right) = (r_{14})_j,$$

$$\delta \theta_j^n - \delta \theta_{j-1}^n - \frac{h}{2}\left(\delta p_j^n + \delta p_{j-1}^n\right) = (r_{15})_j,$$

The boundary conditions (2.31) are written as

$$\delta f_0^n = 0, \delta g_0^n = 1/\sigma, \delta \theta_0^n = 1, \delta g_j^n = \delta \theta_j^n = 0.$$

Lastly, linear algebraic system and respective boundary data are shifted to a matrix form where the coefficients of unknown quantities δf_j^n, δg_j^n, $\delta q_j^n, \delta \theta_j^n$, and δp_j^n in the fundamental laws are given as:

Coefficient of momentum equation

Coefficient of δf_{j-1}^{n}:

$$(s_{11})_j = \frac{1}{16}(q_j^n + q_{j-1}^n) + \xi^{n-\frac{1}{2}} * \left(\frac{\sigma_\xi}{8\sigma}\right)(q_j^n + q_{j-1}^n) + \frac{\xi^{n-\frac{1}{2}}}{8\mathrm{k}}[(q_j^n + q_{j-1}^n) + (q_j^{n-1} + q_{j-1}^{n-1})]$$

Coefficient of δf_j^n:

$$(s_{12})_j = \frac{1}{16}(q_j^n + q_{j-1}^n) + \xi^{n-\frac{1}{2}} * \left(\frac{\sigma_\xi}{8\sigma}\right)(q_j^n + q_{j-1}^n) + \frac{\xi^{n-\frac{1}{2}}}{8\mathrm{k}}[(q_j^n + q_{j-1}^n) + (q_j^{n-1} + q_{j-1}^{n-1})]$$

Coefficient of δg_{j-1}^{n}: $(s_{13})_j = +\xi\frac{\sigma_\xi}{2\sigma}(g_j^n + g_{j-1}^n) - \frac{\xi^{n-\frac{1}{2}}}{4\mathrm{k}}(g_j^n + g_{j-1}^n)$

Coefficient of δg_j^n: $(s_{14})_j = +\xi\frac{\sigma_\xi}{2\sigma}(g_j^n + g_{j-1}^n) - \frac{\xi^{n-\frac{1}{2}}}{4\mathrm{k}}(g_j^n + g_{j-1}^n)$

Coefficient of δv_{j-1}^{n}:

$$(s_{15})_j = \left(\frac{-1}{2d_1 h}\right) + \frac{1}{16}(f_j^n + f_{j-1}^n) + \xi^{n-\frac{1}{2}} * \left(\frac{\sigma_\xi}{8\sigma}\right)(f_j^n + f_{j-1}^n) + \frac{\xi^{n-\frac{1}{2}}}{8\mathrm{k}}[(f_j^n + f_{j-1}^n) + (f_j^{n-1} + f_{j-1}^{n-1})]$$

Coefficient of δv_j^n:

$$(s_{16})_j = \left(\frac{1}{2d_1 h}\right) + \frac{1}{16}(f_j^n + f_{j-1}^n) + \xi^{n-\frac{1}{2}} * \left(\frac{\sigma_\xi}{8\sigma}\right)(f_j^n + f_{j-1}^n) + \frac{\xi^{n-\frac{1}{2}}}{8\mathrm{k}}[(f_j^n + f_{j-1}^n) + (f_j^{n-1} + f_{j-1}^{n-1})]$$

Coefficient of energy equation

Coefficient of $\delta\theta_{j-1}^{n}$: $(s_{21})_j = -\frac{\xi^{n-\frac{1}{2}}}{8\mathrm{k}}[g_j^n + g_{j-1}^n + g_j^{n-1} + g_{j-1}^{n-1}]$

Coefficient of $\delta\theta_j^n$: $(s_{22})_j = -\frac{\xi^{n-\frac{1}{2}}}{8\mathrm{k}}[g_j^n + g_{j-1}^n + g_j^{n-1} + g_{j-1}^{n-1}]$

Coefficient of δp_{j-1}^{n}:

$$(s_{23})_j = \left(\frac{-1}{2Prh}\right) + \frac{1}{16}(f_j^n + f_{j-1}^n) + \xi^{n-\frac{1}{2}} * \left(\frac{\sigma_\xi}{8\sigma}\right)(f_j^n + f_{j-1}^n) + \frac{\xi^{n-\frac{1}{2}}}{8\mathrm{k}}[(f_j^n + f_{j-1}^n) - (f_j^{n-1} + f_{j-1}^{n-1})]$$

Coefficient of δp_j^n:

$$(s_{24})_j = \left(\frac{1}{2Prh}\right) + \frac{1}{16}\left(f_j^n + f_{j-1}^n\right) + \xi^{n-\frac{1}{2}} * \left(\frac{\sigma_\xi}{8\sigma}\right)\left(f_j^n + f_{j-1}^n\right) + \frac{\xi^{n-\frac{1}{2}}}{8\mathrm{k}}\left[\left(f_j^n + f_{j-1}^n\right) - \left(f_j^{n-1} + f_{j-1}^{n-1}\right)\right]$$

Non-homogeneous terms

$$(r_{11})_j = \left(f_{j-1}^n - f_j^n\right) + \frac{\mathrm{h}}{2}\left(g_j^n + g_{j-1}^n\right),$$

$$(r_{12})_j = r_{j-\frac{1}{2}}^{n-1} = -\left(\frac{1}{2d_1h}\right)\left[\left(q_j^n - q_{j-1}^n\right) + \left(q_j^{n-1} - q_{j-1}^{n-1}\right)\right] - \left(\frac{1}{16}\right)\left[\left(f_j^n + f_{j-1}^n\right)\left(q_j^n + q_{j-1}^n\right) + \left(f_j^{n-1} + f_{j-1}^{n-1}\right)\left(q_j^{n-1} + q_{j-1}^{n-1}\right)\right] + \xi * \left(\frac{\sigma_\xi}{8\sigma}\right)\left[\left[\left(f_j^n + f_{j-1}^n\right)\left(q_j^n + q_{j-1}^n\right) + \left(f_j^{n-1} + f_{j-1}^{n-1}\right)\left(q_j^{n-1} + q_{j-1}^{n-1}\right)\right] - \left(g_j^n + g_{j-1}^n\right)^2 + \left(g_j^{n-1} + g_{j-1}^{n-1}\right)^2\right] + \xi\left(\frac{1}{8k}\right)\left(\left[\left(g_j^n + g_{j-1}^n\right)^2 + \left(g_j^{n-1} + g_{j-1}^{n-1}\right)^2\right] + \left[\left(q_j^n - q_{j-1}^n\right) + \left(q_j^{n-1} - q_{j-1}^{n-1}\right)\right] * \left[\left(f_j^n + f_{j-1}^n\right) - \left(f_j^{n-1} + f_{j-1}^{n-1}\right)\right]\right),$$

$$(r_{13})_j = m_{j-\frac{1}{2}}^{n-1} = -\left(\frac{1}{2Prh}\right)\left[\left\{\left(p_j^n - p_{j-1}^n\right) + \left(p_j^{n-1} - p_{j-1}^{n-1}\right)\right] - \left(\frac{1}{16}\right)\left[\left(f_j^n + f_{j-1}^n\right) * \left(p_j^n + p_{j-1}^n\right) + \left(f_j^{n-1} + f_{j-1}^{n-1}\right) * \left(p_j^{n-1} + p_{j-1}^{n-1}\right)\right] - \xi * \left(\frac{\sigma_\xi}{8\sigma}\right)\left[\left(f_j^n + f_{j-1}^n\right) * \left(p_j^n + p_{j-1}^n\right) + \left(f_j^{n-1} + f_{j-1}^{n-1}\right) * \left(p_j^{n-1} + p_{j-1}^{n-1}\right)\right] + \xi\left(\frac{1}{8k}\right)\left(\left[\left\{\left(g_j^n + g_{j-1}^n\right) + \left(g_j^{n-1} + g_{j-1}^{n-1}\right)\right\} * \left\{\left(\theta_j^n + \theta_{j-1}^n\right) - \left(\theta_j^{n-1} + \theta_{j-1}^{n-1}\right)\right\}\right] - \left[\left\{\left(p_j^n + p_{j-1}^n\right) + \left(p_j^{n-1} + p_{j-1}^{n-1}\right)\right\} * \left\{\left(f_j^n + f_{j-1}^n\right) - \left(f_j^{n-1} + f_{j-1}^{n-1}\right)\right\}\right]\right).$$

The whole system can simply be written in matrix form, as

$$\bar{A}\bar{\delta} = \bar{r}, \tag{2.33}$$

where

$$\bar{A} = \begin{bmatrix} C_0 & D_0 & & & & & & \\ B_1 & C_1 & D_1 & & & & & \\ & B_2 & C_2 & D_2 & & & & \\ & & \ddots & \ddots & \ddots & & & \\ & & & \ddots & \ddots & \ddots & & \\ & & & & \ddots & \ddots & \ddots & \\ & & & & & B_{L-1} & C_{L-1} & D_{L-1} \\ & & & & & & B_L & C_L \end{bmatrix}, \bar{\delta} = \begin{bmatrix} \delta_0 \\ \delta_1 \\ \delta_2 \\ \vdots \\ \vdots \\ \vdots \\ \delta_{L-1} \\ \delta_L \end{bmatrix}, \bar{r} = \begin{bmatrix} r_0 \\ r_1 \\ r_2 \\ \vdots \\ \vdots \\ \vdots \\ r_{L-1} \\ r_L \end{bmatrix} \quad (2.34)$$

,

and

$$C_0 = \begin{bmatrix} 1 & & & & \\ 0 & 1 & & & \\ 0 & 0 & 0 & & \\ & -1 & -h/2 & 0 & \\ & & 0 & -1 & -h/2 \end{bmatrix}, D_l = \begin{bmatrix} 0 & & & & \\ 0 & 0 & & & \\ 0 & 0 & 0 & & \\ & 1 & -h/2 & 0 & \\ & & 0 & 1 & -h/2 \end{bmatrix};$$

$$l = 0,1,..L-1,$$

$$B_l = \begin{bmatrix} -1 & -h/2 & 0 & 0 & 0 \\ (s_{11})_l & (s_{13})_l & (s_{15})_l & 0 & 0 \\ 0 & 0 & 0 & (s_{21})_l & (s_{23})_l \\ & & & & \end{bmatrix}; \quad l = 1,2,...L,$$

$$C_l = \begin{bmatrix} 1 & -h/2 & 0 & & \\ (s_{12})_l & (s_{14})_l & (s_{16})_l & 0 & 0 \\ 0 & 0 & 0 & (s_{22})_l & (s_{24})_l \\ & -1 & -h/2 & 0 & 0 \\ & & & -1 & -h/2 \end{bmatrix}; \; l = 1,2,...L-1,$$

$$C_J = \begin{bmatrix} 1 & -h/2 & 0 & & \\ (s_{12})_l & (s_{14})_l & (s_{16})_l & 0 & \\ 0 & 0 & 0 & (s_{22})_l & (s_{24})_l \\ & 1 & 0 & 0 & 0 \\ & & 0 & 1 & 0 \end{bmatrix},$$

$$r_0 = \begin{bmatrix} 0 \\ 0 \\ 0 \\ (r_{14})_1 \\ (r_{15})_1 \end{bmatrix}, r_j = \begin{bmatrix} (r_{11})_l \\ (r_{12})_l \\ (r_{13})_l \\ (r_{14})_{l+1} \\ (r_{15})_{l+1} \end{bmatrix}, r_J = \begin{bmatrix} (r_{11})_L \\ (r_{12})_L \\ (r_{13})_L \\ 0 \\ 0 \end{bmatrix},$$

$$\delta_j = \begin{bmatrix} \delta f_l^n \\ \delta g_l^n \\ \delta q_l^n \\ \delta \theta_l^n \\ \delta p_l^n \end{bmatrix}; l = 0,1,2,...,L; n = 0,1,...,N.$$

After writing in matrix form, the block tri-diagonal procedure is implemented for the solution of the system.

For the purpose of authentication of the current numerical method, a comparison with the already existing results in literature is quite necessary. Hence, Table 2.1 is added to complete this task. We clearly see from the Table that our results of the skin-friction coefficient and the local Nusselt number are very close to the existing results reported in Refs. [18], [19] and [40]. This provides confidence in the present numerical scheme. We use the same procedure to solve Eqs. (2.10), (2.11) and (2.12) numerically in order to make the further analysis.

Table 2.1: Comparison of present results with already published data when $Pr = 0.7$ and $\alpha = 0$.

	Present	Rees and Pop [18]	Hossain and Pop [19]	Mehmood et al. [40]
$C_{fx}(\mathrm{Re}_x)^{1/2}$	−0.44375	−0.4438	−0.4439	−0.44375
Nu_x $(\mathrm{Re}_x)^{-1/2}$	−0.34924	−0.3492	−0.3509	−0.34924

2.4 Results and discussion

The numerical results are used to examine the entropy generation phenomenon in the flow with the help of graphs shown in Figs. 2.2-2.11. The entropy number is plotted against the variable ξ for different values of amplitude of surface oscillations. It is noticed that the entropy generation is high for small ξ and reduces gradually in the downstream direction. The reason behind this trend is the fact of less temperature and velocity gradients at the wall at downstream than at upstream. Moreover, it is also noted that the magnitude of oscillation in entropy number increases as the parameter α increases. Fig. 2.3 is sketched to see the behavior of entropy generation across the

boundary layer. It is seen from the figure that entropy number is higher near the wall and vanishes in the freestream flow region. To discriminate the entropy generation rates corresponding to the viscous and thermal dissipation the Bejan number is plotted in Figs. 2.4 and 2.5 against variables ξ and η, respectively. Fig. 2.4 demonstrates that the size of fluctuations in Be increases as one moves in downstream direction which indicates that the dominancy of irreversibility due to viscous or thermal dissipation also fluctuates. Fig. 2.5 shows that near wall irreversibility is dominated by heat transfer effects however far away from the wall is the region of fluid friction dominancy. Besides, the heat transfer and fluid friction irreversibility rates are equal near $\eta = 0.9$ (roughly).

Figures 2.6-2.9 unveil the behavior of entropy generation phenomenon for different values of group parameter ω. It is revealed from Figs. 2.6 and 2.7 that entropy number rises as ω increases. Such type of results are quite expected since an increase in ω gives rise to the viscous dissipation effects which causes the production of entropy. In addition, increasing amplitude of oscillation in entropy number profiles is noticed as ω increases. This is because of the strong frictional effects of the fluid particles which produce more fluctuations in the velocity gradient. Figs. 2.8 and 2.9 demonstrate that an increase in ω results in reduction of heat transfer irreversibility and an increase of fluid friction irreversibility is a consequence of it. It is further noticed that in the upstream region the discrimination between fluid friction and heat transfer irreversibilities is possible. However, in the downstream region the oscillations in the Bejan number profile amplify and thus the distinction of irreversibilities varies.

Figure 2.10 shows the effects of Prandtl number on the total entropy generation number. It is noticed that the entropy production rises in the flow as the Prandtl number increases. This shows that the entropy production in the fluids having large Prandtl

numbers is high. Fig. 2.11 depicts that the heat transfer irreversibility dominates in the fluids having large *Pr* values and fluid friction irreversibility dominates for small *Pr* values.

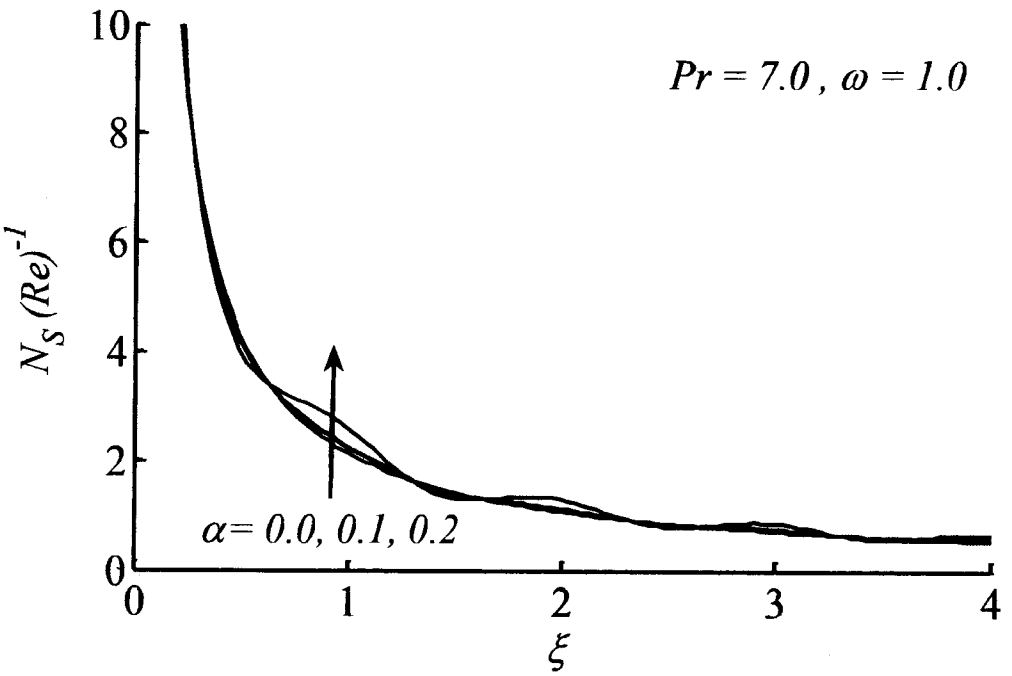

Fig. 2.2: N_s against ξ for different α.

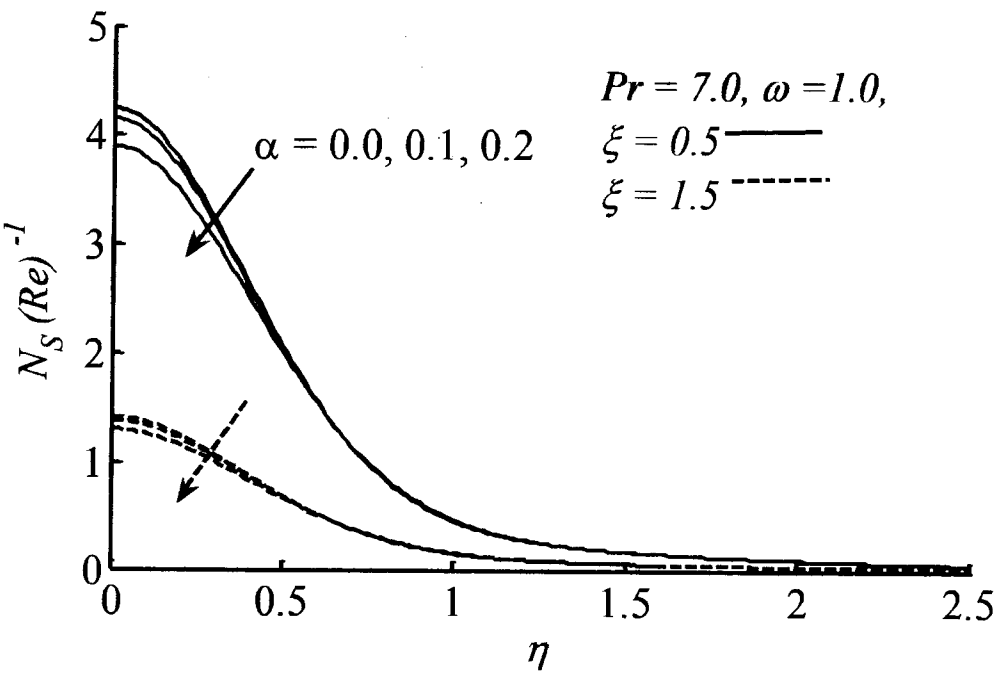

Fig. 2.3: N_s against η for different α.

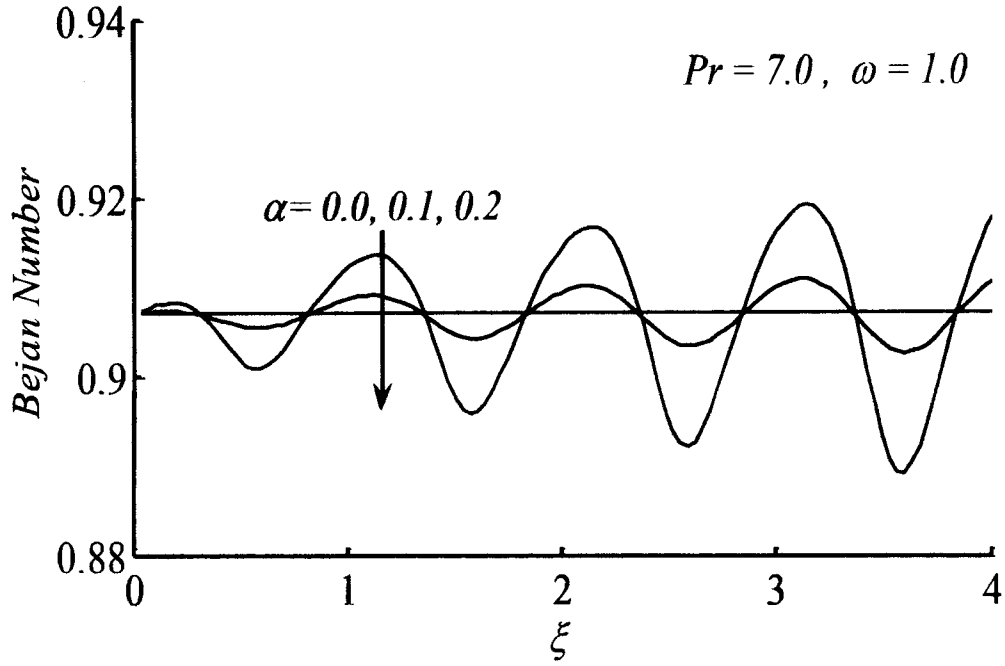

Fig. 2.4: Graph of the Bejan number for different value of α at $\eta = 0$.

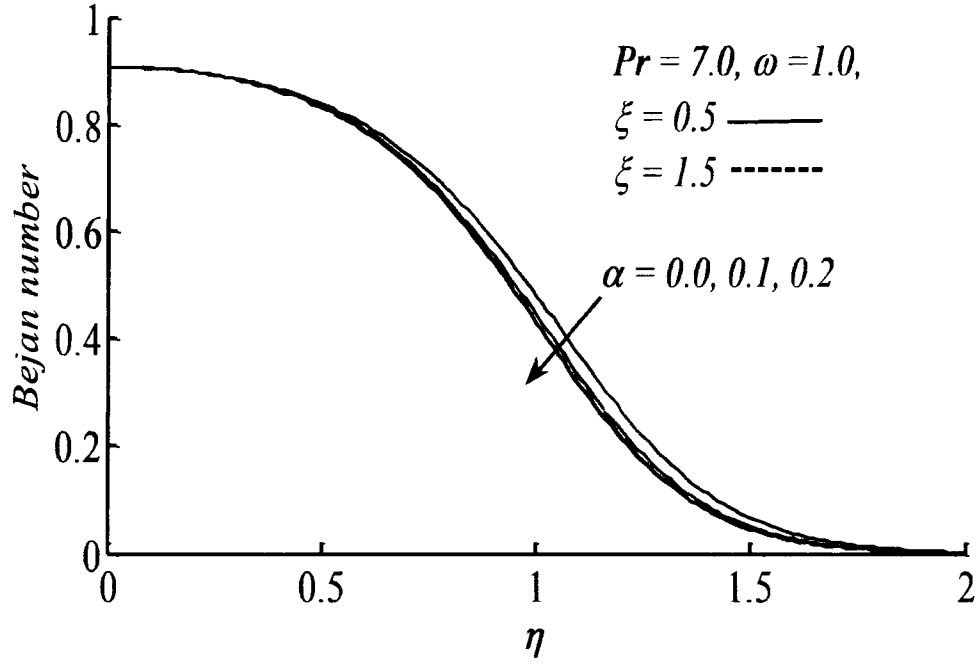

Fig. 2.5: Graph of the Bejan number for different α.

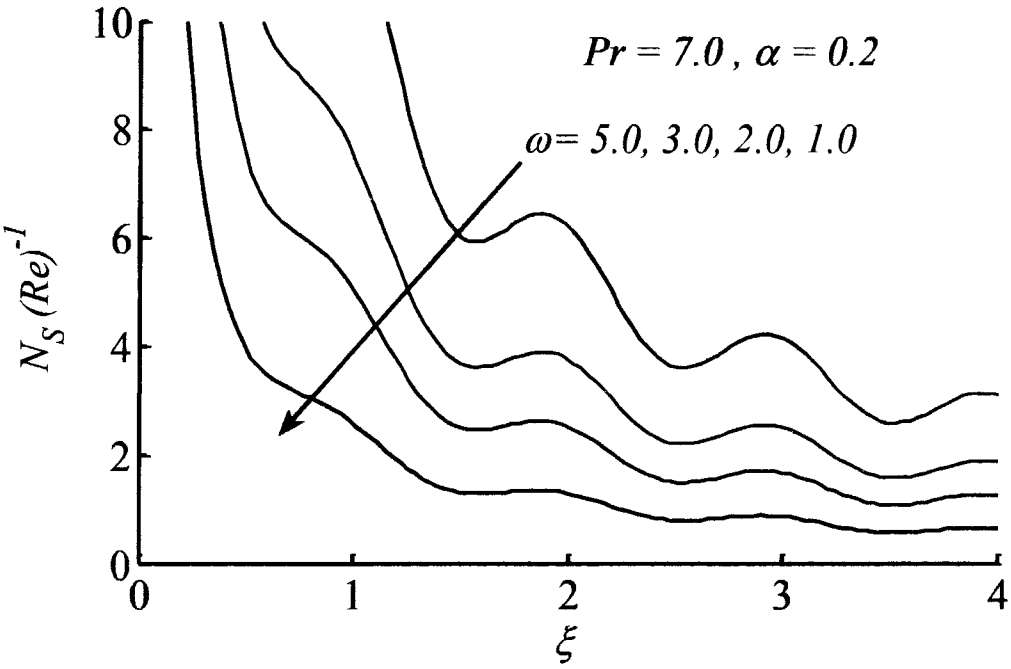

Fig. 2.6: Behavior of on N_s for different ω at $\eta = 0$.

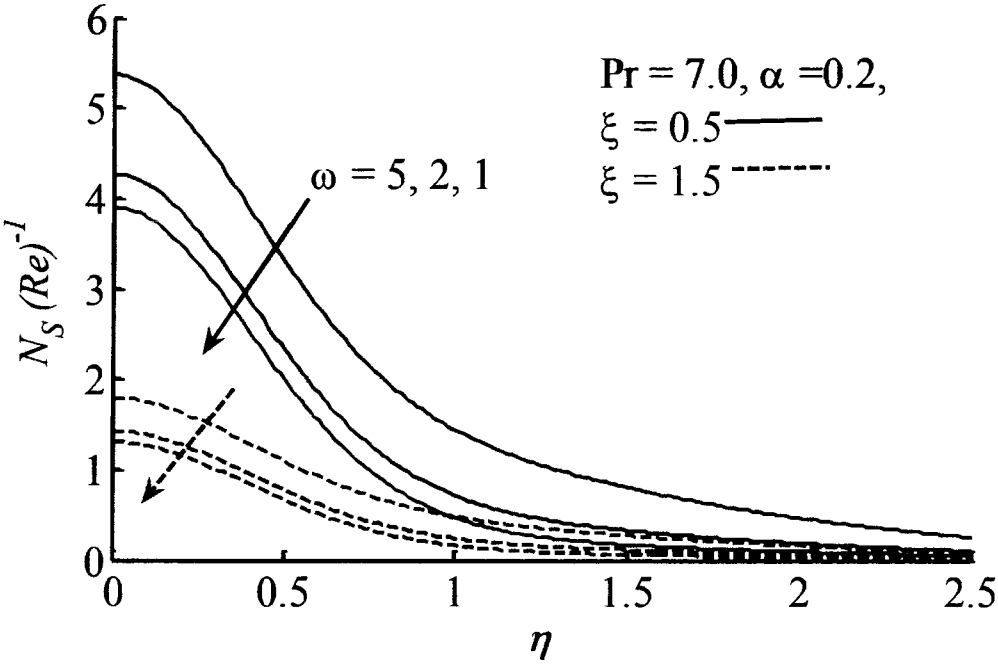

Fig. 2.7: Effect of varying ω on N_s when plotted against η.

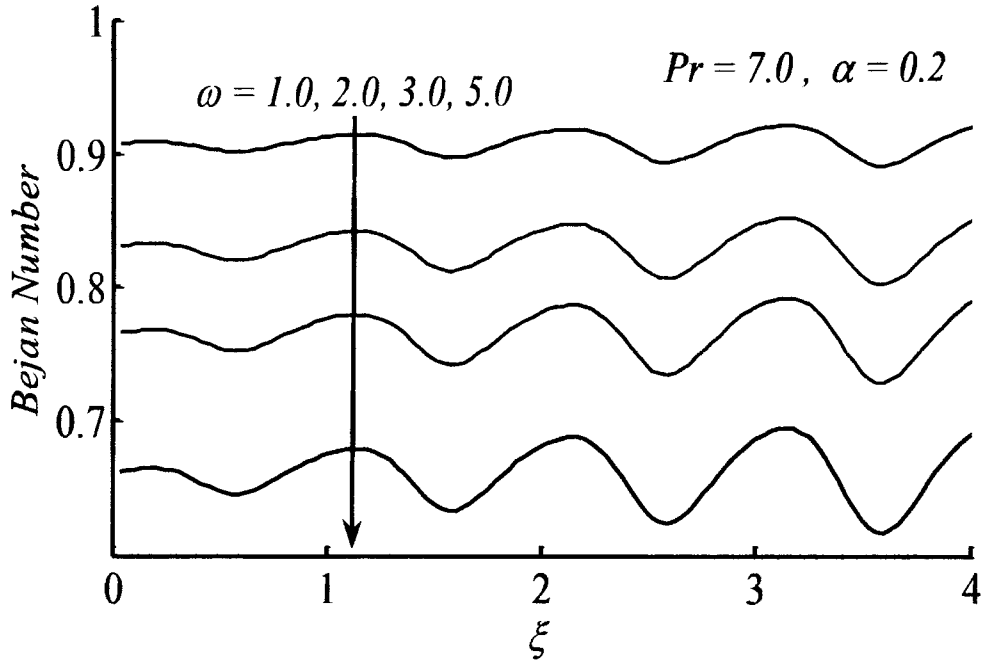

Fig. 2.8: Variation of the Bejan number for different ω at $\eta = 0$.

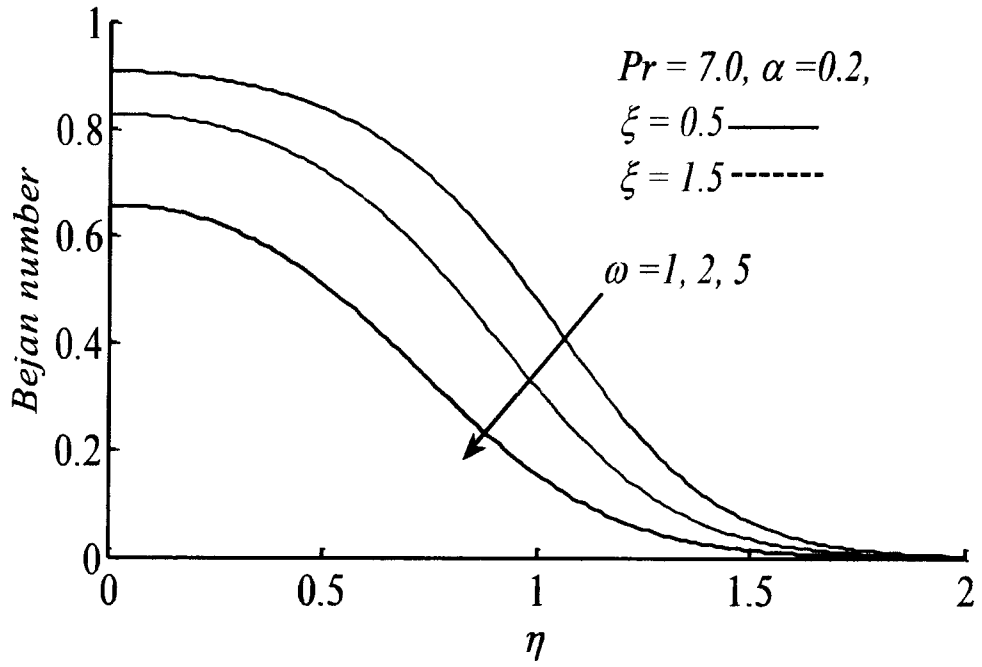

Fig. 2.9: Plot of Bejan number for different ω.

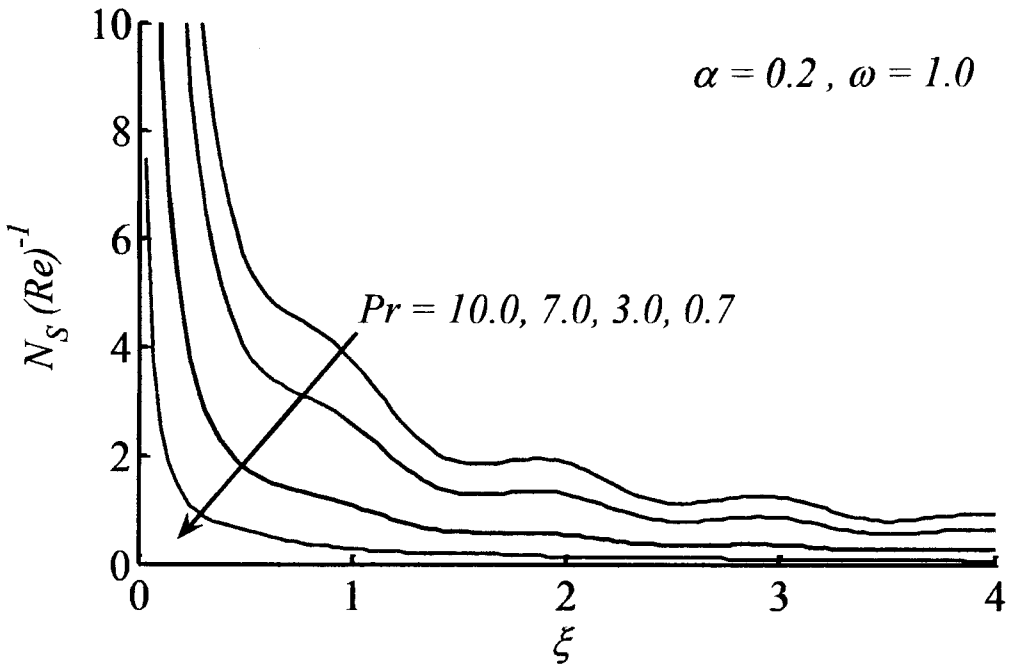

Fig. 2.10: N_s against ξ for different values of Pr at $\eta = 0$.

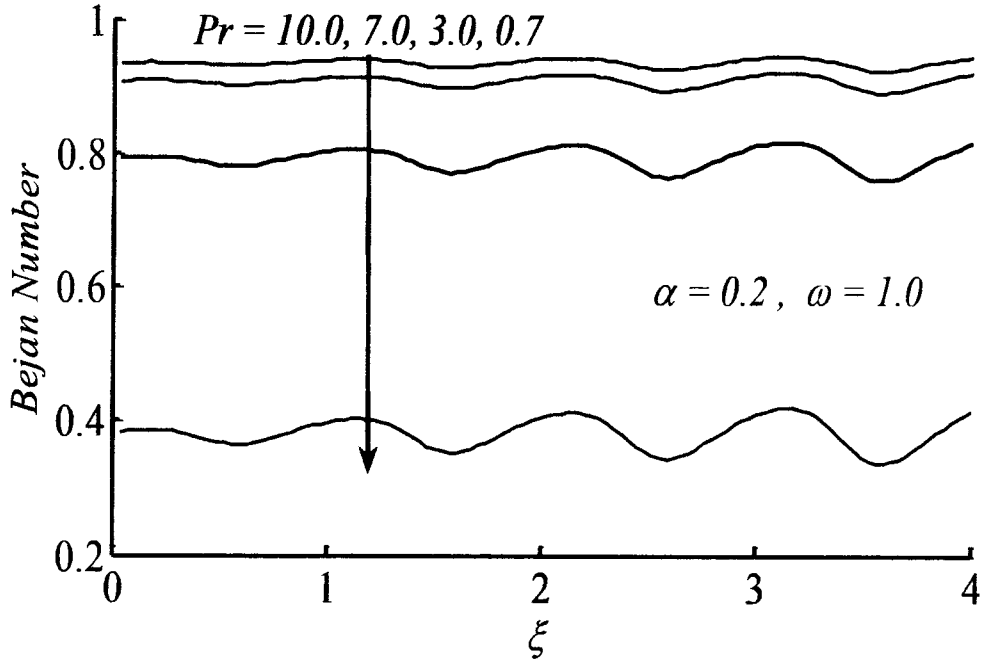

Fig. 2.11: Effects of Pr on the Bejan number at $\eta = 0$.

2.5 Concluding remarks

In this chapter, the second law of thermodynamics is investigated in a convective heat transfer over a continuous horizontally moving wavy surface. A numerical scheme is applied to calculate accurate velocity and temperature profiles. The numerical results are used to calculate the entropy generation. This study reveals that, the entropy generation is high in upstream region and low in the downstream region. In the upstream region, the involvement of heat transfer and viscosity in the entropy production is distinguishable due to less fluctuations. However, in the downstream region the fluctuations in the Bejan number are high due to which dominancy of heat transfer and fluid friction irreversibility varies. The present analysis will be helpful on further research on irreversibility minimization and entropy generation in energy convergence systems, heat exchangers, and thermal design.

Chapter 3

Impact of horizontal wavy surface on entropy generation in nanofluid: Tiwari and Das model

In this chapter we aim to investigate the combined effect of surface texture and nanoparticles upon entropy generation phenomenon in a viscous flow over a moving wavy surface. Due to high thermal conductivity of the nanoparticles, nanofluid is very much beneficial in the thermal transport mechanism. In the present investigation Tiwari and Das model has been used and the mixing of nanoparticles Cu and Fe_3O_4 in the regular fluid are considered. Impact of these nanoparticles upon entropy production has been reported. Results reveal that Fe_3O_4 base nanofluid is quite beneficial to reduce the production of entropy as compared to Cu base nanofluid.

3.1 Problem formulation

3.1.1 Nanofluid: thermo-physical properties

In the literature, several theoretical and experimental models are available for describing the homogenous (single-phase) and non-homogenous (two-phase) nanofluids. To model a single-phase nanofluid, two important models namely the Tiwari and Das [25] and Buongiorno [26] models are available in literature to discuss the convective transport phenomenon of nanofluid. The model by Tiwari and Das, discusses the effective properties of the nanoparticles whereas the Brownian motion and thermophoresis are considered in Boungiorno model. Therefore, to capture the contribution of nanoparticles by considering the material properties of the particles in the thermal analysis, the model of Tiwari and Das is utilized. Because of the existence

of these particles in the pure fluid, the material properties of mixture such as effective dynamic viscosity, density, effective thermal conductivity, and heat capacity are altered. Different models have been utilized by the scientists for the effective dynamic viscosity. The model of viscosity for nanoparticles (spherical shaped) as a function of volume fraction was proposed by Einstein [140-142] which is limited to 2 % volume fraction only. Later on, Brinkman [143] determined a new relation for viscosity by considering the volume fraction up to 4% in the form

$$\mu_{nf} = \frac{\mu_f}{(1-\phi)^{2.5}}. \tag{3.1}$$

Brinkman model is suitable for the current analysis due to moderate range of volume fraction and easy for mathematical handling. Under the rule of mixture, the effective density of nanofluid has been modelled as

$$\rho_{nf} = (1-\phi)\rho_f + \phi\rho_p, \tag{3.2}$$

which has good agreement with experimental data. The thermal heat capacity is defined as the amount of heat required to increase the temperature up to 1 Kelvin of substance having 1 Kg mass. It depends upon simple mixing theory of nanofluid and is written as

$$(\rho c_p)_{nf} = (1-\phi)(\rho c_p)_f + \phi(\rho c_p)_p. \tag{3.3}$$

Thermal conductivity of the mixture of liquid and solid was first introduced by Maxwell [135] in 1873. He recognized that the addition of solid particles in liquid enhances the thermal conductivity of mixture and proposed the following relation

$$\frac{\kappa_{nf}}{\kappa_f} = \frac{(\kappa_p + 2\kappa_f) - 2\phi(\kappa_f - \kappa_p)}{(\kappa_p + 2\kappa_f) + \phi(\kappa_f - \kappa_p)}. \tag{3.4}$$

Also, Maxwell proposed the concept of thermal diffusivity of nanofluid which is the ratio of thermal conductivity and heat capacity of nanofluid. In heat transport phenomenon of nanofluid it is given as

$$\alpha_{nf}^{*} = \frac{\kappa_{nf}}{(\rho c_p)_{nf}}. \tag{3.5}$$

3.1.2 Mathematical model

Consider a steady flow due to a horizontal wavy sheet moving uniformly in $\bar{x}$-direction. The flow is two-dimensional in nature whose velocity varies continuously with the variable '$\bar{x}$' which makes the flow non-similar. The wavy surface is assumed to be surrounded by the ambient nanofluid. The surface shape is described by the function which is given in Eq. (1.13) and shown along with the coordinate system in Fig. 3.1. The surface is held at a constant temperature T_w and the ambient temperature is T_∞ such that $T_w > T_\infty$.

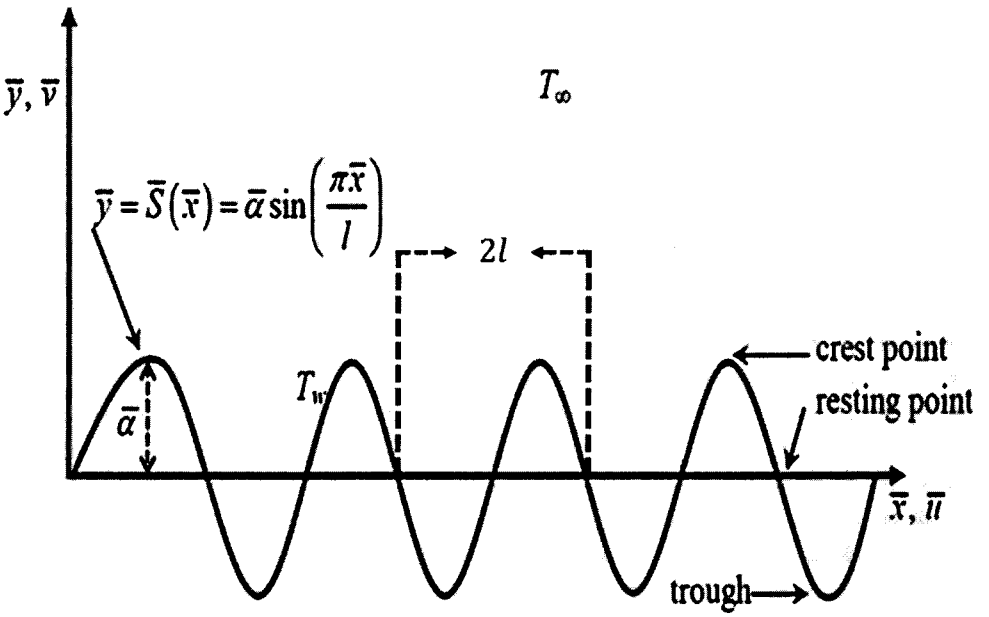

Figure 3.1: Schematic diagram with coordinate system.

According to this model the mass, momentum, and energy conservation laws in component form are described as

$$\frac{\partial \bar{u}}{\partial \bar{x}} + \frac{\partial \bar{v}}{\partial \bar{y}} = 0, \tag{3.6}$$

$$\bar{u}\frac{\partial \bar{u}}{\partial \bar{x}} + \bar{v}\frac{\partial \bar{u}}{\partial \bar{y}} = -\frac{1}{\rho_{nf}}\frac{\partial \bar{p}}{\partial \bar{x}} + \nu_{nf}\nabla^2\bar{u}, \tag{3.7}$$

$$\bar{u}\frac{\partial \bar{v}}{\partial \bar{x}} + \bar{v}\frac{\partial \bar{v}}{\partial \bar{y}} = -\frac{1}{\rho_{nf}}\frac{\partial \bar{p}}{\partial \bar{y}} + \nu_{nf}\nabla^2\bar{v}, \tag{3.8}$$

$$\bar{u}\frac{\partial T}{\partial \bar{x}} + \bar{v}\frac{\partial T}{\partial \bar{y}} = \alpha^*_{nf}\nabla^2 T, \tag{3.9}$$

where ρ_{nf}, $\alpha^*_{nf,}$ and ν_{nf} represents the density, thermal diffusivity, and kinematic viscosity of the nanofluid. The corresponding boundary conditions for the moving wavy surface are listed in Eqs. (2.5a) & (2.5b). For the dimensionless form of the governing system and the boundary condition, use is made of the dimensionless quantities given in Eq. (2.6) and (2.9). Thus, the non-similar governing equations are therefore written as [for detail derivation see ref [42]].

$$\frac{1}{d_1}f''' + \frac{1}{2}ff'' - \xi\frac{\sigma_\xi}{\sigma}(ff'' - f'^2) = \xi\left[f'\frac{\partial f'}{\partial \xi} - f''\frac{\partial f}{\partial \xi}\right], \tag{3.10}$$

$$\frac{d}{d_2 Pr}\theta'' + \frac{1}{2}f\theta' + \xi\frac{\sigma_\xi}{\sigma}f\theta' = \xi\left[f'\frac{\partial \theta}{\partial \xi} - \theta'\frac{\partial f}{\partial \xi}\right]. \tag{3.11}$$

The material parameters d, d_1, and d_2 are given by

$$\left.\begin{aligned} d = \frac{\kappa_{nf}}{\kappa_f}, d_1 = \frac{1}{(1-\phi)^{-2.5}}\left[1 - \phi + \phi\left(\frac{\rho_p}{\rho_f}\right)\right], \\ d_2 = \left[1 - \phi + \phi\left(\frac{(\rho c_p)_p}{(\rho c_p)_f}\right)\right], \end{aligned}\right\} \tag{3.12}$$

where ϕ denotes the concentration of nanoparticle, ρ, c_p, and k denote the density, heat capacity and thermal conductivity of the fluid, respectively. The subscripts 'p', 'f', and 'nf' mention the nanoparticle, base fluid, and the nanofluid, respectively. The boundary data in non-dimensional form is written as

$$\left.\begin{aligned} f(\xi,0) = 0,\ f'(\xi,0) = \frac{1}{\sigma},\ \theta(\xi,0) = 1, \\ f'(\xi,\infty) = 0,\ \theta(\xi,\infty) = 0. \end{aligned}\right\} \tag{3.13}$$

The skin-friction at the wall and the Nusselt number are

$$C_{fx} = \frac{\tau_w}{\rho_f U^2},\ Nu_x = \frac{\bar{x}q_w}{\kappa_f(T_w - T_\infty)}, \tag{3.14}$$

where τ_w and q_w are the shear stress and heat flux at the wall, respectively and are obtained as

$$\tau_w = \mu_{nf}(\nabla\bar{u}\cdot\hat{n})_{y=0},\ q_w = -\kappa_{nf}(\nabla T\cdot\hat{n})_{y=0}. \tag{3.15}$$

In above equations, $\hat{n} = (n_x, n_y) = (-\sigma_\xi/\sigma, 1/\sigma)$ indicates unit normal vector on the sinusoidal boundary. Using Eqs. (2.6), (2.9) and (3.15) in Eqs. (3.14) the required skin-friction coefficient at the wall and the Nusselt number have the following form:

$$\begin{aligned} C_{fx}Re^{\frac{1}{2}} &= \frac{x^{-\frac{3}{2}}}{\sigma^{\frac{3}{2}}(1-\phi)^{2.5}} f''(\xi,0), \\ Nu_xRe^{-\frac{1}{2}} &= -\frac{\sqrt{x}}{\sqrt{\sigma}}\frac{\kappa_{nf}}{\kappa_f}\theta'(\xi,0). \end{aligned} \tag{3.16}$$

3.2 Entropy analysis

On the basis of second law of thermodynamics the local entropy generation for nanofluid in rectangular coordinate system can be written as

$$\begin{aligned} S_G = \frac{\kappa_{nf}}{T_\infty^2}\left[\left(\frac{\partial T}{\partial\bar{x}}\right)^2 + \left(\frac{\partial T}{\partial\bar{y}}\right)^2\right] \\ + \frac{\mu_{nf}}{T_\infty}\left[2\left[\left(\frac{\partial\bar{u}}{\partial\bar{x}}\right)^2 + \left(\frac{\partial\bar{v}}{\partial\bar{y}}\right)^2\right] + \left(\frac{\partial\bar{u}}{\partial\bar{y}} + \frac{\partial\bar{v}}{\partial\bar{x}}\right)^2\right], \end{aligned} \tag{3.17}$$

where the thermal conductivity (k_{nf}) and the viscosity (μ_{nf}) of nanofluid are two major causes of irreversibility. The first term represents the irreversibility due to heat transfer while the second term describes the fluid friction irreversibility. Entropy generation number is defined by Bejan [1], which is the ratio of volumetric entropy generation to the characteristic entropy generation rate. Using the set of dimensional variables listed in Eqs. (2.6) & (2.9) the entropy generation number is described by the following equation:

$$\frac{N_S}{Re} = \frac{S_G}{S_{G_0}} = \frac{d}{\xi}\theta'^2 + \frac{d_1\omega\sigma^2}{\xi}f''^2 = N_H^* + N_F^*, \tag{3.18}$$

where d and d_1 are material parameters defined in Eq. (3.12), $Br = \mu_f U_w^2/k_f(T_w - T_\infty)$ is the Brinkman number, and $S_{G_0} = k_f(\Omega_T/l)^2$ is the characteristic entropy. In Eq. (3.18) N_H^* and N_F^* denote the entropy generation due to heat transfer and fluid friction, respectively. The Bejan number Be for the current problem is given by

$$Be = \frac{d\theta'^2}{d\theta'^2 + d_1\omega\sigma^2 f''^2}. \tag{3.19}$$

3.3 Results and discussion

The governing nonlinear system (3.10) and (3.11) along with boundary data (3.13) is solve numerically with the aid of Keller-Box method. The scheme of solution has already been illustrated through previous chapter. We use the solution to make the further entropy analysis by inspecting the influence of physical quantities upon entropy production with the help of graphs shown in Figs. 3.2-3.12. In Fig. 3.2 entropy number is plotted against the variable ξ for variation in parameter α. Profiles indicate that, high entropy production is noted in the upstream region and low in the downstream region. The reason behind this behavior of irreversibility is that the temperature and velocity gradients are high at upstream location. A careful look on the figure reveals that the entropy generation decreases at the resting points as the aspect ratio α increases. However, it increases at the crest and trough points of wavy surface. The Bejan number is plotted in Fig. 3.3 to see the discriminating features of heat transfer and fluid friction irreversibilities against the variable ξ in presence of Cu and Fe_3O_4-water nanoparticles. From the figure it is observed that overall heat transfer irreversibility dominates over fluid friction irreversibility at all resting points and irreversibility due to fluid friction augments at the crest/trough points of the surface. However, for nanofluid based on

Fe_3O_4 nanoparticles the Bejan number is higher as compare to Cu-water base nanofluid. This indicates that Fe_3O_4-water based nanofluids are highly efficient in producing the heat transfer irreversibility and thus good for heat transfer augmentation problems. Moreover, the amplitude of oscillations in the Bejan number is high for the case of Cu-water base nanofluid in downstream which indicates that it is less efficient for the heat transfer augmentation process.

Figure 3.4 indicates that the entropy number augments as group parameter ω increases because of fluid friction enhancement. Moreover, oscillation in the entropy number due to presence of Cu-water based nanofluid is higher than Fe_3O_4-water based nanofluid as ω increases. Fig. 3.5 illustrates that the Bejan number reduces as the group parameter ω increases which indicates the dominancy of fluid friction irreversibility for both types of nanofluids. The graph of the Bejan number shown in Fig. 3.6 indicates that fluid friction irreversibility increases as the volume concentration of nanoparticles increases. This happened because the increasing volume concentration causes an increase in the viscosity of the nanofluid which consequently leads to increase the friction factor.

Figures 3.7-3.12 show the graphs of the entropy number and the Bejan number against the variable η. Fig. 3.7 demonstrates that the entropy decreases as the aspect ratio α increases for both types of nanoparticles. Moreover, the entropy is high near the wall and dies out when one moves away from the surface. However, the entropy generation due to transfer of heat is dominant near the wall and irreversibility due to fluid friction is dominant in free stream region (see Fig. 3.8). Fig. 3.9 demonstrates that the total entropy generation number increases as the group parameter increases. Fig. 3.10 shows that with increasing value of group parameter ω, the Bejan number decreases due to dominancy of fluid friction irreversibility. However, Fe_3O_4 nanoparticles display ability to persist heat transfer effect. Fig. 3.11 reveals that the entropy generation number N_s

increases as ϕ increases. This is because viscous effects due to the nanoparticles concentration increase and consequently enhance the overall irreversibility. From Fig. 3.12 it is noted that as the value of ϕ increases the Bejan number reduces near the surface showing the strengthening of fluid friction irreversibility however an inverse behavior is seen in the main stream where heat transfer effects become stronger.

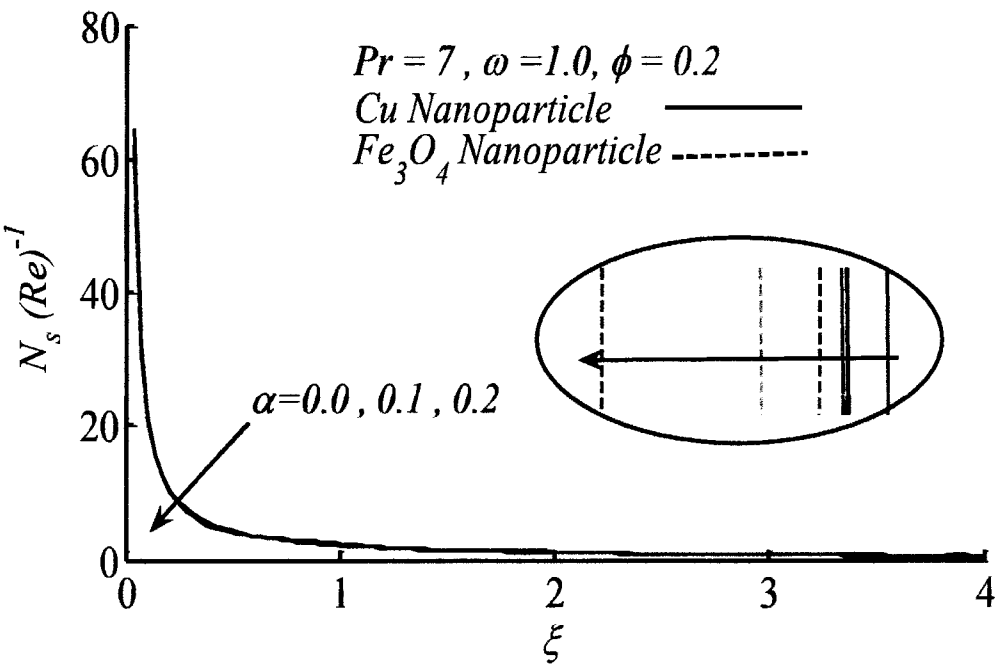

Fig. 3.2: Entropy number N_s for different α.

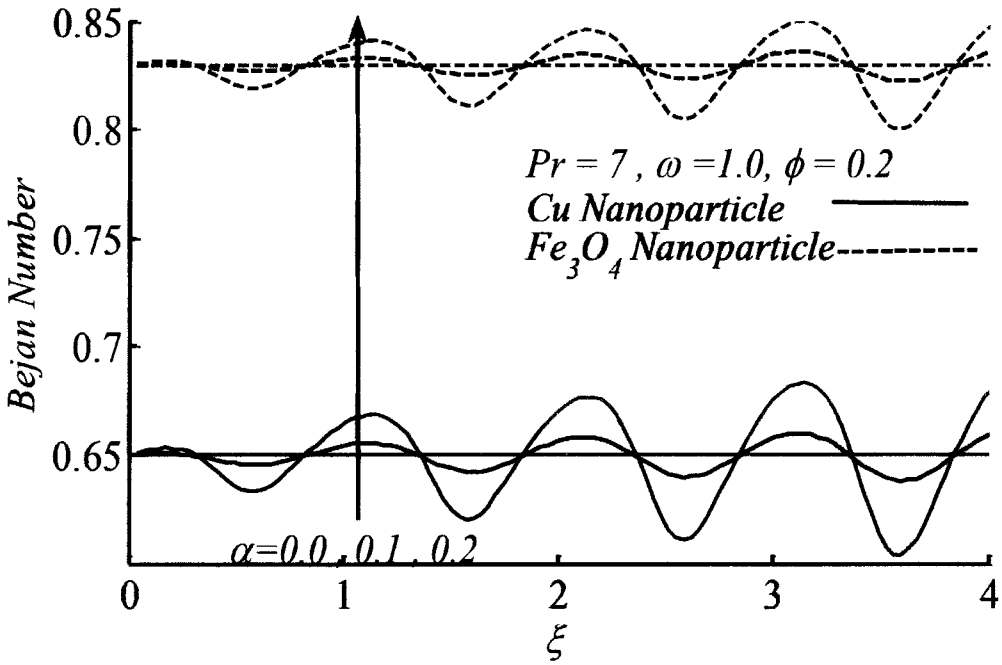

Fig. 3.3: Bejan number for different α.

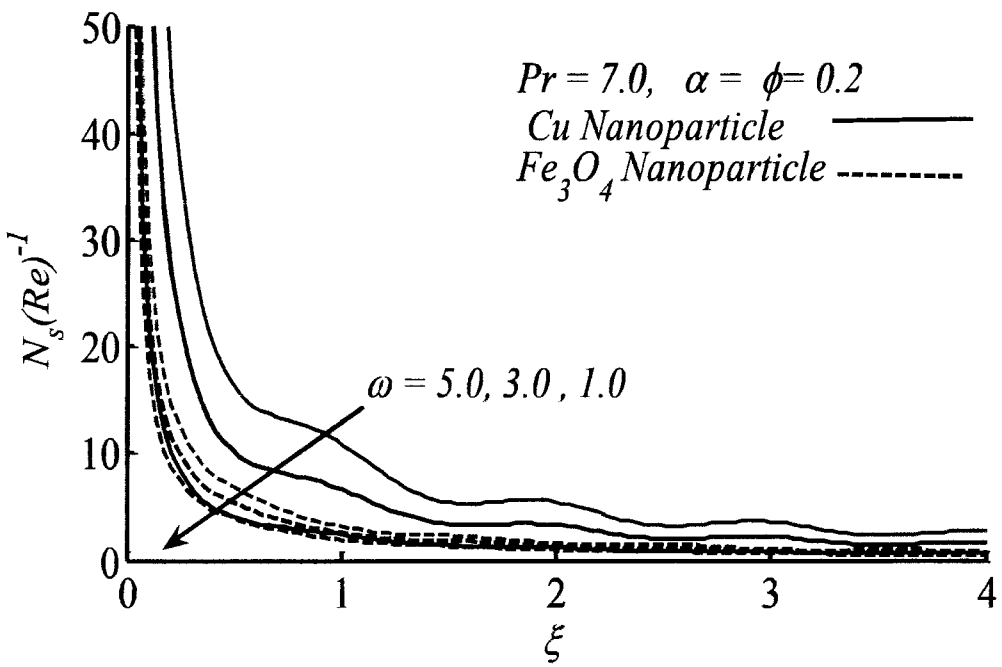

Fig. 3.4: Entropy number N_s for different ω.

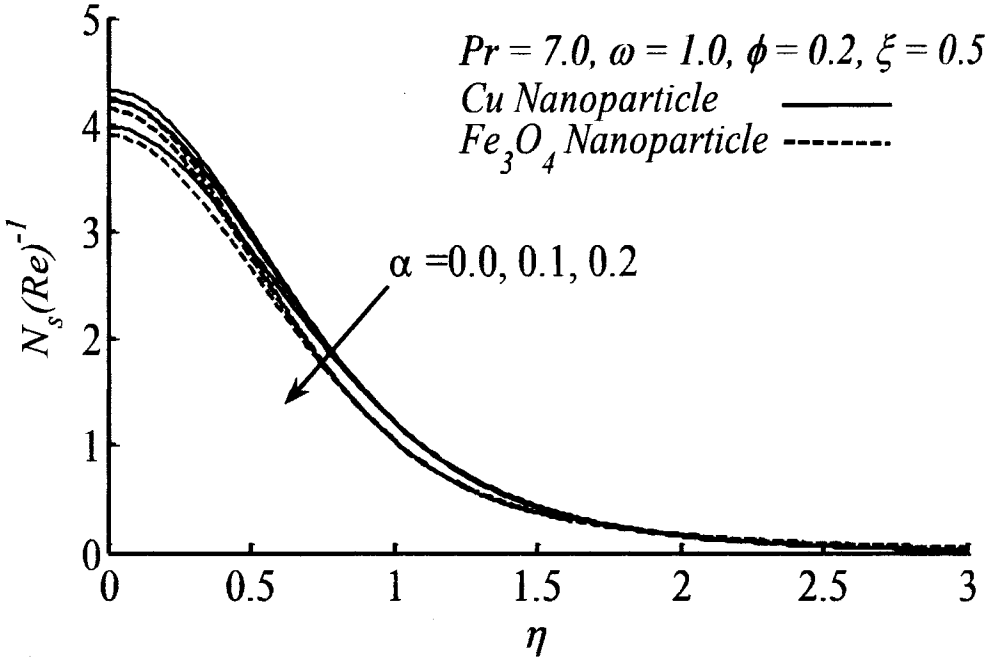

Fig. 3.7: Entropy number N_s for different α.

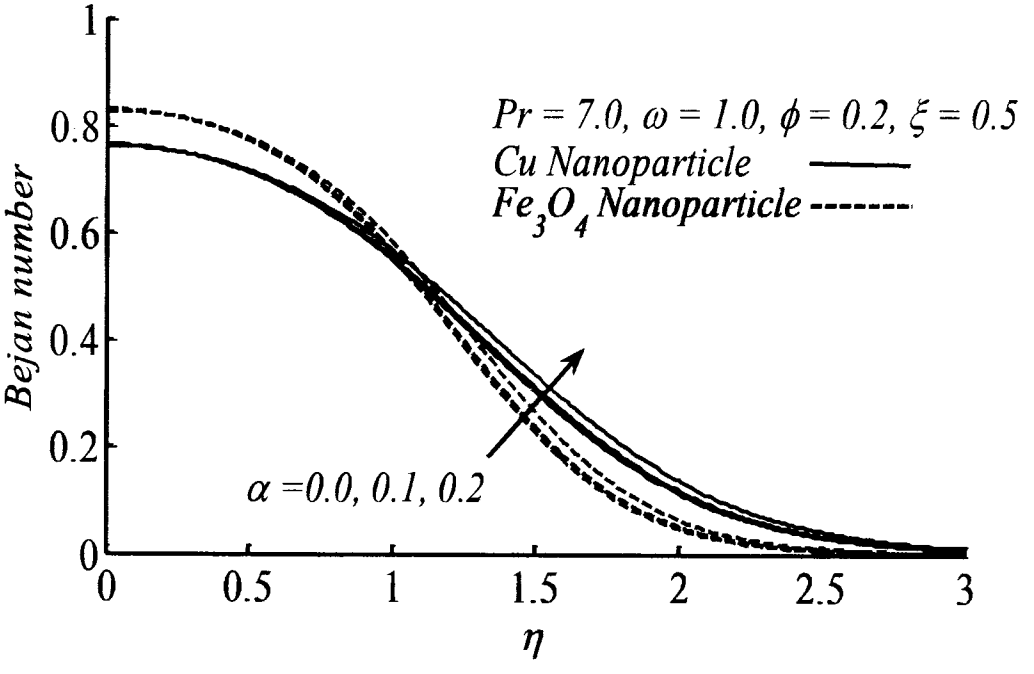

Fig. 3.8: Bejan number for different α.

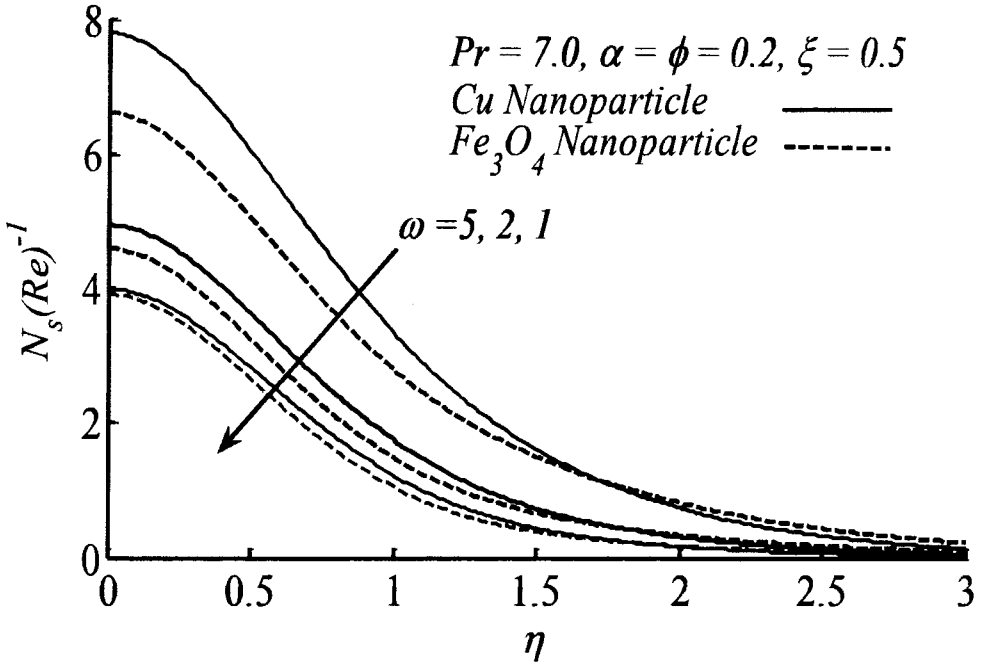

Fig. 3.9: Entropy number N_s for different ω.

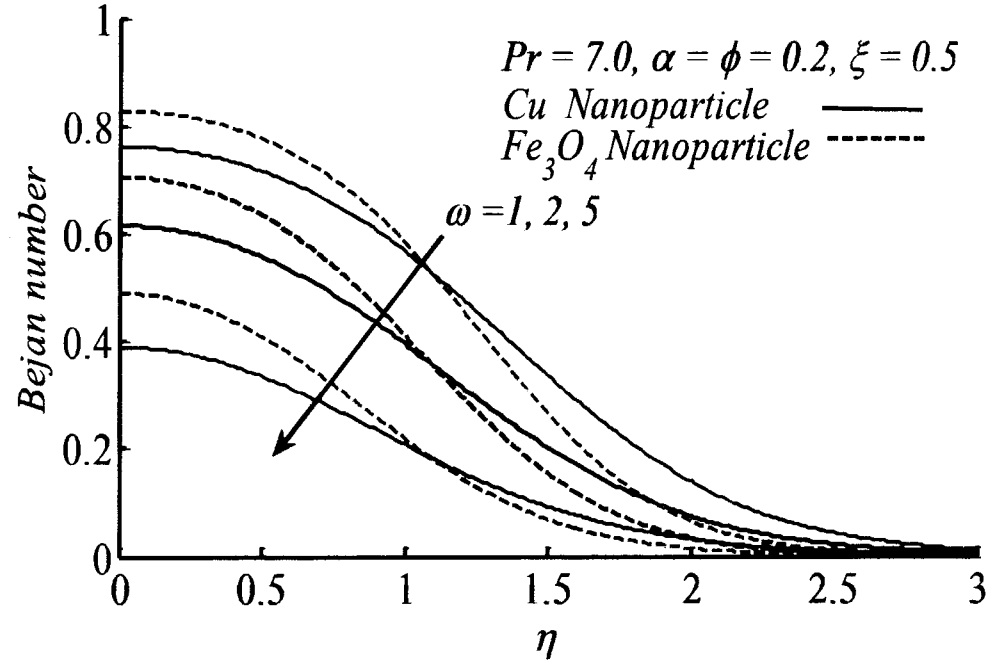

Fig. 3.10: Bejan number for different ω.

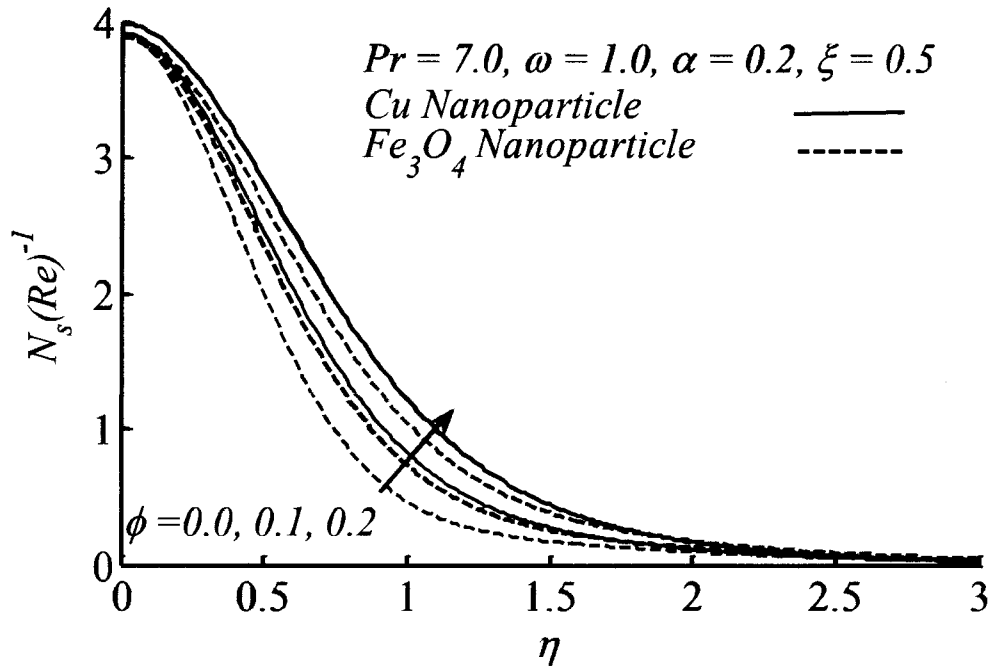

Fig. 3.11: Entropy number N_s for different ϕ.

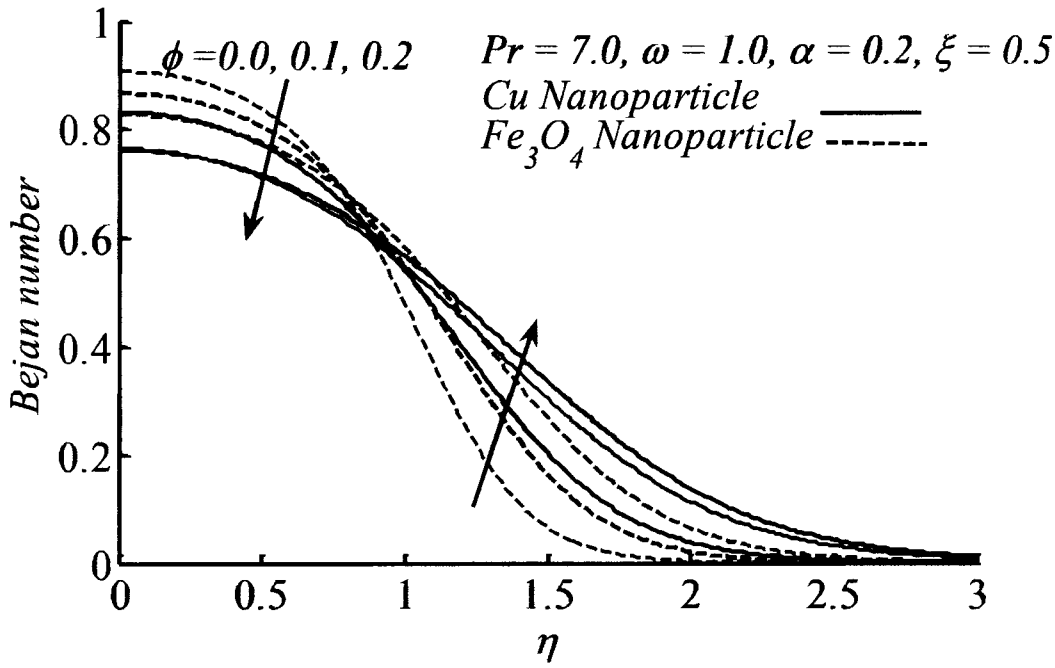

Fig. 3.12: Bejan number for different ϕ.

3.4 Final remarks

In the current chapter, entropy production under the combined effects of surface texture and nanofluid over a continuously moving wavy surface is studied. Numerical results are obtained for non-similar flow and heat transfer equations via Keller Box scheme. The numerical results are plotted in different graphs to see the effect of surface texture and nanofluid on the entropy phenomenon. The findings are as under:

- The total entropy generation reduces and rises at the resting points and crest/trough points of the surface, respectively, as the magnitude of oscillations increases.

- Nanofluid based on Fe_3O_4 nanoparticles reduces entropy more efficiently as compared to the nanofluid based on Cu nanoparticles. Since Fe_3O_4-water based nanofluid is more capable of producing heat transfer irreversibility and thus good for heat transfer augmentation problems.

- The volume concentration of nanoparticles should be kept under a certain range since it leads to increase the fluid friction irreversibility and thus results in increasing the total entropy of the system.

- Graphical results show that the entropy generation by the transfer of heat is dominant close to the boundary and fluid friction irreversibility is dominant in distant region.

- Enhancement of group parameter leads to decrease the Bejan number rapidly in case of Cu nanoparticles as compared to the nanoparticles of Fe_3O_4.

Chapter 4

Entropy analysis due to a moving isothermal wavy surface in nanofluid using Buongiorno model

Irreversibility phenomenon due to the existence of nanoparticles in the base fluid for viscous flow caused by the uniform motion of the wavy plate is the objective of this chapter. The utilized model for the presentation of nanofluid is the Buongiorno model in which the Brownian motion and thermophoresis effects are considered. The non-flat surface texture of the wavy plate does not allow the similarity solution to exist. Due to which the problem is non-similar in nature. Impact of various controlling parameters upon Bejan number and entropy production number are examined. It is found that entropy production decreases in the vicinity of the plate due to thermophoresis parameter.

4.1 Problem formulation

We consider the flow of viscous incompressible nanofluid over a wavy plate which is moving uniformly in $\bar{x}$-direction. The constant surface-temperature of the wavy plate is represented by T_w while T_∞ represents the fluid temperature outside the boundary layer. Additionally, the fluid temperature T_∞ is smaller than the temperature T_w of the surface. The differentiable sinusoidal function shown in Eq. (1.13) describes the texture of the sinusoidal surface. The wavy plate is assumed to be situated horizontally where the $\bar{x}$-coordinate coincides with the mean location of the wavy surface while the $\bar{y}$-axis runs normal to it, as given in Fig. 2.1. In view of the coordinate system $(\bar{x}, \bar{y})$ the

governing equations of the two-dimensional nanofluid flow under the foregoing assumptions, can be written as suggested by Buongiorno [26]:

$$\frac{\partial \bar{u}}{\partial \bar{x}} + \frac{\partial \bar{v}}{\partial \bar{y}} = 0, \tag{4.1}$$

$$\bar{u}\frac{\partial \bar{u}}{\partial \bar{x}} + \bar{v}\frac{\partial \bar{u}}{\partial \bar{y}} = -\frac{1}{\rho}\frac{\partial \bar{p}}{\partial \bar{x}} + \nu\nabla^2\bar{u}, \tag{4.2}$$

$$\bar{u}\frac{\partial \bar{v}}{\partial \bar{x}} + \bar{v}\frac{\partial \bar{v}}{\partial \bar{y}} = -\frac{1}{\rho}\frac{\partial \bar{p}}{\partial \bar{y}} + \nu\nabla^2\bar{v}, \tag{4.3}$$

$$\bar{u}\frac{\partial T}{\partial \bar{x}} + \bar{v}\frac{\partial T}{\partial \bar{y}} = \alpha^*\nabla^2 T + \tau^*\left[D_B(\nabla T.\nabla C) + \frac{D_T}{T_\infty}(\nabla T.\nabla T)\right], \tag{4.4}$$

$$\bar{u}\frac{\partial C}{\partial \bar{x}} + \bar{v}\frac{\partial C}{\partial \bar{y}} = D_B\nabla^2 C + \frac{D_T}{T_\infty}\nabla^2 T, \tag{4.5}$$

where D_B and D_T designate the Brownian and thermophoresis parameters, respectively. The associated boundary conditions can be expressed as (see [40])

$$\begin{gathered}\bar{y} = \bar{S}(\bar{x}):\ \bar{u}\bar{t}_{\bar{y}} - \bar{v}\bar{t}_{\bar{x}} = 0, \bar{u}\bar{t}_{\bar{y}} + \bar{v}\bar{t}_{\bar{x}} = U, T = T_w, C = C_w \text{ for all } \bar{x} > 0,\\ \bar{y} \to \infty:\ \bar{u} = \bar{v} = 0, \bar{p} = p_\infty, T = T_\infty, C = C_\infty \quad \text{for all } \bar{x} > 0,\\ \bar{x} = 0:\ \bar{p} = p_\infty, T = T_\infty \text{ , for all } \bar{y} \neq 0\,.\end{gathered} \tag{4.6}$$

We now set up the following suitable transformations to convert the above system of non-linear PDE's into an equivalent non-dimensional form:

$$\begin{gathered}\xi = x = \frac{\bar{x}}{l}, y = \frac{\bar{y}}{l}, u = \frac{\bar{u}}{U}, \alpha = \frac{\bar{\alpha}}{l}, S = \frac{\bar{S}(\bar{x})}{l}, v = \frac{\sqrt{Re}}{U}(\bar{v} - S_\xi\bar{u}),\\ p = \frac{\bar{p}}{\rho U^2}, \theta(\xi,\eta) = \frac{T-T_\infty}{T_w-T_\infty}, \varphi(\xi,\eta) = \frac{C-C_\infty}{C_w-C_\infty}, \psi(\xi,\eta) = \sqrt{\xi}f(\xi,\eta),\\ \eta = \frac{(\bar{y} - \bar{S}(\bar{x}))\sqrt{Re}}{l\sigma\sqrt{\xi}}y, u = \frac{\partial\psi}{\partial x}, v = -\frac{\partial\psi}{\partial y}, Re = \frac{Ul}{\nu}, \tau^* = \frac{(\rho c)_p}{(\rho c)_f}.\end{gathered} \tag{4.7}$$

Using the transformations described in Eq. (4.7) the system of equations (4.2)-(4.5) in dimensionless form reads as

$$f''' + \frac{1}{2}ff'' + \xi\frac{\sigma_\xi}{\sigma}(ff'' - f'^2) = \xi\left[f'\frac{\partial f'}{\partial \xi} - f''\frac{\partial f}{\partial \xi}\right], \tag{4.8}$$

$$\frac{1}{Pr}\theta'' + \frac{1}{2}f\theta' + \xi\frac{\sigma_\xi}{\sigma}f\theta' + (N_b\theta'\varphi' + N_t\theta'^2) = \xi\left[f'\frac{\partial \theta}{\partial \xi} - \theta'\frac{\partial f}{\partial \xi}\right], \tag{4.9}$$

$$\frac{1}{Le}\left(\varphi'' + \frac{N_b}{N_t}\theta''\right) + \frac{1}{2}f\varphi' + \xi\frac{\sigma_\xi}{\sigma}f\varphi' = \xi\left[f'\frac{\partial\varphi}{\partial\xi} - \varphi'\frac{\partial f}{\partial\xi}\right], \tag{4.10}$$

where $N_b = \frac{\tau^* D_B(C_w - C_\infty)}{\nu}, N_t = \frac{\tau^* D_T(T_w - T_\infty)}{T_\infty \nu}, Le = \frac{\nu}{D_B}$, are the Brownian motion parameter, thermophoresis parameter, and Lewis number, respectively. The dimensionless form of boundary conditions is given by

$$\left.\begin{array}{c} f(\xi,0) = 0,\ f'(\xi,0) = {}^1/_\sigma, \theta(\xi,0) = 1, \varphi(\xi,0) = 1 \\ f'(\xi,\infty) = 0, \theta(\xi,\infty) = 0, \varphi(\xi,\infty) = 0. \end{array}\right\} \tag{4.11}$$

The physical quantities of interest are described as

$$C_{fx} = \frac{\tau_w}{\rho U^2}, Nu_x = \frac{\bar{x}q_w}{k(T_w - T_\infty)}, Sh_x = \frac{\bar{x}\bar{q}_m}{D_B(C_w - C_\infty)}, \tag{4.12}$$

where the first term is skin-friction coefficient, second is local Nusselt number, and third is local Sherwood number that explains the mass transfer at the wall. The quantities τ_w, q_w, and $\bar{q}_m$ are obtained by the following relations

$$\begin{gathered} \tau_w = \mu_{nf}(\nabla\bar{u}.\hat{n})_{y=0}, \qquad q_w = -\kappa_{nf}(\nabla T.\hat{n})_{y=0}, \\ \bar{q}_m = -D_B(\nabla C.\hat{n})_{y=0}. \end{gathered} \tag{4.13}$$

After using Eqs. (4.7) and (4.13) in Eq. (4.12), following relations of physical quantities are achieved:

$$\begin{gathered} C_f = C_{fx}Re^{\frac{1}{2}} = \frac{\xi^{-\frac{3}{2}}}{\sigma^{\frac{3}{2}}}f''(\xi,0), \quad Nu = Nu_x Re^{-\frac{1}{2}} = -\frac{\xi^{\frac{1}{2}}}{\sigma^{\frac{1}{2}}}\theta'(\xi,0), \\ Sh = Sh_x Re^{-\frac{1}{2}} = -\frac{\xi^{\frac{1}{2}}}{\sigma^{\frac{1}{2}}}\varphi'(\xi,0). \end{gathered} \tag{4.14}$$

4.2 Entropy generation

In an engineering system, the loss of useful work is simply related to the entropy production. The volumetric entropy expression for viscous incompressible nanofluid, as proposed by Bejan [1-4], in the Cartesian coordinate system is expressed as:

$$S_G = \frac{\kappa}{T_\infty^2}\left[\left(\frac{\partial T}{\partial \bar{x}}\right)^2 + \left(\frac{\partial T}{\partial \bar{y}}\right)^2\right] + \frac{\mu}{T_\infty}\left[2\left(\left(\frac{\partial \bar{u}}{\partial \bar{x}}\right)^2 + \left(\frac{\partial \bar{v}}{\partial \bar{y}}\right)^2\right) + \left(\frac{\partial \bar{u}}{\partial \bar{x}} + \frac{\partial \bar{u}}{\partial \bar{y}}\right)^2\right] + \frac{RD_B}{C_\infty}\left[\left(\frac{\partial C}{\partial \bar{x}}\right)^2 + \left(\frac{\partial C}{\partial \bar{y}}\right)^2\right] + \frac{RD_B}{T_\infty}\left[\left(\frac{\partial T}{\partial \bar{x}}\right)\left(\frac{\partial C}{\partial \bar{x}}\right) + \left(\frac{\partial T}{\partial \bar{y}}\right)\left(\frac{\partial C}{\partial \bar{y}}\right)\right]. \tag{4.15}$$

The first part of the above expression arises because of the heat transfer irreversibility, second part appears by virtue of viscous dissipation, and the local entropy generation in view of concentration of nanoparticles is appearing in the third part. Following expression in dimensionless form for entropy number is obtained by applying Eq. (4.7) to Eq. (4.15):

$$\frac{N_s}{Re} = \frac{S_G}{S_{G_0}} = \frac{1}{\xi}\theta'^2 + \frac{Br}{\xi\,\Omega_T}\sigma f''^2 + \frac{\lambda}{\xi}\left(\frac{\Omega_C}{\Omega_T}\right)\theta'\varphi' + \frac{\lambda}{\xi}\left(\frac{\Omega_C}{\Omega_T}\right)^2\varphi'^2, \tag{4.16}$$

where $\Omega_C = \frac{\Delta C}{C_\infty}$, and $\lambda = RD_BC_\infty/\kappa$ are the concentration differences and nanoparticles mass transfer parameter, respectively. Entropy number is unable to classify the dominancy of irreversibility mechanism. To overcome this difficulty Bejan number is constructed to analyze the irreversibility mechanism. Bejan number Be is formed by dividing the heat transfer irreversibility to the total entropy production. For the present analysis, Bejan number (Be) has the following form:

$$Be = \frac{\frac{1}{\xi}\theta'^2}{\frac{1}{\xi}\theta'^2 + \frac{Br}{\xi\,\Omega_T}\sigma f''^2 + \frac{\lambda}{\xi}\left(\frac{\Omega_C}{\Omega_T}\right)\theta'\varphi' + \frac{\lambda}{\xi}\left(\frac{\Omega_C}{\Omega_T}\right)^2\varphi'^2}. \tag{4.17}$$

4.3 Solution scheme and grid independence

Numerical solution of the governing non-linear partial differential equations (4.8)-(4.10) with the boundary conditions (4.11) for various values of pertinent parameters is achieved by Keller-box method [136,139]. Details of the scheme have been given in chapter 2. According to this finite-difference scheme the given nonlinear PDE's are converted into a system of first order PDE's. For linearization of the system, the

Newton's scheme is used. Block tridiagonal elimination technique is employed for the solution of the obtained system. The code is developed in the computational software MATLAB.

The grid independent test for the numerical results of the considered problem has been conducted by taking various step lengths for η and ξ variables. It has been shown that numerical results remain unchanged when $\Delta\eta = \Delta\xi < 0.01$. Therefore, we have taken step size $\Delta\eta = \Delta\xi = 0.005$. For the present solution algorithm, grid independence test is tabulated in Table 4.1.

Table 4.1: Gird independence by taking $\alpha = 0.2,\ Pr = 7.0, Le = 10.0, Nt = Nb = 0.$

No of grid points η direction With fix $\eta = 15$.	No of grid points ξ direction With fix $\xi = 0.5$	$-C_f$	Nu	Sh
150	10	0.44680	1.3378	1.6224
300	50	0.42889	1.3292	1.6106
1050	70	0.42765	1.3283	1.6092
1500	100	0.42672	1.3279	1.6087
3000	100	0.42672	1.3279	1.6087
6000	100	0.42672	1.3279	1.6087

4.4 Results and discussion

In the current section, the influence of physical parameters upon velocity, temperature, concentration, Bejan number, and entropy production profiles are depicted. Figures 4.1-4.2 explore the influence of thermophoresis and Brownian motion parameters on velocity, temperature and concentration profiles. Thermal conductivity of the fluid increases as a result of higher values of N_t and N_b and hence this enhancement augments the temperature profile. Similar effects on concentration profile occur due to increment in N_t as seen in Fig. 4.1 while on the other hand due to increase in N_b it reduces the concentration of nanoparticle which are shown in Fig. 4.2. Figures 4.3-4.5 show the graphs of Bejan number against η for different parameters. Figure 4.3 illustrates the influence of wavy amplitude α, Lewis number Le, and the Prandtl

number Pr, on the Bejan number. The Bejan number increases as Pr and α increase and attains a peak value close to the wavy surface while in free-stream region the fluid friction irreversibility is dominant. Similar behavior is observed with the variation in Le number except near the wavy surface. Figure 4.4 shows the effect of nanoparticle mass transfer parameter λ and Brinkman number Br on Be. The contribution in entropy production owing to the transfer of heat is weakened on surface as λ strengthens, while it attains a maximum value a bit away from the surface. For distant area, fluid friction irreversibility with diffusion irreversibility controls the entropy production. Similar effects are observed, as Br increases. Observation of Fig. 4.5 indicates that, Bejan number reduces as N_b and N_t are increased near the wavy surface but reverse influence is observed in distant region. For a particular values of N_b or N_t, Be increases to reach the peak value and gradually decreases within the boundary layer region. In free- stream region, Bejan number approaches to zero which means that heat transfer irreversibility effects are negligible.

Figure 4.6-4.10 represent the graphs of Be against ξ for different physical parameters. These graphs illustrate that, with the increment of ξ, heat transfer irreversibility is dominant. Figures 4.6-4.7 illustrate that, Bejan number enhances as Br and λ augments. Figure 4.8 depicts that, the enhancement of Brownian and thermophoresis parameters leads to decrease the Bejan number in the upstream region and negligible effects are observed in the downstream region with variation of these parameters. Figure 4.9 depicts the influence of Pr and Le on Bejan number. With decreasing value of Le, Bejan number increases in upstream region but no prominent effects are seen in downstream region. Bejan number increases, as Pr increases. It is noted from Fig. 4.10 that the fluctuations in Bejan number are more pronounced in increasing direction of ξ, as α increases.

Figures 4.11-4.14 show the graphs of entropy generation number against ξ. Graphical results show that, the irreversibility is high in upstream region which reduces gradually in downstream region. Figure 4.11 shows that, with the enhancement of λ, variation in entropy profile is not prominent but the value of entropy generation enhances with the increment of Br. According to Fig. 4.12 the entropy generation decreases, with augmentation of N_t and N_b. It is observed from Fig. 4.13 that there is no significant effect in downstream region with the variation of Lewis number. However, with the increasing values of Pr entropy profile is enhanced. The effects of Le, Pr, and α on entropy number are depicted in Fig. 4.14. Results show that, with the augmentation of Le, the entropy number enhances in the region closer to the plate. Physically, temperature profile increases with the increase in Le and hence entropy generation enhances. However, there appears no significant effect in distant region. For increasing values of Pr, slightly variation in entropy number occurs in the region close to the plate and far away from the plate but in the intermediate flow region entropy number attains its peak value (around $\eta = 0.5$). Entropy generation enhances with the decrement of the wavy amplitude α near the surface.

Figure 4.15 illustrates the influence of N_t and N_b on entropy profile. Entropy number decreases close to the boundary with increasing N_t and N_b but the opposite effects are noticed for far away region. Physically, an increase in N_t means that the thermophoresis force enhances and hence nanoparticles tend to move from hot surface to cold region. However, the temperature and velocity gradient is large near the boundary, therefore entropy production is high close to the surface and is negligible for distant region. The consequences of λ and Br on entropy production number is reported in Fig. 4.16. By increasing the Br number, the resistance among the fluid particles increases. Consequently, the fluid is heated up which causes the increment in entropy

production. Same results are achieved for the parameter λ because increments in λ means concentration of nanoparticle increases which intensifies the temperature inside the boundary layer region. Also, entropy profile illustrates that the wavy boundary serves as a strong source of entropy production. Since the flow investigated in this study is non-similar in nature, therefore the results reported in this study have been computed at certain local values of the involved variables.

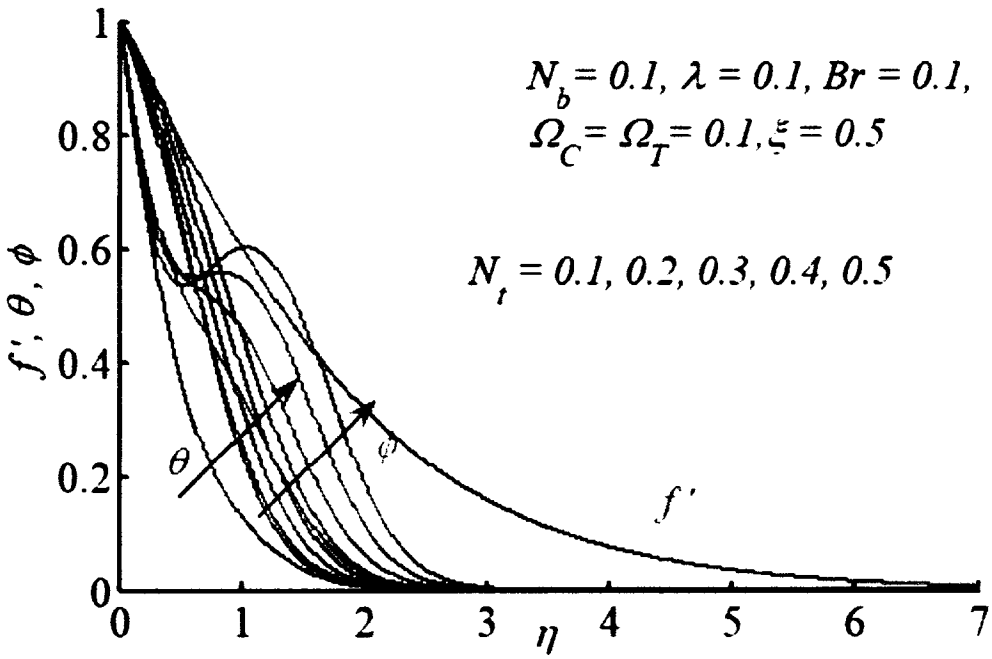

Fig. 4.1: Velocity, temperature, and concentration profiles against η for different N_t.

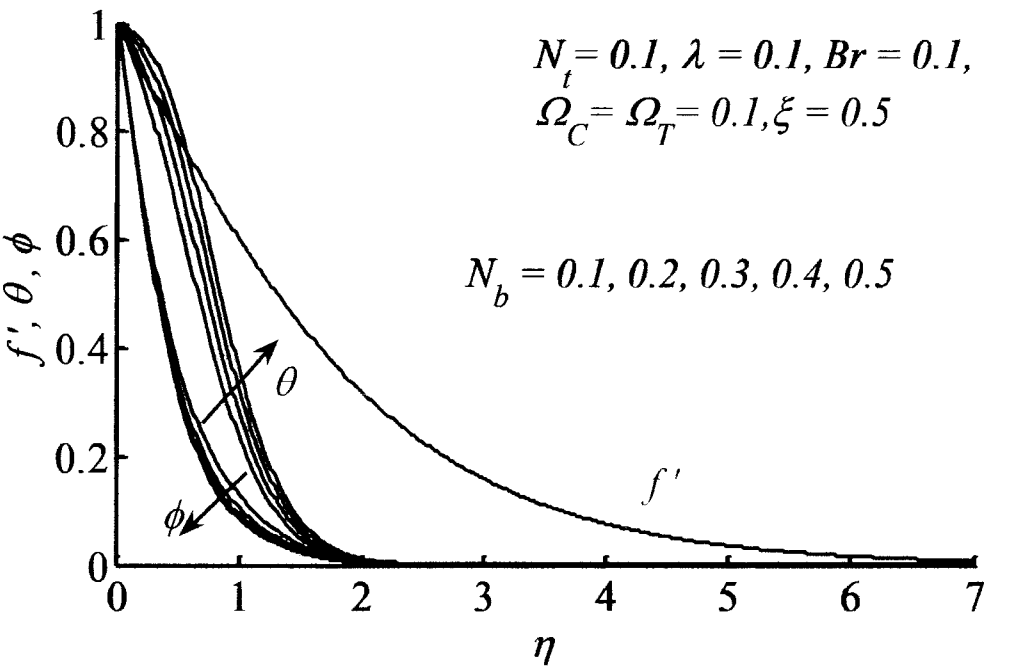

Fig. 4.2: Velocity, temperature, and concentration profiles against η for different N_b.

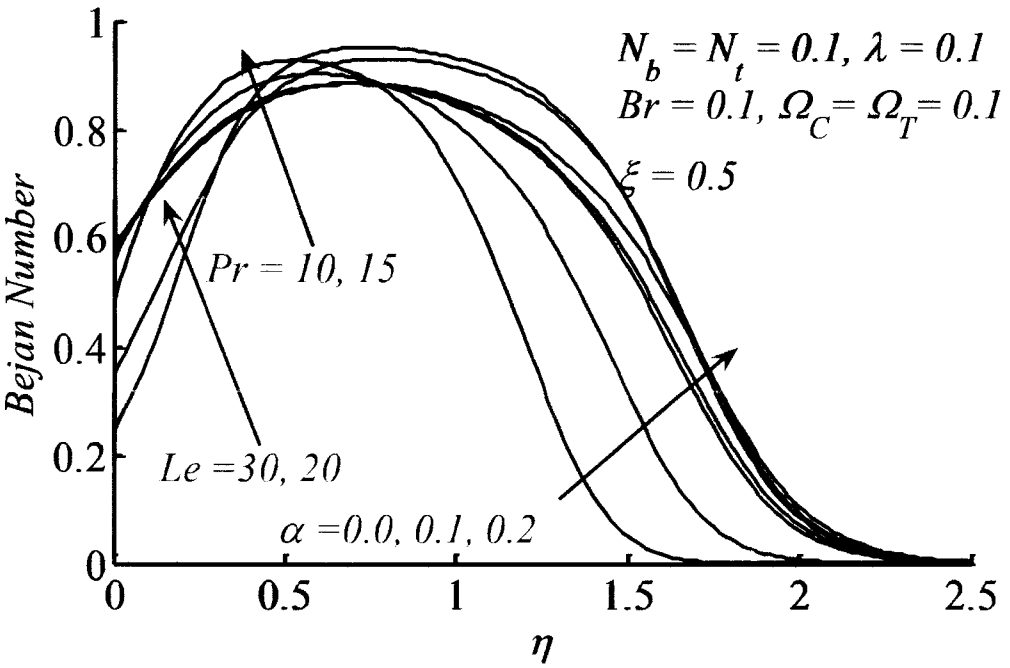

Fig. 4.3: *Be* plotted against η for different *Pr*, *Le*, & α.

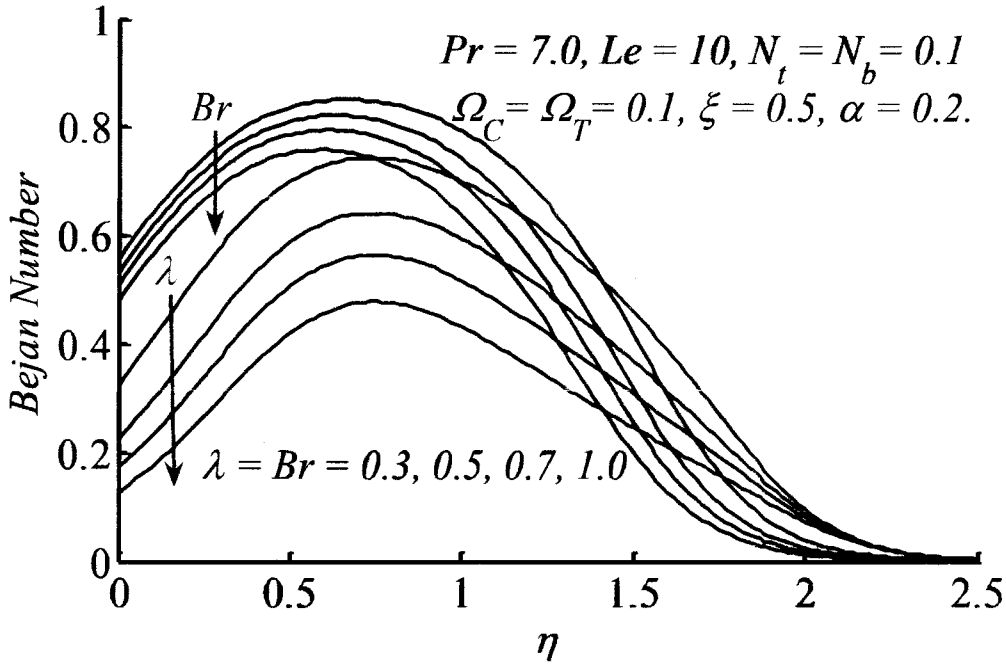

Fig. 4.4: *Be* verses η for various values of Br, & λ.

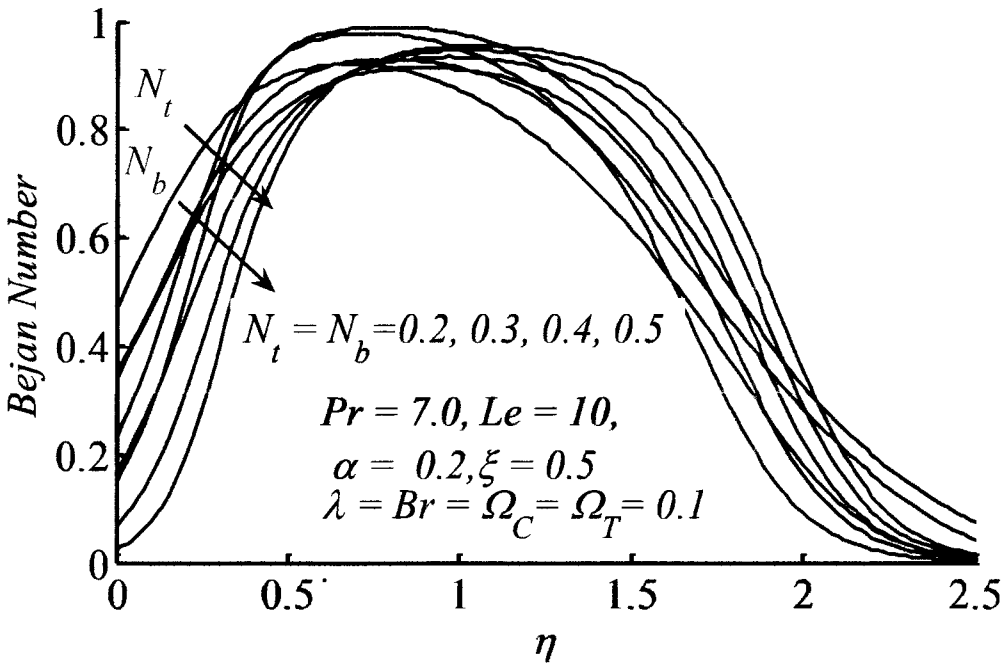

Fig. 4.5: *Be* against η for different N_t, & N_b.

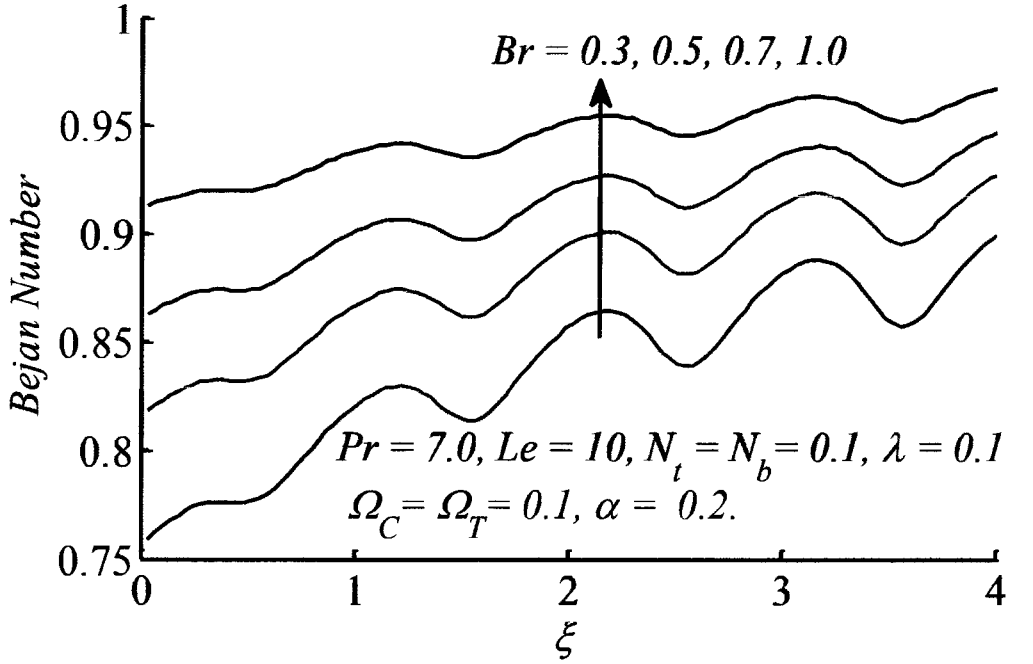

Fig. 4.6: Variation of Be for different Br at $\eta = 0$.

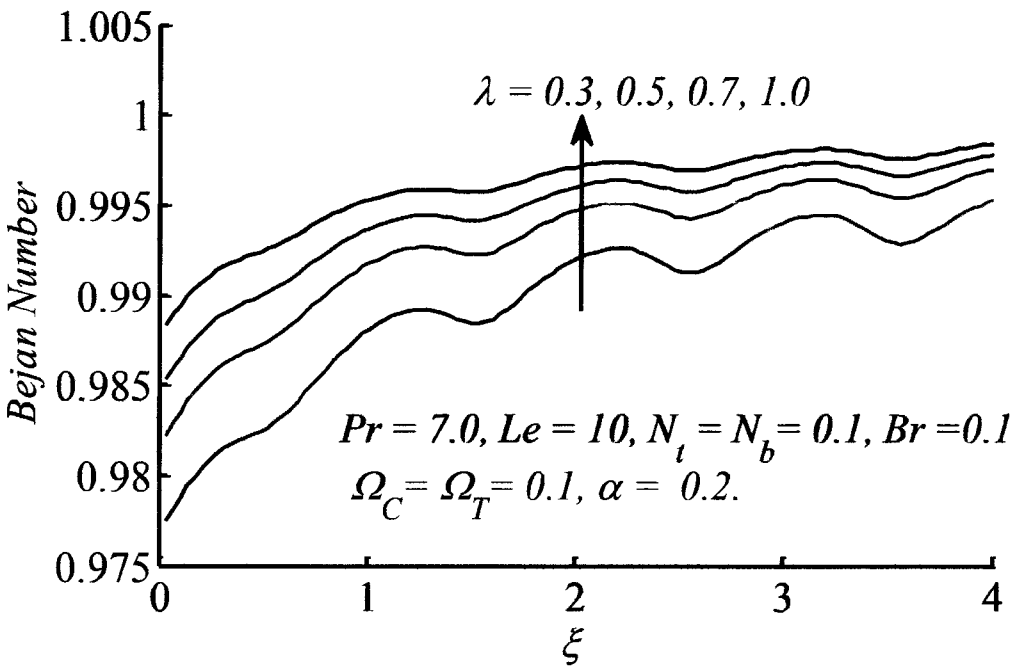

Fig. 4.7: Behavior of Be for different λ at $\eta = 0$.

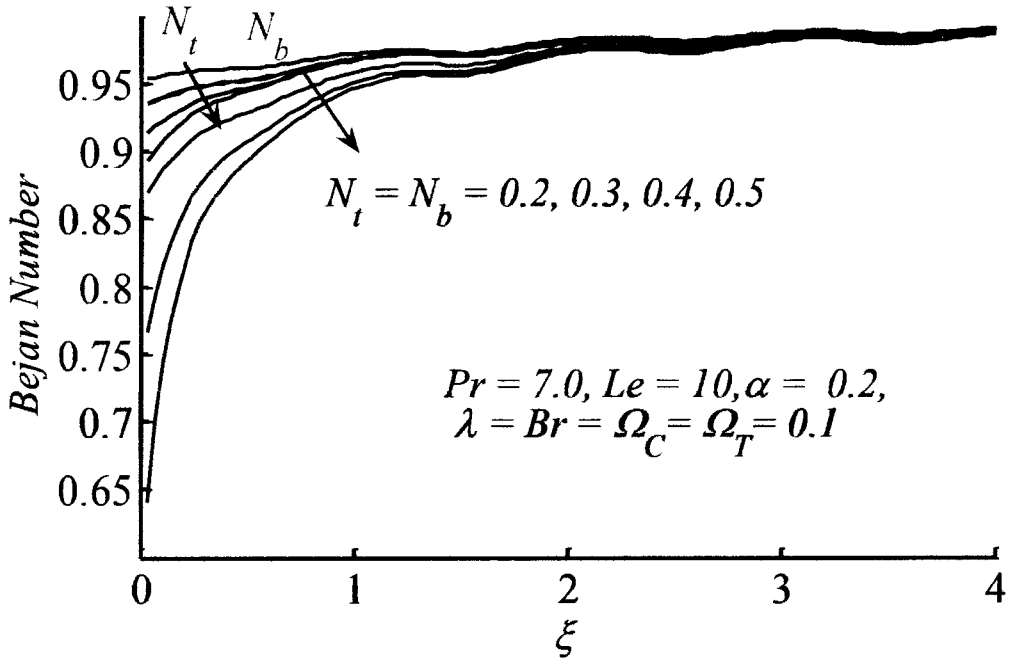

Fig. 4.8: Be plotted for different N_t & N_b at $\eta = 0$.

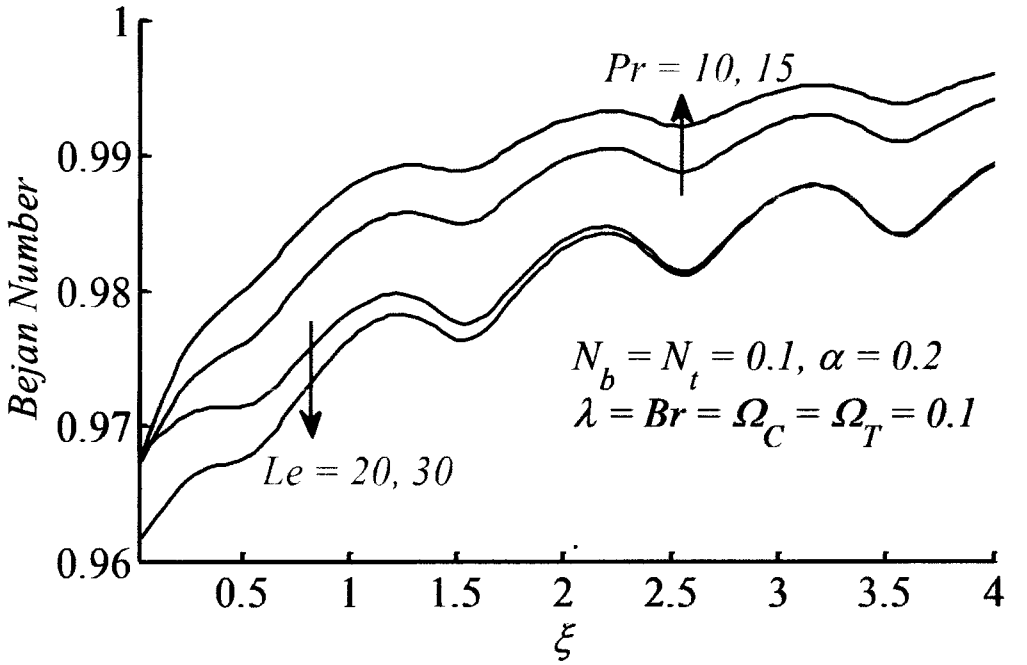

Fig. 4.9: Be graph for different Le & Pr at $\eta = 0$.

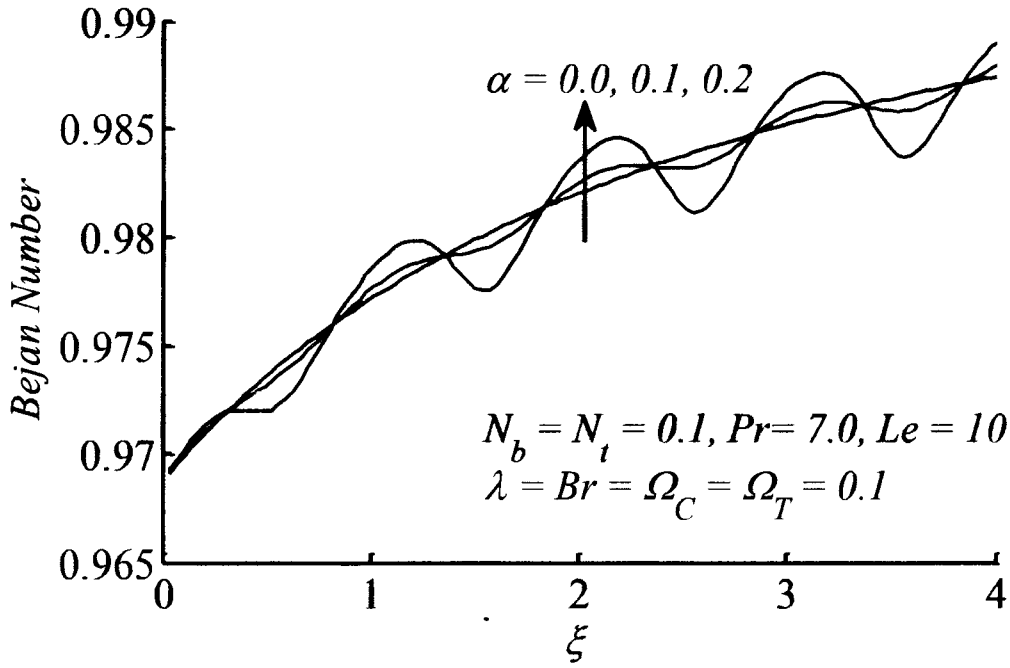

Fig. 4.10: Plot of Be for different α at $\eta = 0$.

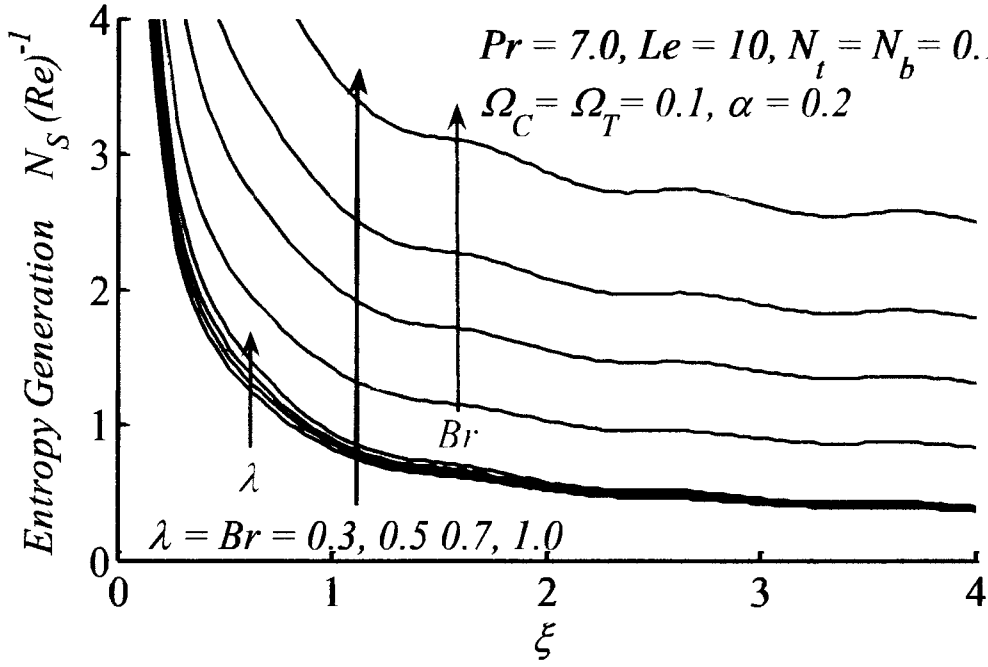

Fig. 4.11: Graph of N_S for different Br & λ at $\eta = 0$.

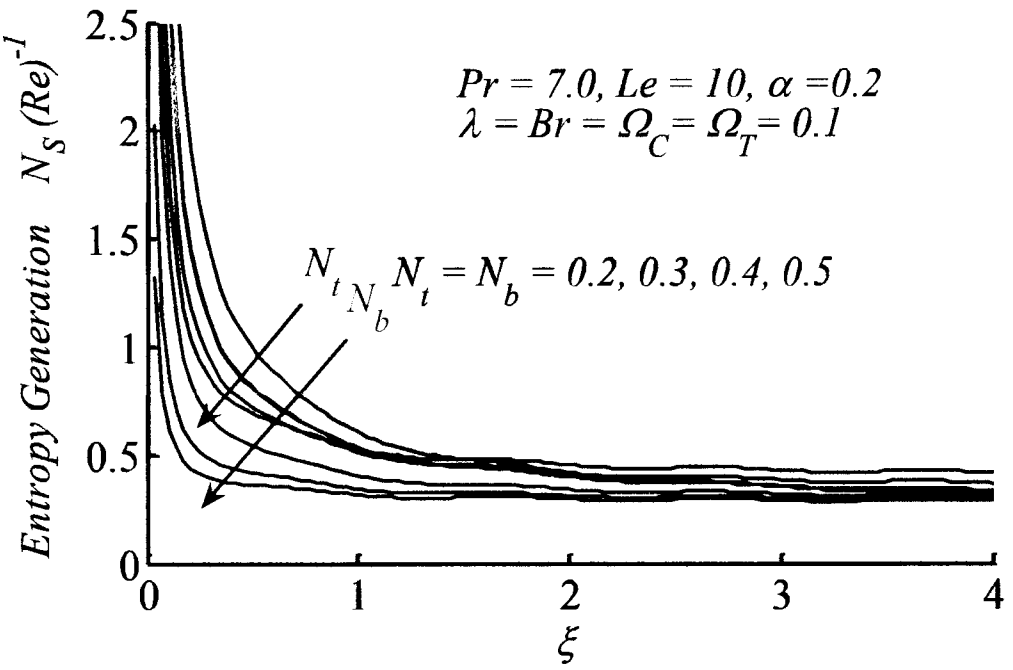

Fig. 4.12: Variation of N_S for various N_t & N_b at $\eta = 0$.

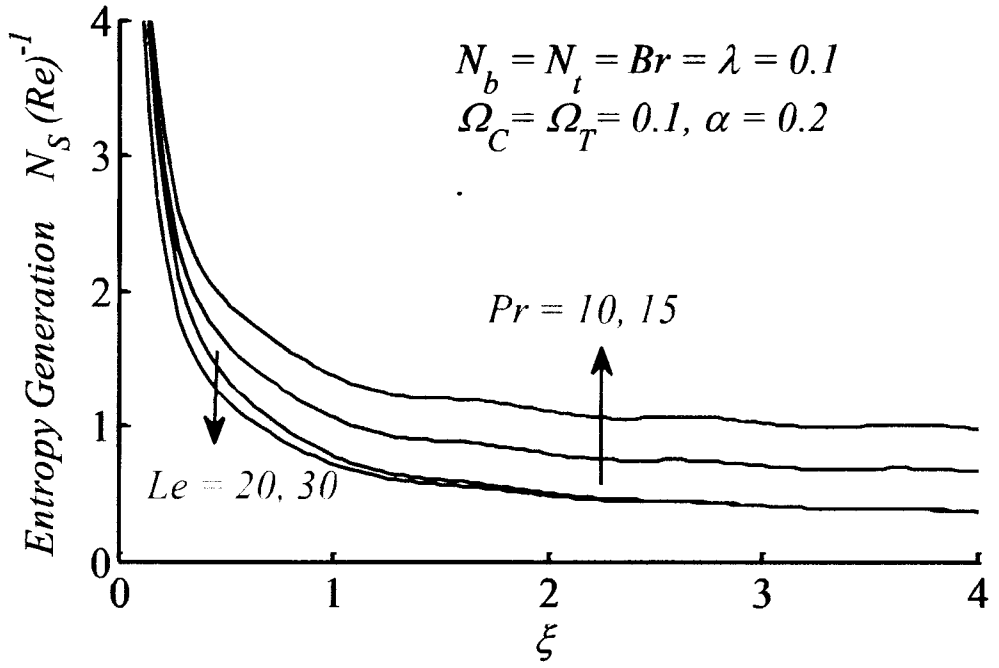

Fig. 4.13: Variation in N_S due to Pr & Le at $\eta = 0$.

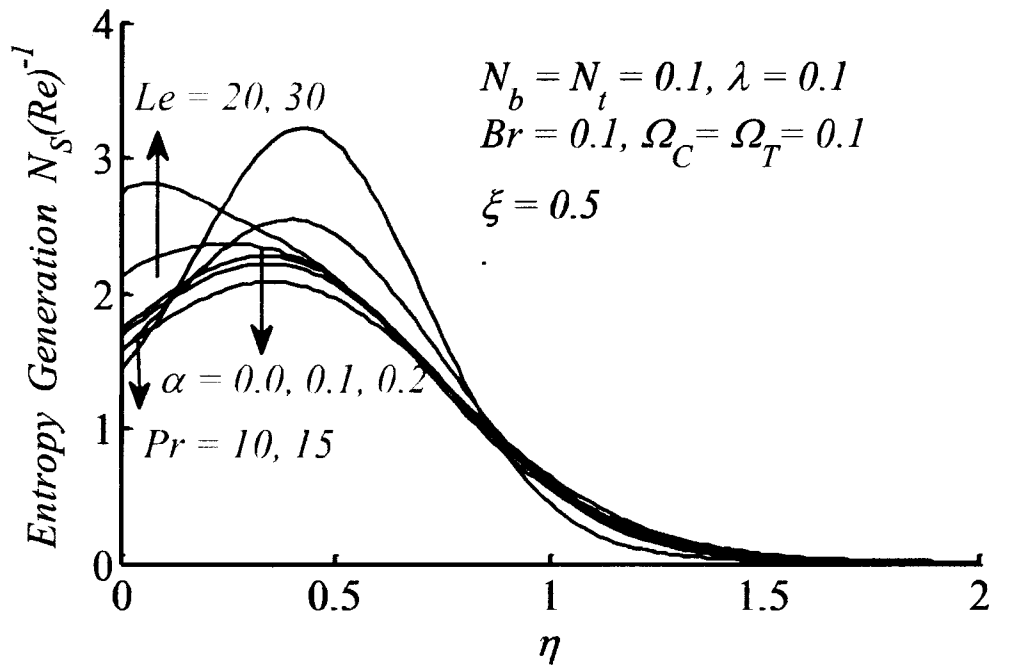

Fig. 4.14: N_S plotted against η for different $Pr, Le, \& \alpha$.

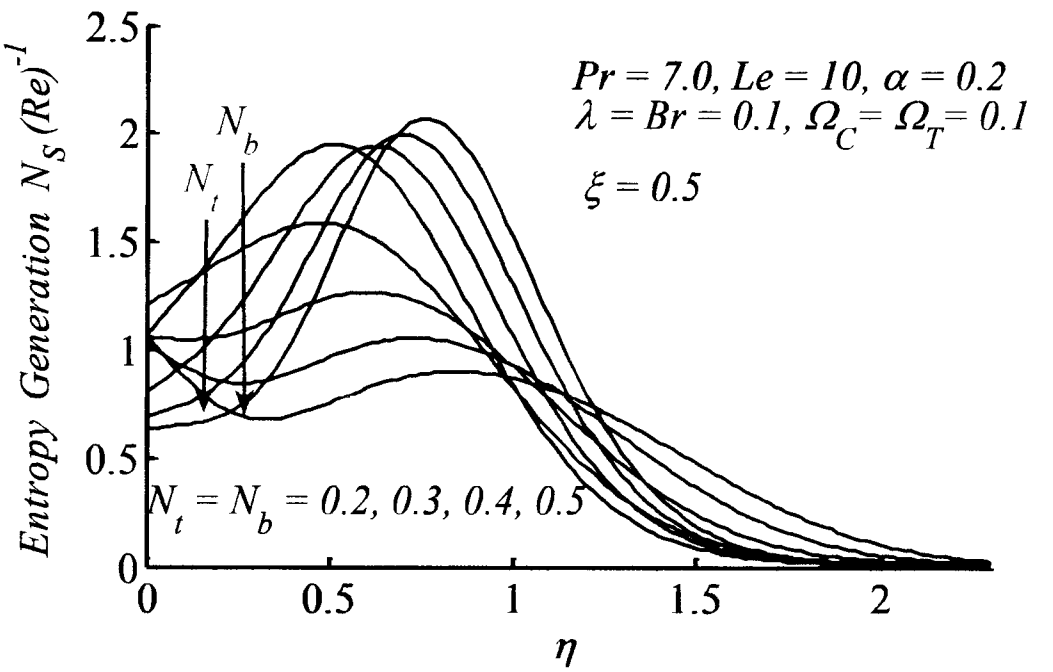

Fig. 4.15: N_S graph for different N_t & N_b.

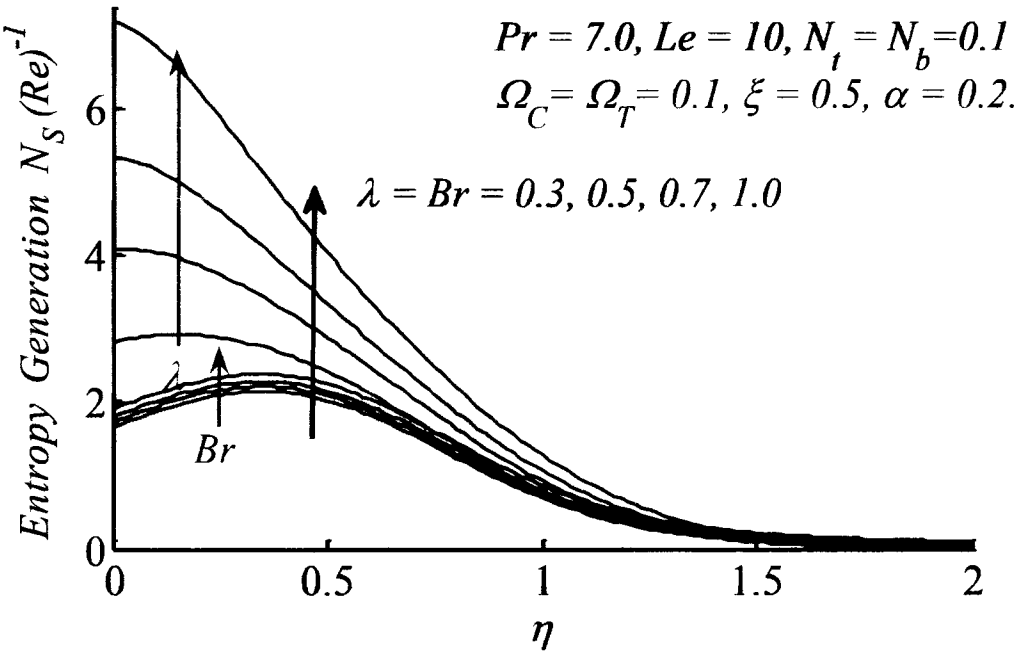

Fig. 4.16: N_S plotted against η for different λ & Br.

4.5 Final remarks

In this chapter, we investigated the combined effects of surface texture and nanofluid on entropy generation phenomenon by utilizing the Buongiorno nanofluid model. It includes the effects of thermophoresis and Brownian motion of nanoparticles in addition to enhanced thermo-physical properties of the mixture. By using temperature, velocity, and concentration profiles, entropy production number and Bejan number have been computed. The main findings of this work are as under:

- Bejan number is decreased with the enhancement of nanoparticle mass transfer parameter λ.
- Increasing the Brownian motion and thermophoresis parameter result in the reduction of Bejan number in the vicinity of the wavy surface but reverse observations are achieved in the faraway region. From the graphical results it is also concluded that in increasing direction of ξ, the entropy profile due to thermal irreversibility are prominent for different pertinent parameters.

- Entropy production augments near the surface of the wavy plate as Le, Br, and λ are enhanced.
- Entropy production decreases due to the augmentation of N_t and N_b in the vicinity of the plate but reverse effects are observed for far away region.

Chapter 5

Entropy generation in mixed convection flow past a vertical wavy surface

Irreversibility phenomenon is numerically investigated for mixed convection flow along a uniformly heated vertical wavy surface. Wavy texture of the plate does not allow for a self-similar solution due to which the nature of the problem is non-similar. Convective heat transfer become mixed convection in current analysis due to buoyancy driven flow and free stream velocity of the fluid in faraway region. The influence of various physical parameters of interest (mixed convection parameter, wavy amplitude, Prandtl number) on entropy generation and Bejan number has been discussed in detail. It is observed that entropy production enhances with an increment in mixed convection parameter.

5.1 Formulation of the problem

Consider a physical model of two-dimensional mix-convection viscous flow along a vertical wavy surface. The flow is laminar, steady, and incompressible. A differentiable periodic function is chosen to defined the wavy surface as given in Eq. (1.13). The surface temperature (T_w) of the plate is considered to be constant and higher than the free stream temperature (T_∞). The geometry and the coordinate system are exemplified through Fig. 5.1.

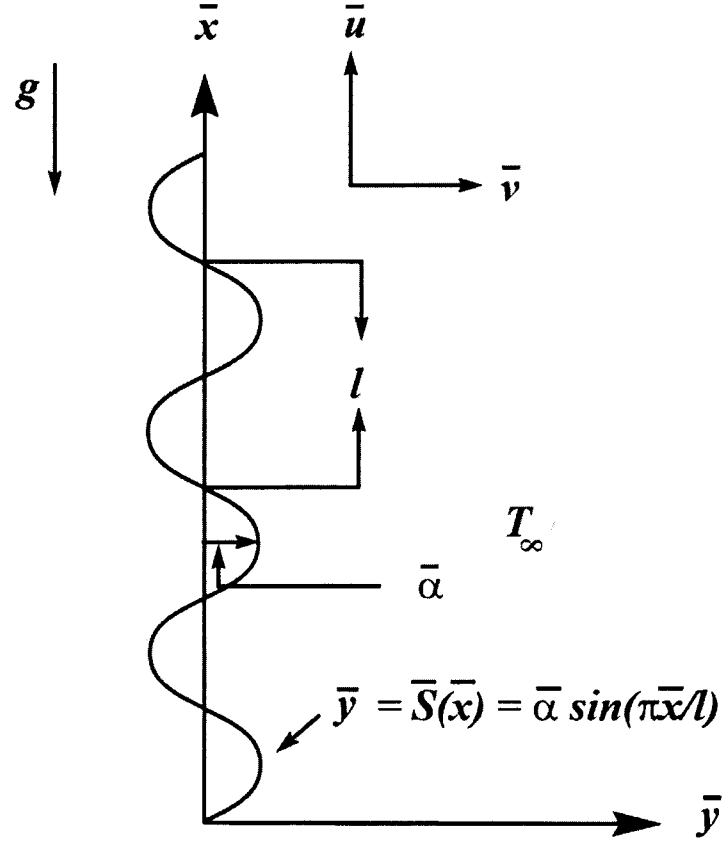

Figure 5.1: Physical model and the coordinate system.

According to this model equations of continuity, momentum, and energy under the usual Boussinesq approximation are:

$$\frac{\partial \bar{u}}{\partial \bar{x}} + \frac{\partial \bar{v}}{\partial \bar{y}} = 0, \tag{5.1}$$

$$\bar{u}\frac{\partial \bar{u}}{\partial \bar{x}} + \bar{v}\frac{\partial \bar{u}}{\partial \bar{y}} = -\frac{1}{\rho}\frac{\partial \bar{p}}{\partial \bar{x}} + \nu\nabla^2\bar{u} + g\beta(T - T_\infty), \tag{5.2}$$

$$\bar{u}\frac{\partial \bar{v}}{\partial \bar{x}} + \bar{v}\frac{\partial \bar{v}}{\partial \bar{y}} = -\frac{1}{\rho}\frac{\partial \bar{p}}{\partial \bar{y}} + \nu\nabla^2\bar{v}, \tag{5.3}$$

$$\bar{u}\frac{\partial T}{\partial \bar{x}} + \bar{v}\frac{\partial T}{\partial \bar{y}} = \frac{k}{\rho C_p}\nabla^2 T + \frac{\mu}{\rho C_p}\left[2\left(\left(\frac{\partial \bar{u}}{\partial \bar{x}}\right)^2 + \left(\frac{\partial \bar{v}}{\partial \bar{y}}\right)^2\right) + \left(\frac{\partial \bar{u}}{\partial \bar{y}} + \frac{\partial \bar{v}}{\partial \bar{x}}\right)^2\right], \tag{5.4}$$

where the velocity components $(\bar{u}, \bar{v})$ are taken along dimensional coordinates $(\bar{x}, \bar{y})$ and g is the gravitational acceleration. For specified geometry the boundary conditions read as

$$\left.\begin{array}{lllll} \bar{y}=\bar{S}(\bar{x}) : \bar{u}=0, & \bar{v}=0, & T=T_w, & \text{for all } \bar{x}>0, \\ \bar{y}\to\infty : \bar{u}=U, & \bar{p}=p_\infty, & T=T_\infty, & \text{for all } \bar{x}>0. \end{array}\right\} \quad (5.5)$$

Prandtl's transposition theorem is utilized for the transformation of sinusoidal boundary into a flat boundary [60] and the subsequent dimensionless variables are employed for the purpose of non-dimensionalization of the system. The dimensionless variables are given by

$$x=\frac{\bar{x}}{l}, y=\frac{\bar{y}-\bar{S}(\bar{x})}{l}\sqrt{Re}, u=\frac{\bar{u}}{U}, v=\frac{\sqrt{Re}}{U}(\bar{v}-S_\xi\bar{u}),$$
$$S=\frac{\bar{S}(\bar{x})}{l},\ p=\frac{\bar{p}}{\rho U^2}, \theta(\xi,\eta)=\frac{T-T_\infty}{T_w-T_\infty},\ Re=\frac{Ul}{\nu}. \quad (5.6)$$

By the utilization of above variables and the assumption that the change in pressure along vertical axis is zero and consequently by the elimination of the term $\partial\bar{p}/\partial\bar{y}$ between Eqs. (5.2) and (5.3), one finds out that

$$u\frac{\partial u}{\partial x}+v\frac{\partial u}{\partial y}=(1+\sigma_x^2)\frac{\partial^2 u}{\partial y^2}-\frac{\sigma_x\sigma_{xx}}{1+\sigma_x^2}u^2+\frac{Gr/Re^2}{1+\sigma_x^2}\theta, \quad (5.7)$$

$$u\frac{\partial\theta}{\partial x}+v\frac{\partial\theta}{\partial y}=\frac{1+\sigma_x^2}{Pr}\frac{\partial^2\theta}{\partial y^2}+\frac{U^2(1+\sigma_x^2)^2}{\Delta Tv}\left(\frac{\partial u}{\partial y}\right)^2. \quad (5.8)$$

For the most convenient form of Eqs. (5.7)−(5.8), the following set of new variables have been considered:

$$\xi=x,\quad \psi(\xi,\eta)=\xi^{\frac{3}{4}}f(\xi,\eta),\quad \eta=\xi^{-\frac{1}{4}}y,\quad \theta=\theta(\xi,\eta), \quad (5.9)$$

where the dimensionless stream function f depends upon ξ and η simultaneously. The reason is the non-similar nature of this flow which happened due to the non-flat texture of the plate surface. In view of Eq. (5.9) the dimensionless system (5.7)-(5.8) is transformed as

$$(1+\sigma_\xi^2)f'''+\frac{3}{4}ff''-\left(\frac{1}{2}+\frac{\xi\sigma_\xi\sigma_{\xi\xi}}{1+\sigma_\xi^2}\right)f'^2+\frac{Ri}{1+\sigma_\xi^2}\theta$$
$$=\xi\left[f'\frac{\partial f'}{\partial\xi}-f''\frac{\partial f}{\partial\xi}\right], \quad (5.10)$$

$$\frac{1}{Pr}(1+\sigma_\xi^2)\theta''+\frac{3}{4}f\theta'+\xi Ec(1+\sigma_\xi^2)^2f''^2=\xi\left[f'\frac{\partial\theta}{\partial\xi}-\theta'\frac{\partial f}{\partial\xi}\right], \quad (5.11)$$

where $Ri = Gr/Re^2$ represents the mixed convection parameter (characterized by Richardson number) and $Gr = \frac{g\beta(T_w - T_\infty)l^3}{\nu^2}$ is the Grahsof number. The values of Ri $(0 < Ri < 1)$ correspond to the situation of dominant forced convection which ultimately becomes pure forced convection at $Ri = 0$, while the values $Ri > 1$ corresponds to the dominant natural convection phenomenon. It is important to remember that the values of Ri falling in the neighborhood of $Ri = 1.0$ correspond to the situation of mixed convection flow where by the very small or very large values of Ri will correspond to forced convection or free convection flow only, respectively. The parameter Ec represents viscous dissipation facts and is known as Eckert number. The dimensionless form of the boundary conditions in view of Eqs. (5.6) & (5.9) are described as

$$\begin{gathered} f(\xi,0) = 0, \quad f'(\xi,0) = 0, \quad \theta(\xi,0) = 1, \\ f'(\xi,\infty) = 1, \quad \theta(\xi,\infty) = 0. \end{gathered} \tag{5.12}$$

5.2 Entropy generation

The volumetric entropy expression for the current flow problem in dimensional form are described by the Eq. (2.16). The non-dimensional form of volumetric entropy production can be achieved by the utilization of Eqs (5.6) & (5.9);

$$\frac{N_s}{Re} = \frac{S_G}{S_{G_0}} = \frac{(1+\sigma_\xi^2)}{\sqrt{\xi}}\theta'^2 + \frac{Br}{\Omega_T}(1+\sigma_\xi^2)^2\sqrt{\xi}f''^2. \tag{5.13}$$

Since Eq. (5.13) indicates that the heat transfer rate and the fluid viscosity are the major contributors towards the generation of entropy. Therefore, it is also important to identify that which one (among these two) is the dominant contributor. To answer this question the Bejan number (Be) is constructed to analyze the dominancy of heat transfer irreversibility or the viscous irreversibility in the process of entropy production.

Bejan number is found by dividing the thermal irreversibility to the total entropy. For the present analysis the Bejan number (Be) has the following form:

$$Be = \frac{(1+\sigma_\xi^2)\theta'^2}{(1+\sigma_\xi^2)\theta'^2 + \frac{Br}{\Omega_T}(1+\sigma_\xi^2)^2 \xi f''^2}. \tag{5.14}$$

Expression (5.14) also signifies the contribution of surface waviness which is by no means a trivial involvement. Therefore, it must be investigated in detail in order to understand the merits and de-merits of the wavy surface towards entropy generation.

5.3 Solution methodology

Since the governing system of equations has variable coefficients which are periodic in nature so that the exact solution as well as an asymptotic solution is not possible. Therefore, in order to find the solution of Eqs. (5.10-5.11) with the associated boundary conditions (5.12), an implicit finite difference method known as Keller-Box scheme [136, 139] has been utilized. The reason of the utilization of this method is that it is designed especially for the boundary layer flows by Keller and Cebeci. The Keller-Box discretization is fully coupled at each step which reflects the physics of parabolic system. Moreover, the choice of Keller-Box method is based upon its great simplicity; great suitability, second-order accuracy with arbitrary spacing, and attractive extrapolation features.

5.4 Results and discussion

In order to understand the influence of involved imperative variables on entropy number (N_S) and the Bejan number (Be), several graphs are plotted in Figs. 5.2-5.12. Figures 5.2-5.3 depict the graphs of entropy generation number against ξ for two distinct characters of mixed convection parameter Ri, i.e. for $Ri > 1$ and $Ri < 1$. The impact of Pr and α on entropy production is also discussed. Figure 5.2 illustrates that

the production of entropy is high when $Ri = 2.5$ as compared to $Ri = 0.5$, which means that entropy generation number is high in a case when the flow is induced by natural convection. Also, oscillation in entropy number is more prominent for $Ri = 2.5$ with the variation of α. Similar pattern is observed with the variation of Prandtl number. In both the figures fluctuations in N_s are high in downstream region for the flow induced by free convection. Moreover, N_s is observed to be an increasing function of ξ for $Ri = 2.5$ while a decreasing function of ξ for $Ri = 0.5$. This fact signifies that the entropy production in a natural convection flow can be minimized by introducing a forced flow. The effect of mixed convection parameter Ri on N_s, plotted against η are depicted in Fig. 5.4. It is observed that with an increase in the values of Ri, the entropy generation profile is augmented. The large values of Ri mean that the buoyancy effects are dominant and consequently the entropy generation at the surface is more significant. This fact highlights that to minimize the entropy generation in natural convective flow, a forced flow should be introduced there simultaneously, as observed above.

The dependence of entropy generation on Prandtl number is illustrated through Fig. 5.5. Results display that the entropy production reduces monotonically as one moves away from the surface. Moreover, its dependence upon Pr is seen to be in significant. Bejan number, as a function of ξ, is sketched through Fig. 5.6 for wavy amplitude α. Overall, the results depict that for natural convection and forced convection flow, Bejan number attains its optimal value in the upstream region. It means that the thermal irreversibility is dominant in upstream region which continuously decreases to die out in the downstream region. However, Bejan number takes higher values in case of forced convection flow which is opposite to the case of entropy production. Moreover, the amplitude of Be curves increases by increasing α, though which is not any significant. Figure 5.7 establishes the impact of Prandtl number upon Be. With the enhancement of

Pr, Bejan number increases in both cases (buoyancy driven natural convection and forced convection dominated flow). However, it is noted that in the downstream region the variation in Be (along ξ) is more prominent with the variation of Pr. Bejan number Be is sketched against η for two distinct characters of mixed convection parameter Ri in Figs. 5.8 and 5.9. At higher value of Ri, Be attains small value at the surface of the plate, which indicates that the major contributor in the production of entropy is the viscosity of a fluid. However, the reverse effects are observed on Be at the surface in the case of large Ri which highlights the dominancy of thermal irreversibility. Moreover, in main flow region Be approaches to its maximum value (which is 1) in both cases (forced and free convection flows) which also indicates that the major contribution is the thermal irreversibility in the production of entropy. As one moves away from the boundary, Be continuously decreases and dies out by showing that the irreversibility is totally controlled by viscous dissipation in faraway region. The impact of wave amplitude α on Bejan number Be is depicted in Fig. 5.8. Increasing trend is seen in Be with the intensification of α. The influence of Pr on Be is illustrated in Fig. 5.9. Graphical results show that in the locality of vertical wavy surface, Be increases with the augmentation of Prandtl number, but the reverse influence is noticed in faraway region from the surface.

A graph of Bejan number Be plotted against η with the variation of Ri is depicted in Fig. 5.10. Reduction in Be is observed as Ri strengthens. For large values of Ri (natural convection flow), fluid friction irreversibility is dominant at the surface, while for smaller Ri (forced convection flow) thermal irreversibility is dominant at the boundary. Overall, as discussed earlier, in faraway region the irreversibility is totally dependent upon viscous dissipation and in the case of natural convection flow this dependency is quickly achieved. The influence of Eckert number on entropy generation number and

Bejan number are discussed through Figs. 5.11-5.12. It is seen that variation of entropy production is more prominent in the downstream region for the case of dominant natural convection. Bejan number approaches to zero (viscous dissipation dominant) with the enhancement of Eckert number.

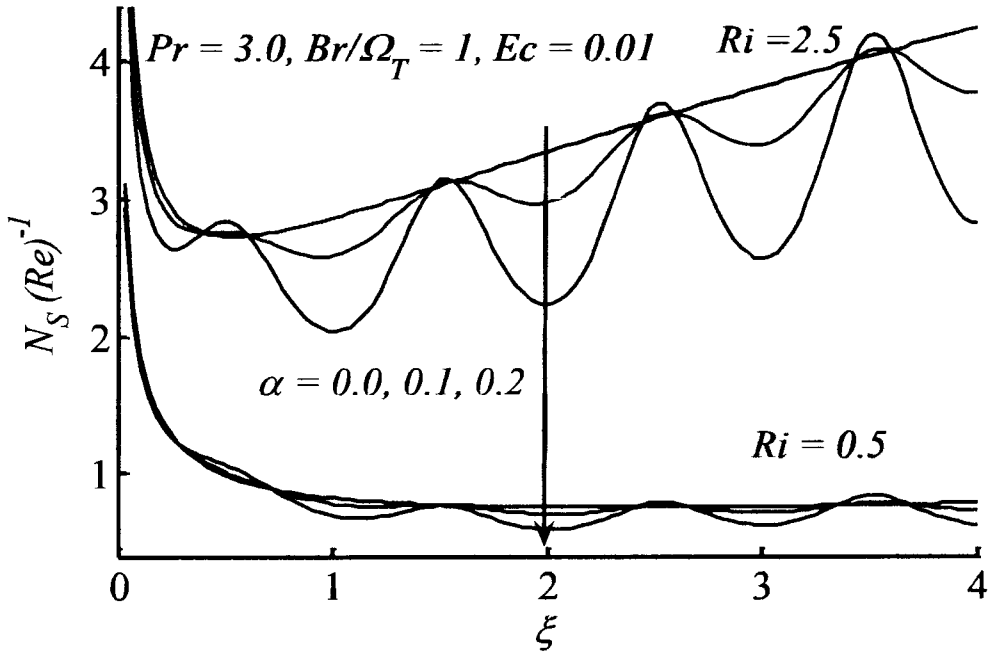

Fig. 5.2: Effect of wavy amplitude on entropy generation number.

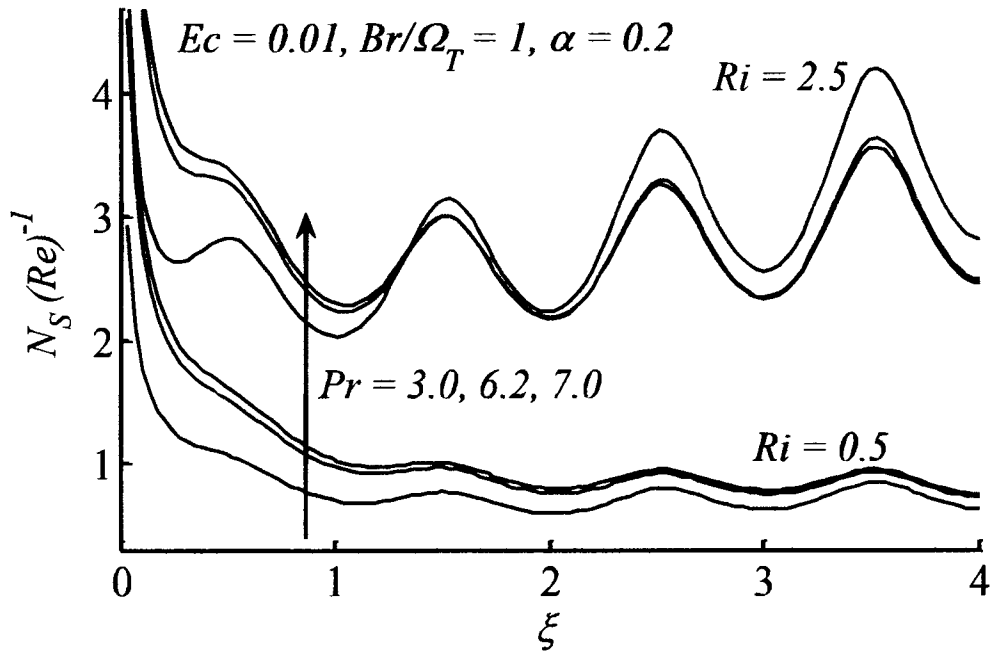

Fig. 5.3: Entropy generation profile plotted against ξ at different Prandtl number.

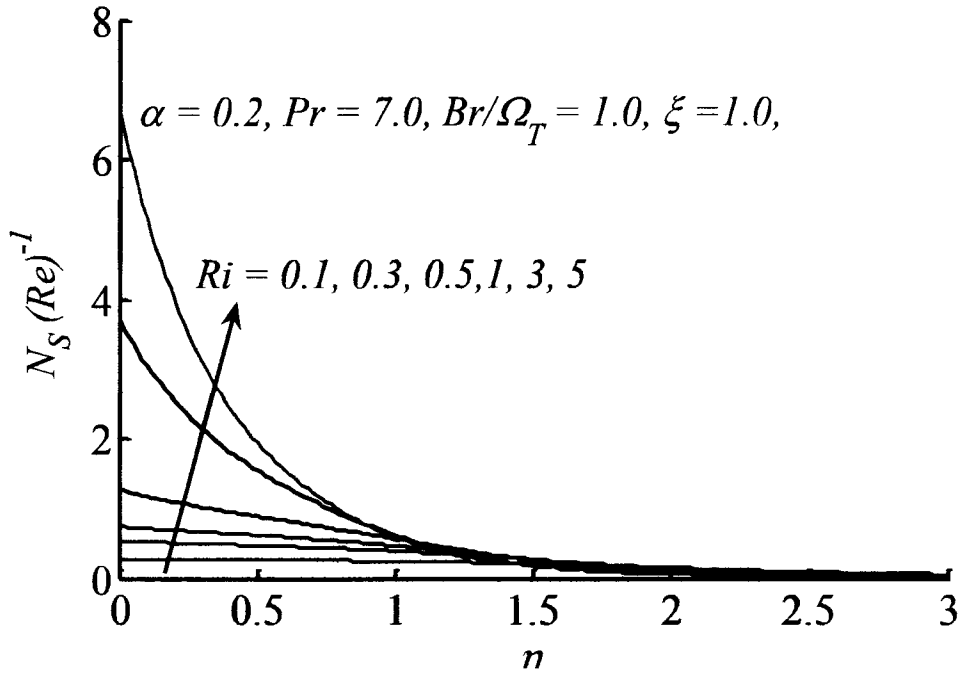

Fig. 5.4: Influence of Richardson number on entropy profile at $\xi = 1.0$.

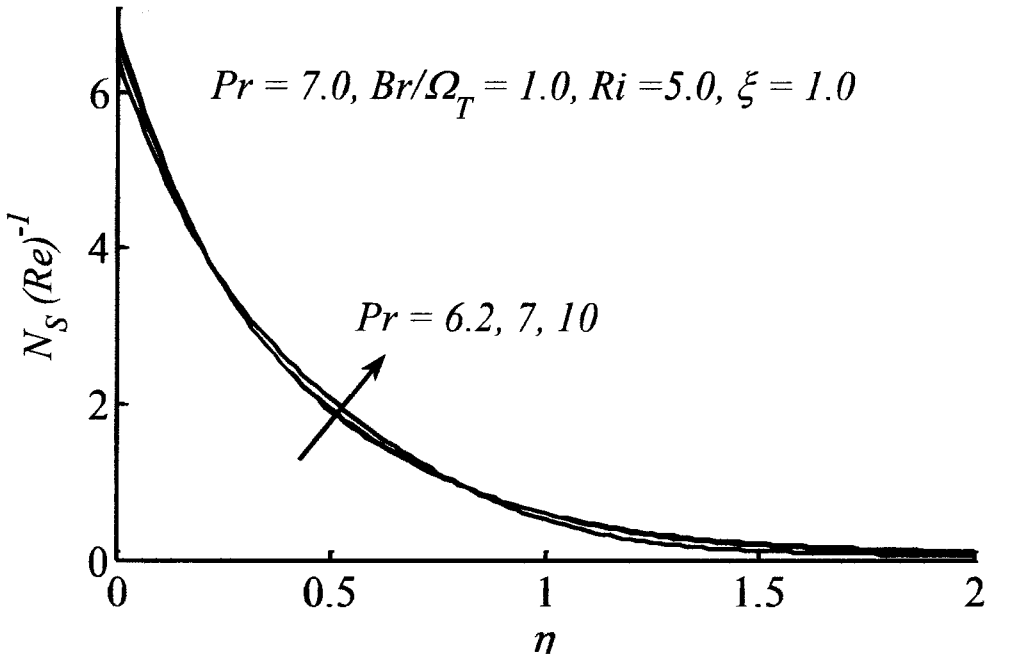

Fig. 5.5: Dependence of entropy profile on Prandtl number at $\xi = 1.0$.

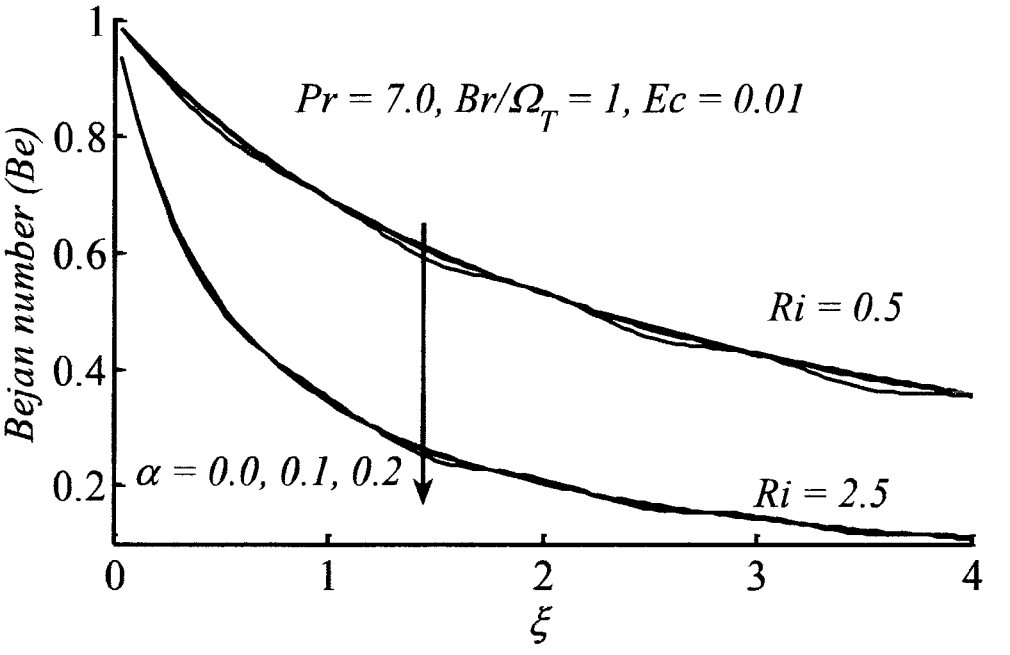

Fig. 5.6: Effects of wavy amplitude on Bejan number when plotted against ξ.

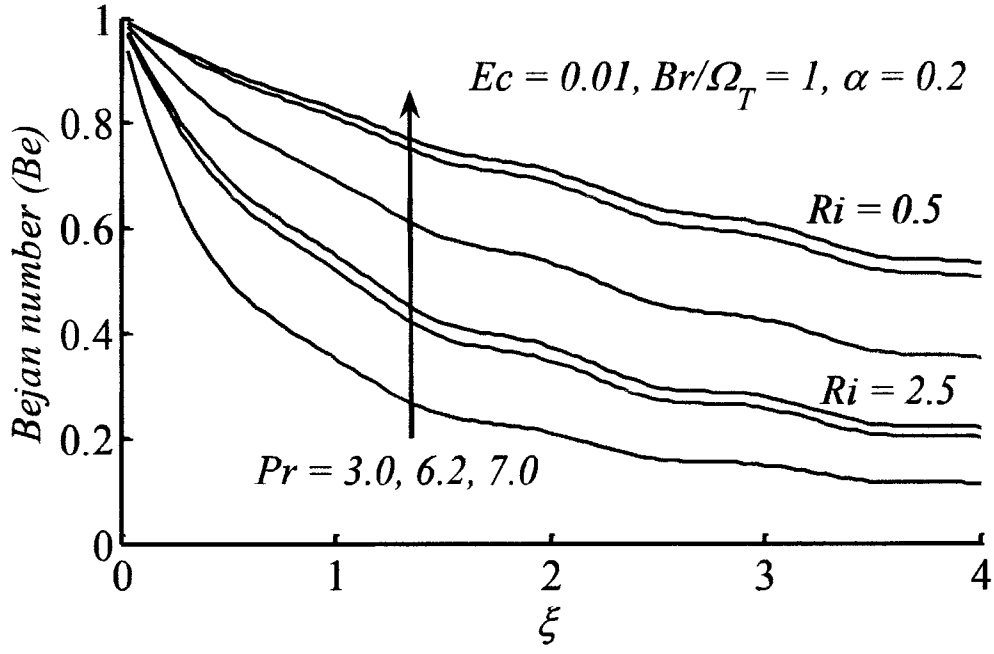

Fig. 5.7: Local Bejan number plotted at different Prandtl number.

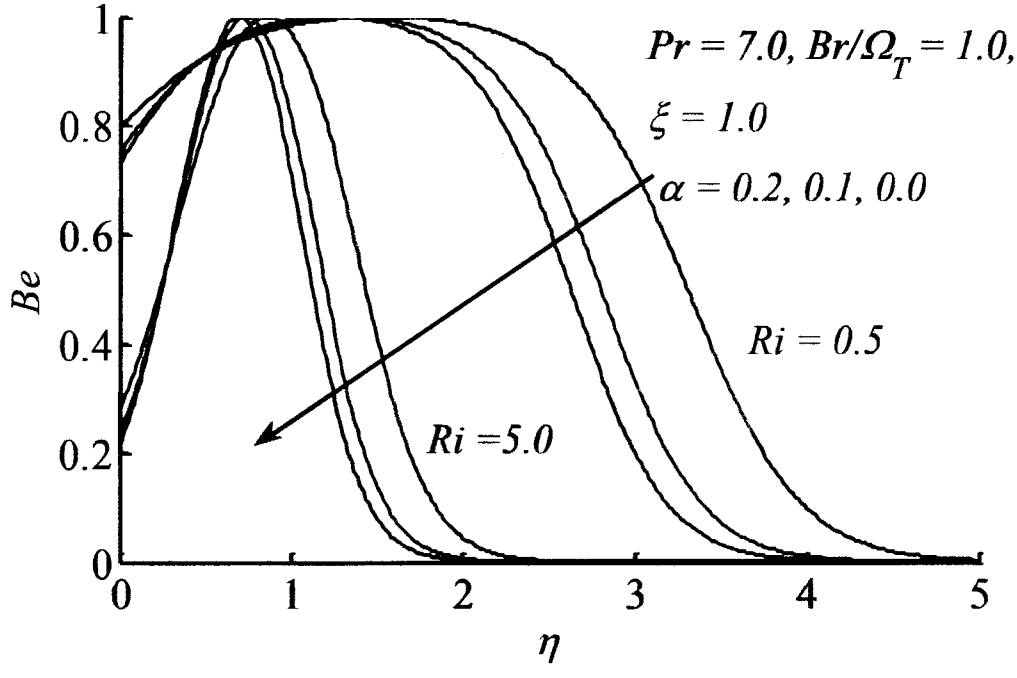

Fig. 5.8: Bejan number plotted for selected values of wavy amplitude.

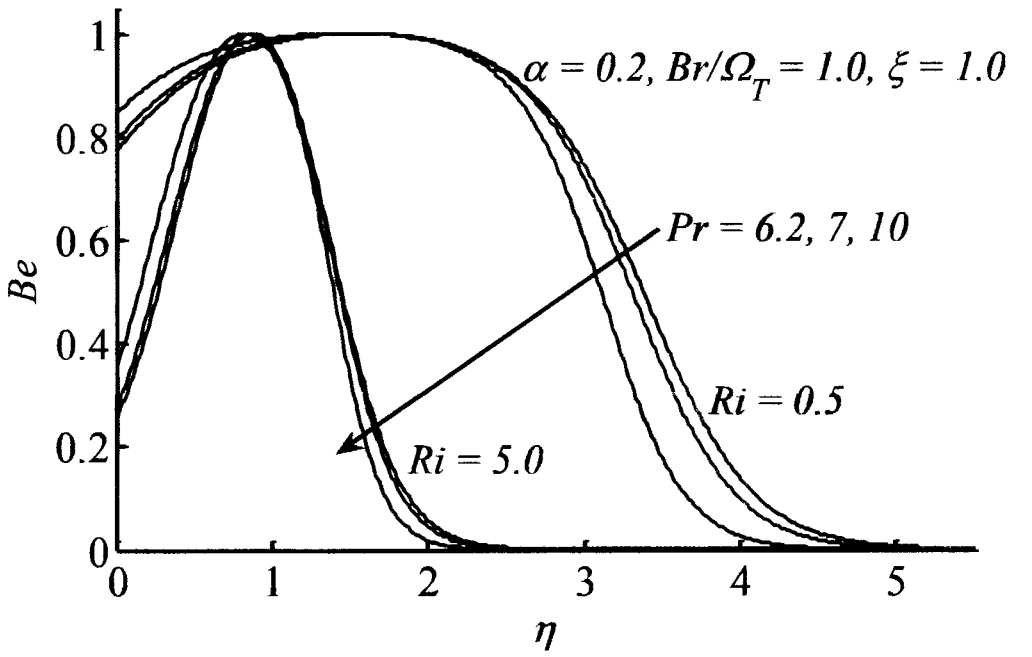

Fig. 5.9: Impact of Prandtl number on Bejan number for two fixed values of Richardson number.

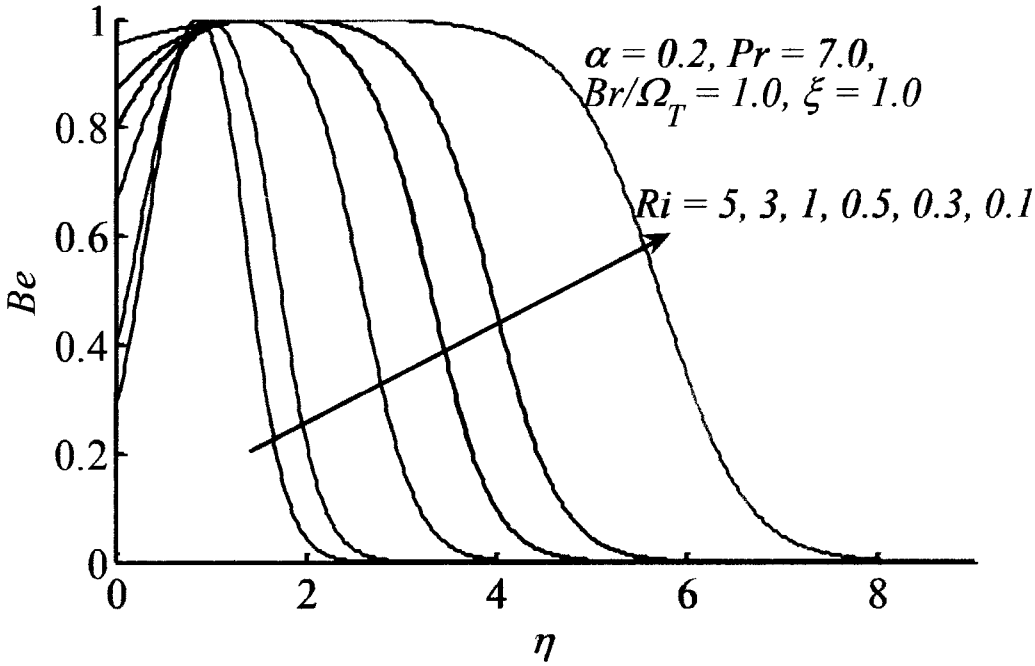

Fig. 5.10: Influence of mixed convection parameter on Bejan number.

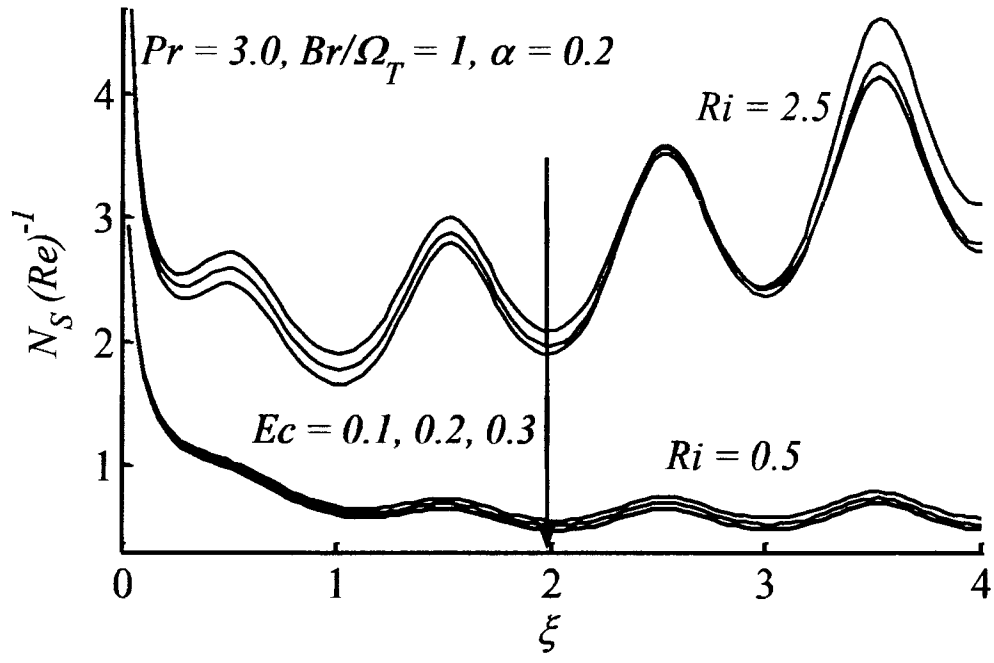

Fig. 5.11: Entropy generation number plotted against ξ at different Eckert number.

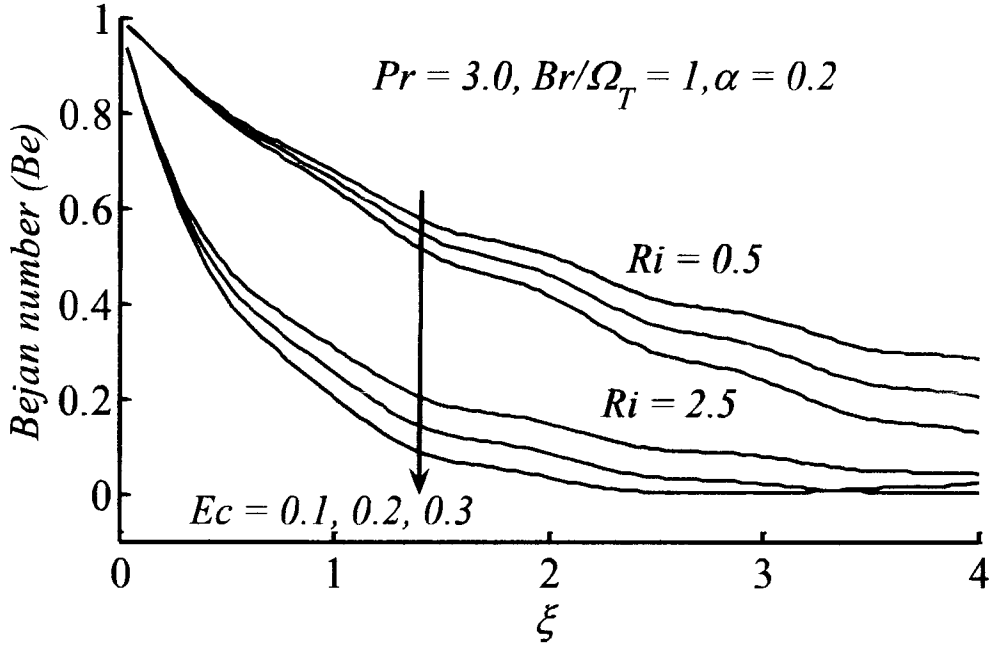

Fig. 5.12: Impact of Eckert number on Bejan number

5.5 Final remarks

The present chapter investigates the entropy production phenomenon in forced and free convection flow over heated wavy plate. The numerical results are utilized to analyze the irreversibility analysis in mixed convection flow. It is revealed that entropy generation augments when the flow is induced by natural convection. In order to minimize the entropy of a natural convection system, a forced convection phenomenon is useful to be introduced. The dependence of entropy generation upon amplitude to wavelength ratio is more significant for the natural convection flow. Bejan number reduces due to the increment of mixed convection parameter. In upstream region, the contribution of thermal irreversibility in entropy production is dominant in both types of flows (natural and forced convection flow).

Chapter 6

Irreversibility analysis of mixed convection flow past an inclined wavy surface

The subject of current communication is the study of entropy generation in mixed convection flow under the influence of non-flatness of the considered inclined surface. Due to the consideration of non-flat surface texture, convective transport process is significantly altered. Thus, the investigation of entropy generation phenomenon for a mixed convection flow over such a non-flat (wavy) surface is quite natural. The particularly chosen periodic surface texture of the sheet is an essential reason for the similarity breaking. So the problem becomes non-similar in nature and the rate of entropy generation does not remain alike on the whole longitudinal domain. Such a non-similar nature of the flow makes it possible to visualize the variation in entropy generation in the down-stream direction. The role of involved physical parameters in the irreversibility analysis has been investigated in detail and the findings are highlighted through various graphs. It is observed that the entropy production reduces with the decreasing values of inclination angle of the inclined wavy plate.

6.1 Mathematical modelling

Mixed convective flow of viscous incompressible fluid along an inclined wavy surface at an arbitrary angle γ $(0 \leq \gamma \leq \pi/2)$ to the horizontal is considered. The values $\gamma = 0$ and $\gamma = \pi/2$, respectively, refer to the cases of horizontal wavy surface and a vertical wavy surface. The flow is driven by the gravitational force as well as due to the buoyancy force acting due to the presence of a temperature difference. The $\bar{x}$ and $\bar{y}$ components of the Cartesian coordinate system are considered along and normal to the

mean of the wavy plate. It is assumed that the plate possesses a constant temperature T_w which is greater than the ambient temperature T_∞. The function described in Eq. (1.13) represents the nature of the surface texture of the plate. The chosen coordinate system and the geometry of the flow are depicted through Fig. 6.1.

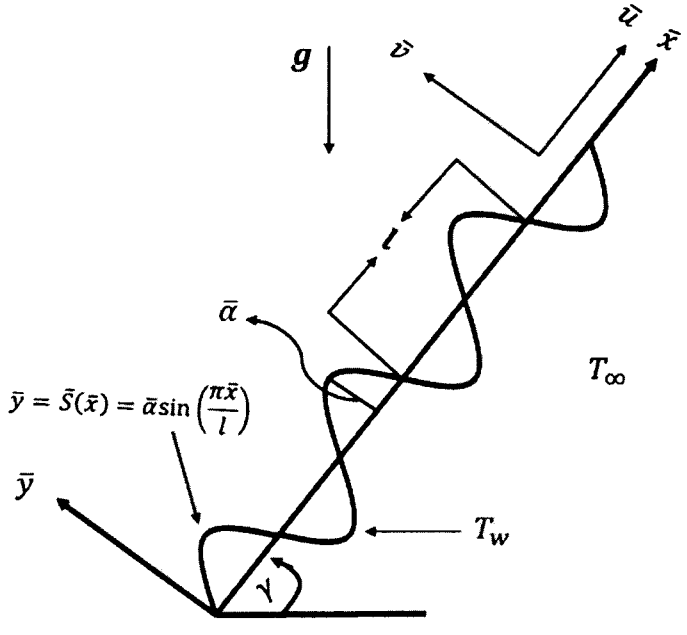

Fig. 6.1: Flow geometry and coordinate system.

By utilizing the above assumptions, the laws of conservation of mass, momentum, and energy are written as:

$$\frac{\partial \bar{u}}{\partial \bar{x}} + \frac{\partial \bar{v}}{\partial \bar{y}} = 0, \tag{6.1}$$

$$\bar{u}\frac{\partial \bar{u}}{\partial \bar{x}} + \bar{v}\frac{\partial \bar{u}}{\partial \bar{y}} = -\frac{1}{\rho}\frac{\partial \bar{p}}{\partial \bar{x}} + \nu\nabla^2\bar{u} + g\beta(T - T_\infty)cos\gamma, \tag{6.2}$$

$$\bar{u}\frac{\partial \bar{v}}{\partial \bar{x}} + \bar{v}\frac{\partial \bar{v}}{\partial \bar{y}} = -\frac{1}{\rho}\frac{\partial \bar{p}}{\partial \bar{y}} + \nu\nabla^2\bar{v} - g\beta(T - T_\infty)sin\gamma, \tag{6.3}$$

$$\bar{u}\frac{\partial T}{\partial \bar{x}} + \bar{v}\frac{\partial T}{\partial \bar{y}} = \frac{k}{\rho C_p}\nabla^2 T. \tag{6.4}$$

The boundary data are described by the Eq. (5.5). For the sake of non-dimensionalization of the system, the set of variables given in Eq. (5.6) is utilized and

the governing system in terms of stream function $\psi(x,y)$ (after the elimination of pressure gradient) can be expressed as

$$\frac{\partial\psi}{\partial y}\frac{\partial}{\partial x}\left(\frac{\partial\psi}{\partial y}\right)-\frac{\partial\psi}{\partial x}\frac{\partial}{\partial y}\left(\frac{\partial\psi}{\partial y}\right)$$
$$=(1+\sigma_x^2)\frac{\partial^2}{\partial y^2}\left(\frac{\partial\psi}{\partial y}\right)-\frac{\sigma_x\sigma_{xx}}{(1+\sigma_x^2)}\left(\frac{\partial\psi}{\partial y}\right)^2 \tag{6.5}$$
$$+\frac{(sin\gamma+\sigma_x cos\gamma)Ri}{1+\sigma_x^2}\theta,$$

$$\frac{\partial\psi}{\partial y}\frac{\partial\theta}{\partial x}-\frac{\partial\psi}{\partial x}\frac{\partial\theta}{\partial y}=\frac{k}{\mu c_p}(1+\sigma_x^2)\frac{\partial^2\theta}{\partial y^2}, \tag{6.6}$$

and the boundary data (5.5) take the following form in terms of stream function ψ

$$\left.\begin{aligned} y=0 \;:\; \frac{\partial\psi}{\partial y}=0, \quad \frac{\partial\psi}{\partial x}=0, \quad \theta=1, \quad \text{for all } x>0,\\ y=\infty \;:\; \frac{\partial\psi}{\partial y}=1, \quad \theta=0, \quad \text{for all } x>0. \end{aligned}\right\} \tag{6.7}$$

A further convenient form (for numerical computation) of the above system is obtained by using the transformations given in Eq. (5.9):

$$(1+\sigma_\xi^2)f'''+\frac{3}{4}ff''-\left(\frac{1}{2}+\frac{\xi\sigma_\xi\sigma_{\xi\xi}}{1+\sigma_\xi^2}\right)f'^2+\frac{(sin\gamma+\sigma_\xi cos\gamma)Ri}{1+\sigma_\xi^2}\theta$$
$$=\xi\left[f'\frac{\partial f'}{\partial\xi}-f''\frac{\partial f}{\partial\xi}\right], \tag{6.8}$$

$$\frac{1}{Pr}(1+\sigma_\xi^2)\theta''+\frac{3}{4}f\theta'=\xi\left[f'\frac{\partial\theta}{\partial\xi}-\theta'\frac{\partial f}{\partial\xi}\right]. \tag{6.9}$$

Accordingly, the boundary data becomes

$$f(\xi,0)=0,\ f'(\xi,0)=0,\theta(\xi,0)=1,f'(\xi,\infty)=1,\theta(\xi,\infty)=0. \tag{6.10}$$

It is worth mentioning that the problem is non-similar in nature due to the variable coefficients appearing on the left-hand side of Eqs. (6.8) and (6.9). Clearly, the function $S(\xi)$ describes the surface texture of the plate and these variable coefficients become constant by taking S_ξ as a constant, thus ensuring a self-similar situation.

6.2 Entropy analysis

For the analysis of entropy production, the expression defined by the Eq. (2.16) in two dimensions are valid in current flow problem. Also, we utilize the same variables and dimensionless parameters as defined in chapter 5 for the attainment of dimensionless form of entropy. Thus, Eq. (5.13) is straight forward valid for the non-similar flow along the inclined sinusoidal surface. So, the difference in the analysis of entropy generation occurs from previous chapter is due to the momentum and energy equations. Similarly, Eq. (5.14) are valid here for Bejan number to analyze the dominancy of heat transfer irreversibility or viscous irreversibility.

6.3 Entropy and Bejan profiles

In present section, entropy generation phenomenon is discussed in detail with the help of graphical pictures. For doing so the non-linear equations (6.8)-(6.9) with the boundary data (6.10) are solved by Keller Box method. Entropy generation number is plotted against η under the influence of different physical parameters in Figs. 6.2-6.5. Entropy number augments by the increasing values of inclination angle (γ) (see Fig. 6.2). In the vicinity of the plate entropy production is high for large values of Richardson number (Ri), which means that a natural convection dominated flow produces large irreversibility. Moreover, when $\gamma = 0$ (horizontal plate) there is no influence of gravity and less entropy generates (see Fig. 6.2) as a consequence. The impact of Prandtl number (Pr) upon entropy profile is explored through Fig. 6.3. Increments in Pr values produce more entropy in the neighborhood of wavy surface but the reverse aspect of Pr is noted away from the solid boundary. Impact of wavy amplitude (α) on the entropy number is depicted through Fig. 6.4. Entropy number decreases with the increase of α near to the surface and in the far-away region there appears no considerable variation. In Fig. 6.5 influence of Brinkman number (Br) upon

entropy profile is depicted. Enhancement of Br augments the irreversibility effects in the neighborhood of wavy plate which continuously goes on decreasing as one moves away from the boundary. This is because the fluid friction is much prominent in the near wall region as compared to the far-away region. Entropy profile plotted against longitudinal variable ξ is inspected through Figs. 6.6-6.8. Figure 6.6 shows an increase in entropy by an increase of Br. Since increase in Br values correspond to further strong viscous dissipation effects and consequently the production of entropy elevates. Moreover, the fluctuations in N_s increase due to increase in Br values as one moves from upstream region to downstream region and the amplitude of oscillations is more in the case of natural convection flow. An interesting role of wavy amplitude α on entropy profile is depicted through Fig. 6.7. The amplitude of Ns-profile increases upon increasing the surface amplitude. This means that a further bumpy surface will cause to further amplify the Ns-oscillations. The variation of entropy number with respect to Pr is illustrated through Fig. 6.8. Obviously, increase in Pr produces more entropy. This means that, the fluids having large viscosity produce more entropy.

In order to identify the dominant character of viscous dissipation or thermal dissipation towards the production of entropy in the boundary layer region, Bejan number is plotted. The effects of wavy amplitude (α), Brinkman number (Br), and inclination angle (γ) on Bejan number (as function of η) are illustrated through Figs. 6.9-6.11. Figure 6.9 explores that the heated surface plays a vital role in the production of entropy at the surface and in its neighborhood but when one moves away from the boundary, viscous dissipation dominates the irreversibility. Further, it is noted that viscous dissipation effects contribute more in case of natural convection dominated flow (see Figs. 6.9-6.11). Moreover, for large values of Br, the viscous dissipation also shows a major role even at the surface of the plate. This fact is highlighted through Fig. 6.10.

Figure 6.11 establishes the influence of inclination angle γ upon Be. An increase in inclination angle γ results to decrease the Be number. In the case of vertical plate, the involvement of viscous dissipation towards the production of entropy is prominent as compared to horizontal surface (zero gravity). Dependence of Be on ξ with the variation of $Br, \gamma,$ and α is illustrated through Figs. 6.12-6.14. Figure 6.12 indicates that in the upstream region, thermal irreversibility is dominant which gradually moves to the downstream region; the dominance of viscous dissipation is achieved with the augmentation of Br. Figure 6.13 reveals that the size of fluctuations in Be reduces by the increase of inclination angle γ. An interesting contribution of the wavy amplitude α in Be is noted through Fig. 6.14. Large wavy amplitude produces more fluctuations in velocity profile due to which velocity and temperature gradient fluctuates and consequently amplitude of Be increases.

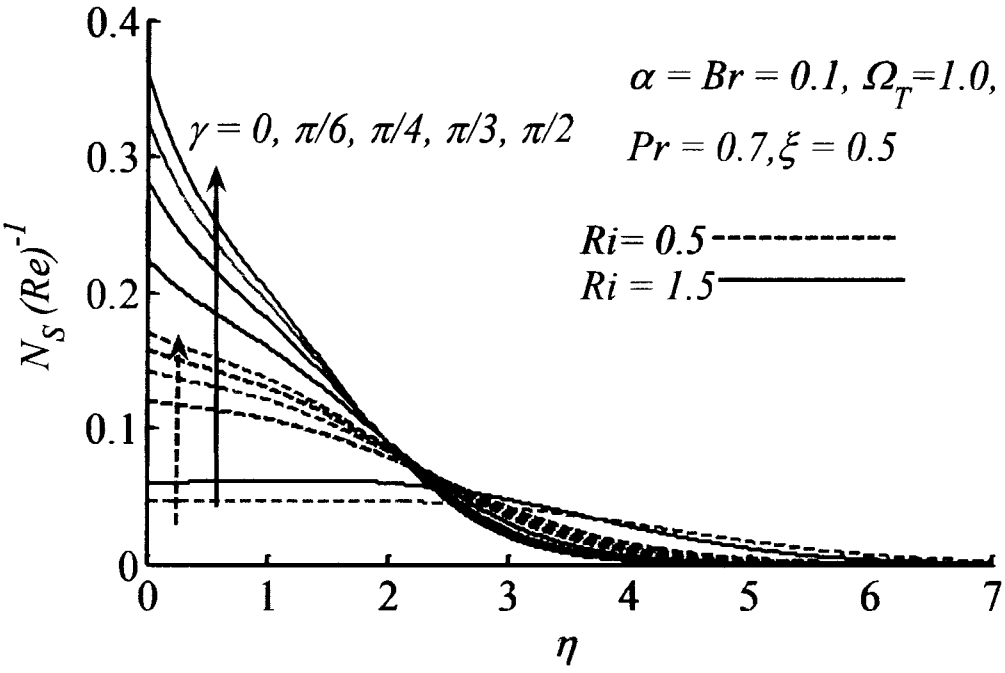

Fig. 6.2: Entropy profile against η for different γ.

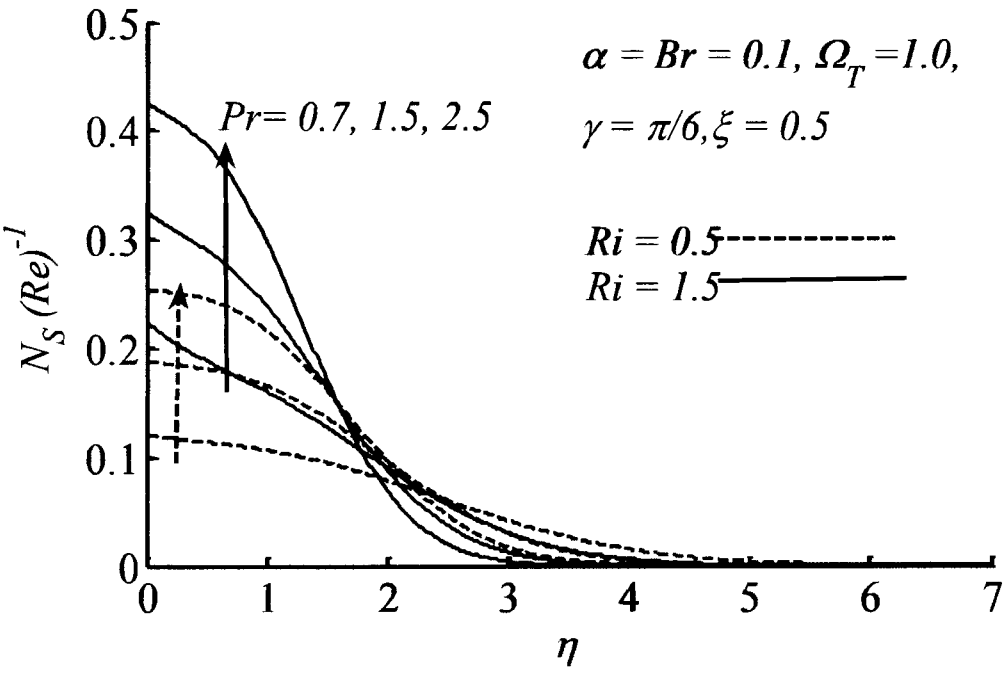

Fig. 6.3: Impact of Prandtl number on entropy generation.

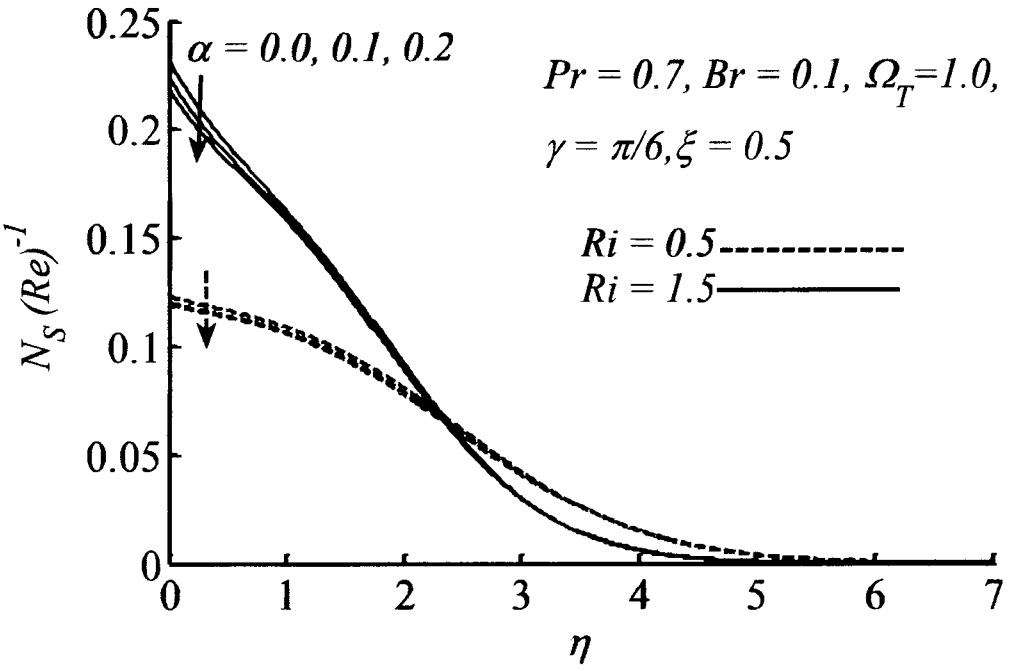

Fig. 6.4: N_s plotted against η for various values of α.

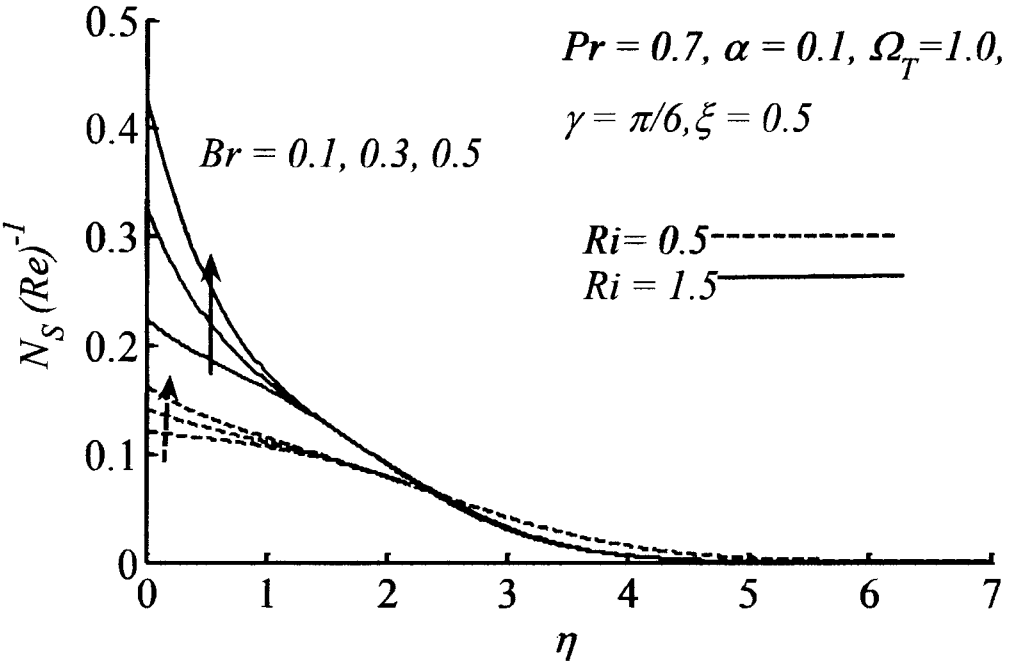

Fig. 6.5: Variation of N_s due to Brinkman number.

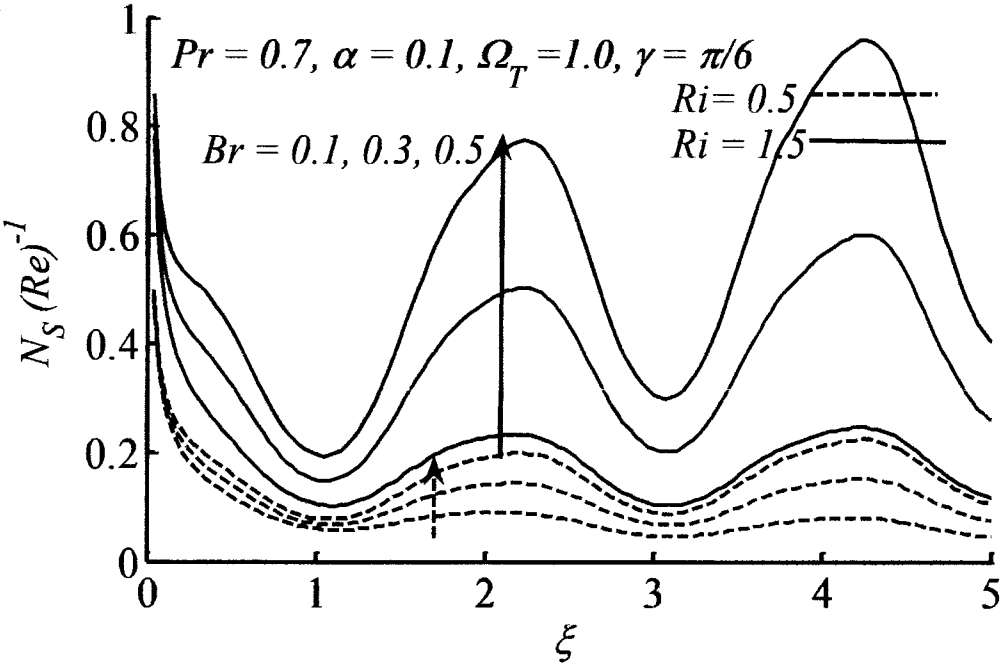

Fig. 6.6: Influence of Br on N_s when plotted against ξ.

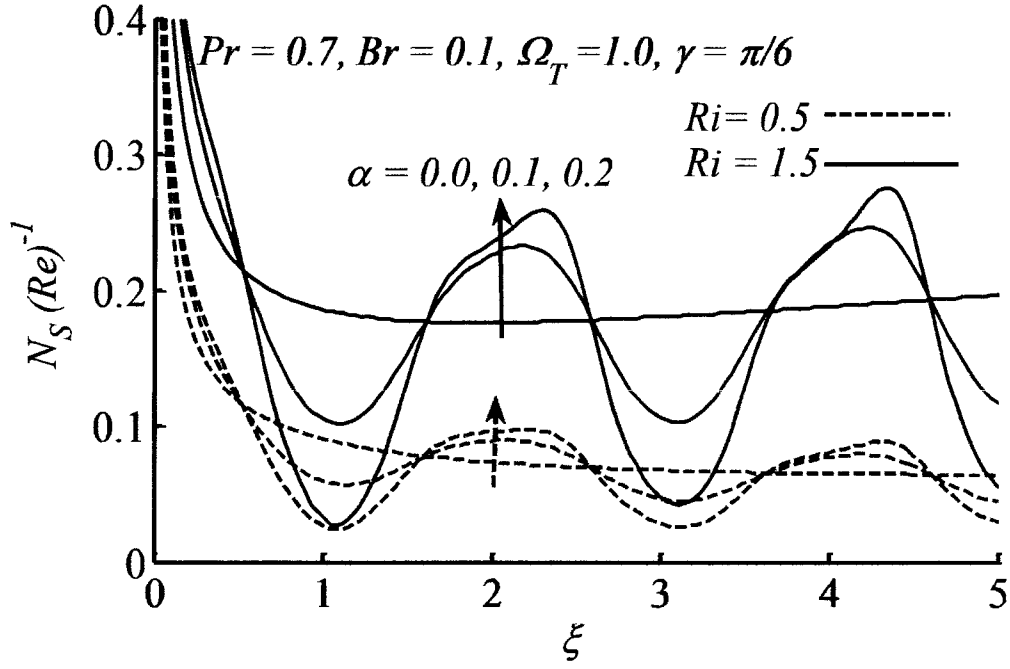

Fig. 6.7: Entropy generation number plotted against ξ for selected values of α.

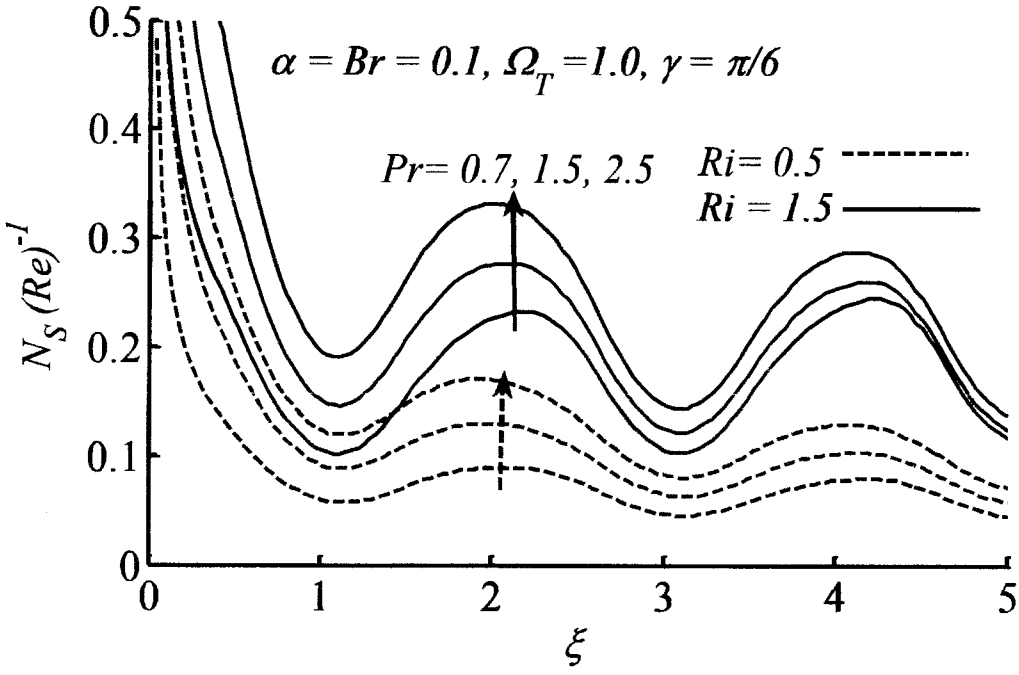

Fig. 6.8: N_s plotted against ξ for various values of Pr.

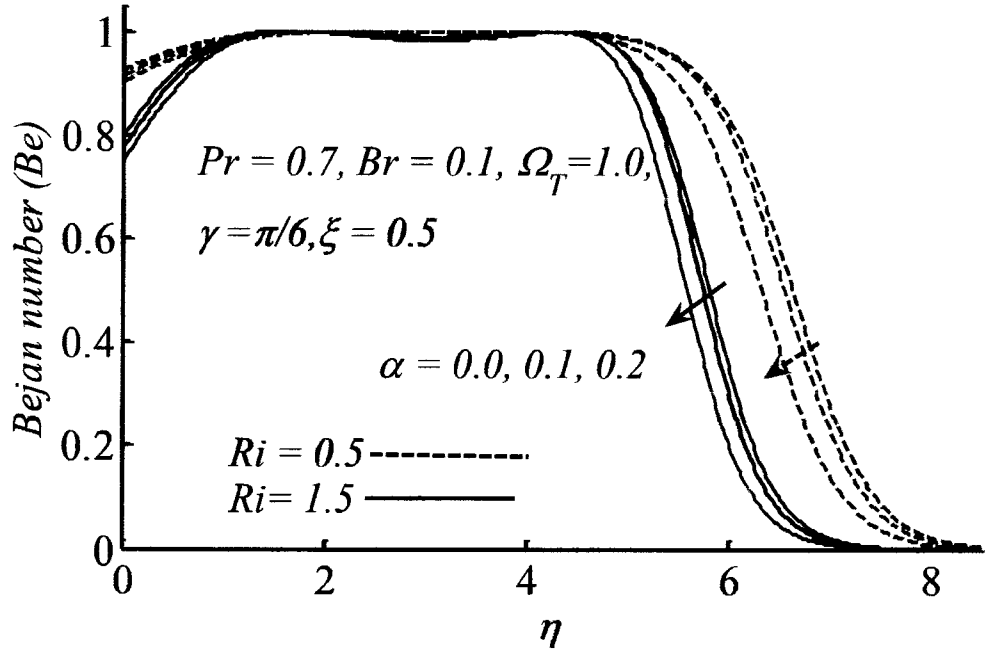

Fig. 6.9: Variation of Bejan number due to α.

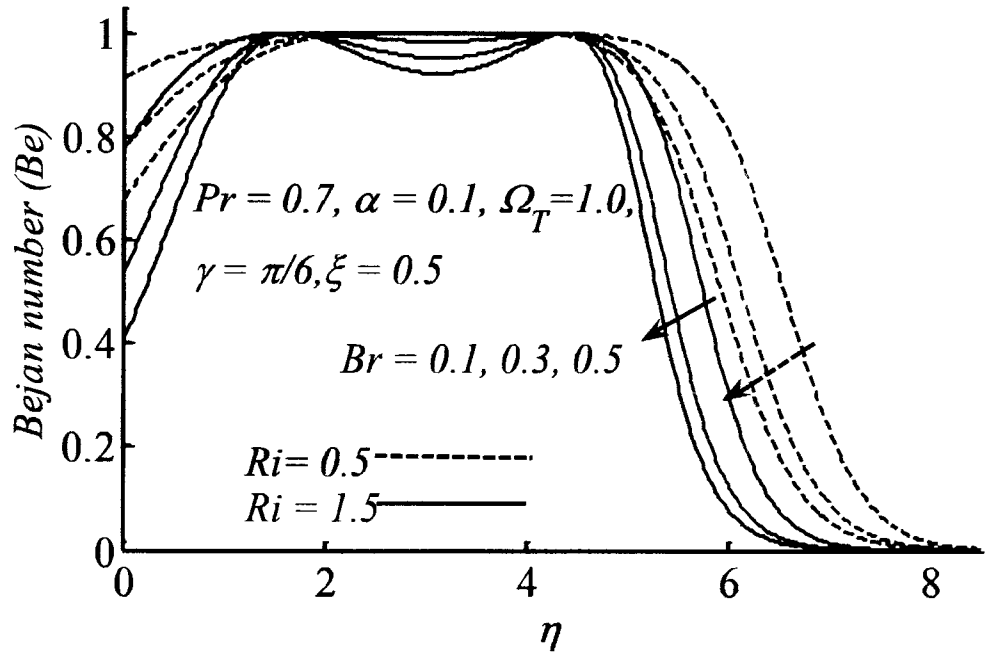

Fig. 6.10: Effects of Br on Be for two fixed values of Ri.

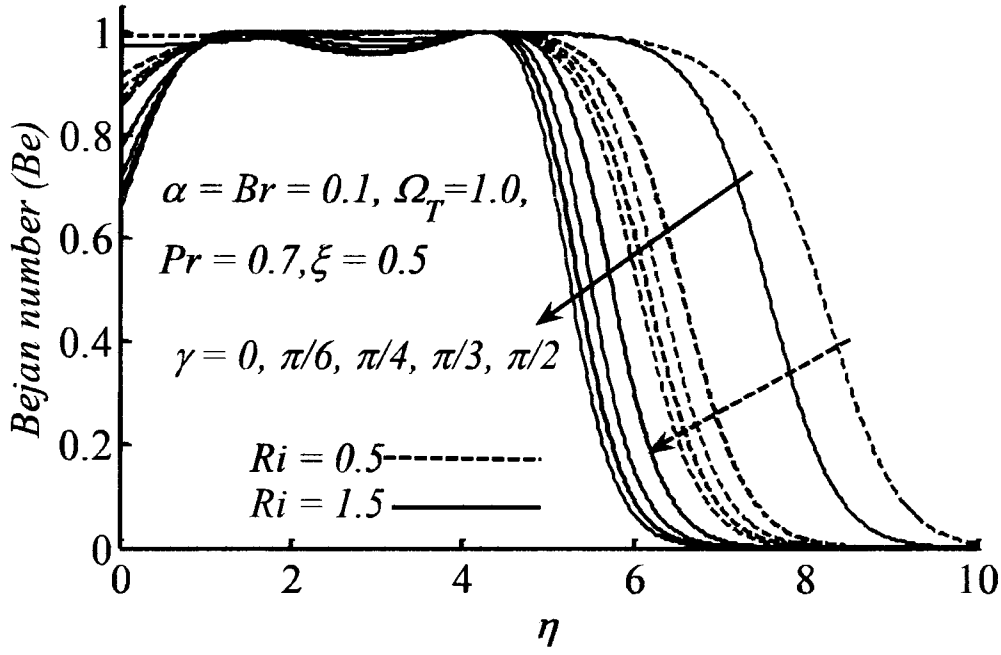

Fig. 6.11: Local Bejan number against η for selected values of γ.

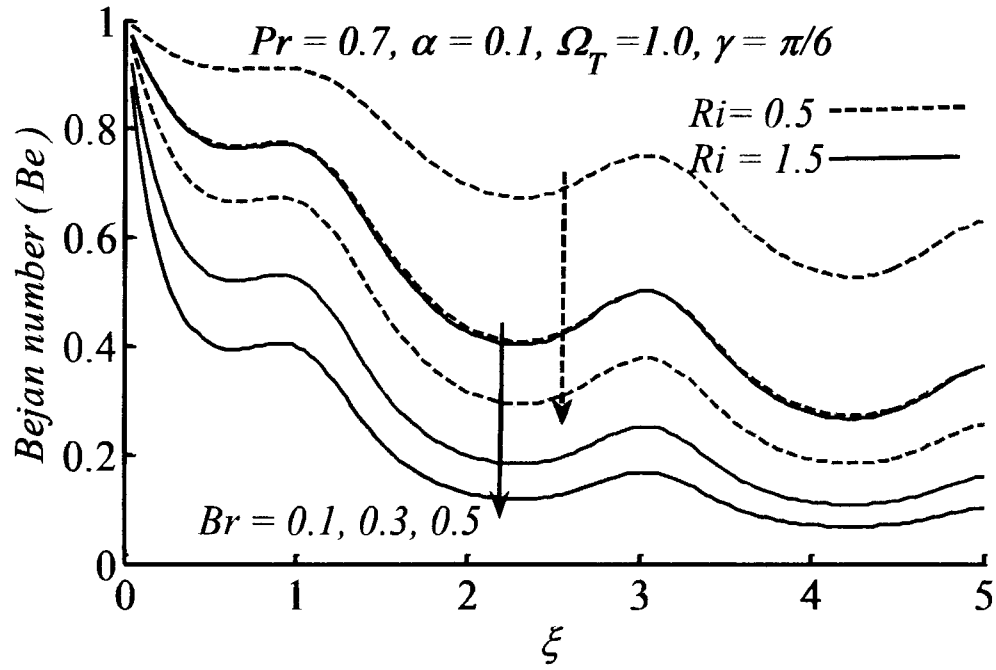

Fig. 6.12: Influence of Br on Be when plotted against ξ.

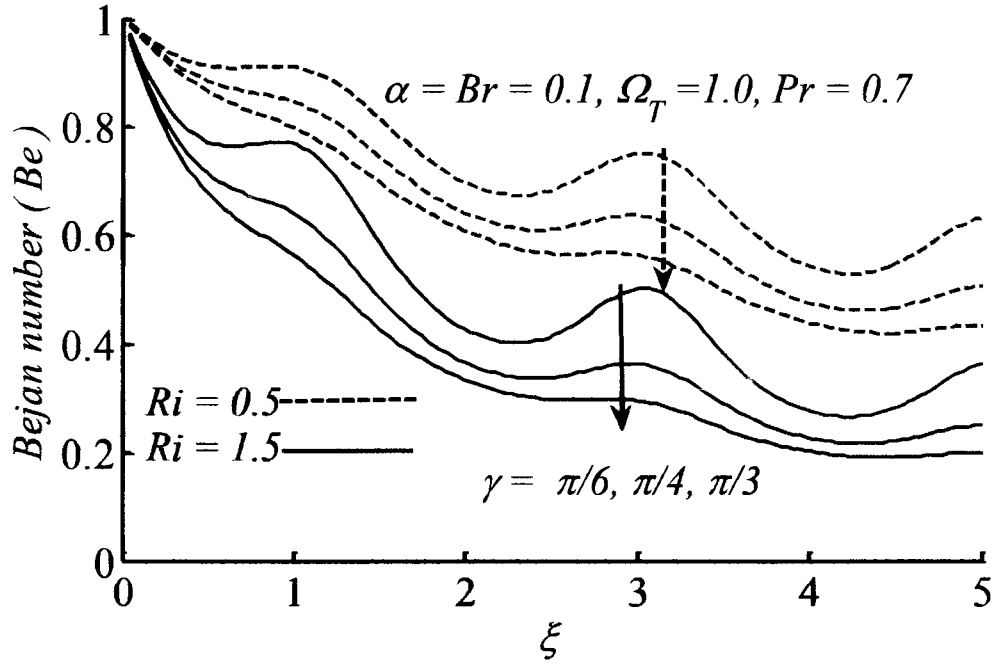

Fig. 6.13: Variation of Be with the inclination angle γ.

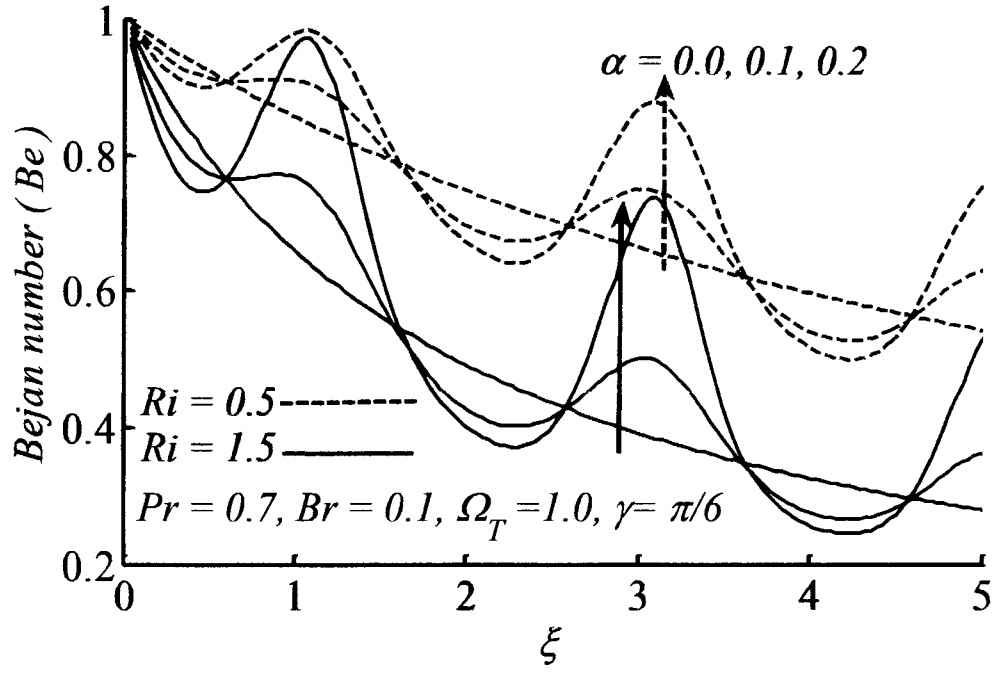

Fig. 6.14: Influence of wavy amplitude on Bejan number.

6.4 Concluding remarks

Entropy generation phenomenon for mixed convection flow upon an inclined sinusoidal plate is studied in the current chapter. An efficient implicit finite difference scheme known as Keller-Box method is employed for the solution of boundary layer equations. The involvement of physical parameters of interest in the production of entropy is elaborated through graphical pictures. It is noted that entropy production is high in the case of large values of inclination angle ($\gamma = \pi/2$) and less entropy production is noticed in the absence of gravitational force ($\gamma = 0$). Considerable variation in entropy number is noticed close to the boundary with the enhancement of viscosity of the fluid. However, for large values of Brinkman number, more entropy produces for the case of natural convection dominated flow. Thus, for the control of entropy production for any physical system of natural convection flow, consideration of forced convection

phenomenon is very much beneficial. On the other hand, Bejan number elaborates that thermal irreversibility is dominant in the upstream region and viscous irreversibility is dominant at downstream. Moreover, fluctuations in the magnitude of entropy increase with the enhancement of wavy amplitude.

Chapter 7

Numerical investigation of entropy generation in mixed convective flow past a vertical wavy cone

In this chapter the problem of entropy generation in mixed convection flow of an incompressible viscous fluid along an isothermal vertical wavy cone is investigated numerically. Analysis is performed to investigate the impact of longitudinal surface curvature on the entropy generation phenomenon in the system. Wavy surface of the cone is a fundamental reason of similarity breaking due to which the complete problem is of non-similar nature. In such kind of flow, not only the thermal transport but also the momentum transport phenomena are non-similar in nature. It is seen that the surface alteration is an easy way to manipulate the rate of entropy production. Such techniques are already in practice to enhance the thermal transport in variety of heat exchangers and are commonly known as passive techniques. The impact of involved physical parameters upon entropy production is studied and the findings regarding the minimization of the loss of useful energy have been reported. Bejan number categorizes the factor (among thermal irreversibility and viscous irreversibility) which plays a dominant role towards the production of entropy.

7.1 Mathematical formulation

Heat transfer analysis of mixed convective flow is considered along vertical wavy cone having half angle γ. The surface of the wavy cone has a temperature T_w and this temperature is higher than the surrounding temperature T_∞. The coordinate system is placed in such a way that the origin coincides with the vertex of the cone while x-axis

runs in the longitudinal direction of the wavy surface and y-axis is measured normal to the surface (see Fig.7.1). The transverse curvature contribution is negligible due to the consideration of large cone angle γ. The sinusoidal function defined in Eq. (1.13) describes the surface of the cone. Consequently, the flow is steady, two-dimensional, and axisymmetric in nature.

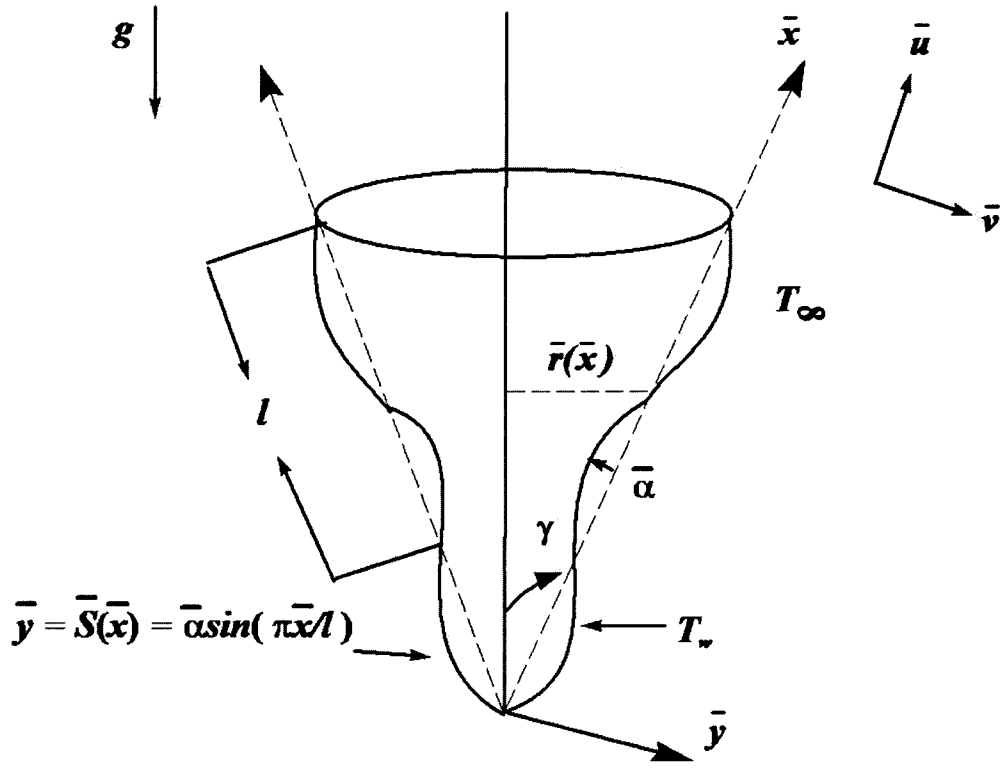

Figure 7.1: Flow geometry and coordinate system.

In view of the above assumptions and by considering the Boussinesq approximation, the physical laws (mass, momentum, and energy conservation) can be read as:

Mass

$$\frac{\partial(\bar{r}\bar{u})}{\partial\bar{x}} + \frac{\partial(\bar{r}\bar{v})}{\partial\bar{y}} = 0, \tag{7.1}$$

Momentum

$$\bar{u}\frac{\partial\bar{u}}{\partial\bar{x}} + \bar{v}\frac{\partial\bar{u}}{\partial\bar{y}} = -\frac{1}{\rho}\frac{\partial\bar{p}}{\partial\bar{x}} + \nu\nabla^2\bar{u} + g\beta(T - T_\infty)cos\gamma, \tag{7.2}$$

$$\bar{u}\frac{\partial \bar{v}}{\partial \bar{x}} + \bar{v}\frac{\partial \bar{v}}{\partial \bar{y}} = -\frac{1}{\rho}\frac{\partial \bar{p}}{\partial \bar{y}} + \nu\nabla^2\bar{v} - g\beta(T - T_\infty)sin\gamma, \tag{7.3}$$

Energy

$$\bar{u}\frac{\partial T}{\partial \bar{x}} + \bar{v}\frac{\partial T}{\partial \bar{y}} = \frac{k}{\rho C_p}\nabla^2 T, \tag{7.4}$$

where $\bar{r}(\bar{x}) = \bar{x}sin\gamma$ is the local radius of the cone and γ denote the half angle of the cone. The boundary conditions are described by the Eq. (5.5). For the sake of non-dimensionalization of the system, the set of variables given in Eq. (5.6) is utilized. In view of the geometry of the cone the nature of flow allows to consider the stream function ψ such that $ru = \partial\psi/\partial y, rv = -\partial\psi/\partial\xi$. Thus the dimensionless form of Eqs. (7.2)-(7.4) in the form of stream function (after eliminating the pressure-gradient) can be expressed as:

$$\begin{aligned}\frac{1}{r}\frac{\partial\psi}{\partial y}\frac{\partial}{\partial\xi}\left(\frac{1}{r}\frac{\partial\psi}{\partial y}\right) - \frac{1}{r}\frac{\partial\psi}{\partial\xi}\frac{\partial}{\partial y}\left(\frac{1}{r}\frac{\partial\psi}{\partial y}\right) \\ = \left(1+\sigma_\xi^2\right)\frac{\partial^2}{\partial y^2}\left(\frac{1}{r}\frac{\partial\psi}{\partial y}\right) - \frac{\sigma_\xi\sigma_{\xi\xi}}{\left(1+\sigma_\xi^2\right)}\left(\frac{1}{r}\frac{\partial\psi}{\partial y}\right)^2 \\ + \frac{\left(1-\sigma_\xi tan\gamma\right)cos\gamma Ri}{1+\sigma_\xi^2}\theta,\end{aligned} \tag{7.5}$$

$$\frac{1}{r}\frac{\partial\psi}{\partial y}\frac{\partial\theta}{\partial\xi} - \frac{1}{r}\frac{\partial\psi}{\partial\xi}\frac{\partial\theta}{\partial y} = \frac{k}{\mu c_p}\left(1+\sigma_\xi^2\right)\frac{\partial^2\theta}{\partial y^2}, \tag{7.6}$$

where the boundary-layer assumption ($Re \to \infty$) has also been implemented. The dominant forced convection flow occurs for the range ($0 < Ri < 1$), which eventually becomes pure forced convection when Ri equals to zero. The flow is completely a natural convection flow when $Ri \to \infty$. Moreover, it is clear from the definition of mixed convection parameter that the mixed convection flow occurs when Ri near or equal to 1. In order to write the above system of equations in a more convenient form we use the following transformations:

$$\psi(\xi,\eta) = r\xi^{3/4} f(\xi,\eta), \qquad \eta = \xi^{-1/4} y, \qquad \theta = \theta(\xi,\eta). \tag{7.7}$$

In view of Eq. (7.7), Eqs. (7.5)-(7.6) and the boundary data have the form:

$$(1+\sigma_\xi^2) f''' + \frac{7}{4} f f'' - \left(\frac{1}{2} + \frac{\xi \sigma_\xi \sigma_{\xi\xi}}{1+\sigma_\xi^2}\right) f'^2 + \frac{(1-\sigma_\xi \tan\gamma)\cos\gamma Ri}{1+\sigma_\xi^2}\theta = \xi\left[f'\frac{\partial f'}{\partial \xi} - f''\frac{\partial f}{\partial \xi}\right], \tag{7.8}$$

$$\frac{1}{Pr}(1+\sigma_\xi^2)\theta'' + \frac{7}{4} f\theta' = \xi\left[f'\frac{\partial \theta}{\partial \xi} - \theta'\frac{\partial f}{\partial \xi}\right], \tag{7.9}$$

$$f(\xi,0) = 0,\ f'(\xi,0) = 0, \theta(\xi,0) = 1, f'(\xi,\infty) = 1, \theta(\xi,\infty) = 0. \tag{7.10}$$

The local-skin friction coefficient and the local Nusselt number are given by

$$C_{fx} = \frac{\tau_w}{\rho U^2},\ Nu_x = \frac{\bar{x} q_w}{k(T_w - T_\infty)}, \tag{7.11}$$

where τ_w is the wall shear stress and q_w is the wall heat flux which are given as

$$\tau_w = \mu(\nabla \bar{u} \cdot \hat{n})_{y=0},\ q_w = -k(\nabla T \cdot \hat{n})_{y=0}, \tag{7.12}$$

in which $\hat{n}$ is the unit normal to the wavy surface. After using Eqs. (5.6), (7.7) and (7.12), the physical quantities of interest given in Eq. (7.11) take the form

$$C_f = C_{fx}(\mathrm{Re}/_x)^{1/4} = \sigma f''(\xi,0),\ Nu = Nu_x(\mathrm{Re}x^3)^{-1/4} = -\sigma\,\theta'(\xi,0). \tag{7.13}$$

7.2 Entropy analysis

Consider the local entropy generation phenomenon for incompressible viscous fluid flow in mixed convection heat transfer process. Since the fluid is viscous and obeys Fourier's law of heat conduction, the expression for entropy production in two dimensions is defined by the Eq. (2.16). Using Eq. (5.6) and the stream function in Eq. (2.16), we obtain the following form of volumetric rate of entropy production

$$S_G = \frac{Re\Delta T^2 \kappa}{l^2 T_\infty^2}\left[\left(1+\sigma_\xi^2\right)\left(\frac{\partial\theta}{\partial y}\right)^2\right] + \frac{\mu U^2 Re}{T_\infty l^2 r^2}\left[\left(1+\sigma_\xi^2\right)^2\left(\frac{\partial^2\psi}{\partial y^2}\right)^2\right]. \quad (7.14)$$

The non-dimensional entropy generation is achieved due to the utilization of characteristic entropy $S_{G_0} = \kappa_f(\Omega_T/l)^2$ and Eq. (7.7), as

$$\frac{N_s}{Re} = \frac{S_G}{S_{G_0}} = \frac{\left(1+\sigma_\xi^2\right)}{\sqrt{\xi}}\theta'^2 + \frac{Br}{\Omega_T}\left(1+\sigma_\xi^2\right)^2\sqrt{\xi}f''^2. \quad (7.15)$$

Since Eq. (7.14) demonstrates that for the production of entropy in any engineering system, existence of velocity and temperature gradients is essential. Moreover, for the analysis of entropy production this expression is fine, but it does not expose that which factor (among these two) is dominant. Bejan number (Be) effectively handles the above-mentioned problem and easily characterizes the dominance of thermal irreversibility or the viscous irreversibility during the process of entropy generation. Bejan number (Be) takes the following form for the current study

$$Be = \frac{\left(1+\sigma_\xi^2\right)\theta'^2}{\left(1+\sigma_\xi^2\right)\theta'^2 + \frac{Br}{\Omega_T}\left(1+\sigma_\xi^2\right)^2\xi f''^2}. \quad (7.16)$$

7.3 Numerical scheme and validation of results

In this section the entropy generation phenomenon has been discussed in detail with the help of graphs. For this purpose, the non-linear boundary layer system with the respective boundary conditions has been solved with the aid of Keller-Box method [136, 139]. The obtained solution is then utilized in Eqs. (7.15) and (7.16) to get the information about the entropy generation number and Bejan number. A comparison with the data available in literature has been made. Table 7.1 gives the comparison of the current results of skin- friction coefficient and Nusselt number with the result

published by Roy [144], and Yih [145]. It shows an excellent agreement which authenticates the present numerical procedure.

Table 7.1: Comparison with the existing data for $f''(0,0)$ and $-\theta'(0,0)$ when $\alpha = \xi = \gamma = 0$.

Pr	$f''(0,0)$			$-\theta'(0,0)$		
	Present	Roy[144]	Yih[145]	Present	Roy[144]	Yih[145]
1	0.76943	0.8600	0.7699	0.51040	0.5275	0.5109
10	0.48770	0.4899	0.4877	1.03399	1.0354	1.0339
100	0.28963	0.2897	0.2896	1.92285	1.9229	1.9226
1000	0.16615	0.1661	0.1661	3.47017	3.4700	3.4696
10000	0.09404	0.0940	0.0940	6.20068	6.1998	6.1984

7.4 Results and discussion

The contribution of the involved physical parameters on the flow phenomenon is examined with the help of several graphs. Before going to the entropy analysis of this flow it is felt convenient to give the velocity and temperature profiles first. This will indeed help to understand the on-going entropy production phenomenon. Figures 7.2-7.3 are the velocity and temperature profiles under the influence of cone half angle (γ), the Prandtl number (Pr), wavy amplitude (α), and the Richardson number (Ri). Clearly, the velocity profile due to Ri and γ augments while the opposite behavior of velocity profile is observed by the increments in α and Pr, as depicted in Fig. 7.2. Figure 7.3 depicts the depreciation of thermal boundary layer due to the augmentation of all these physical parameters. Entropy number is plotted against η in Fig. 7.4 with the variation of γ, Pr, α , and Ri. It is noted that N_s increases with the augmentation of γ, Pr, and Ri while the entropy generation minimizes with the enhancement of wavy amplitude α. This behavior of N_s is more prominent close to the boundary while the generation of irreversibility diminishes in the free-stream region. Physically, those engineering devices which have large wavy amplitude can be chosen to reduce the

losses of useful energy. Moreover, this graph signifies that entropy production is high for the flow due to free convection ($Ri > 1$) as compared to forced convection flow ($Ri < 1$). Thus, irreversibility effects in free convection phenomenon can be reduced by including a forced flow. Moreover, entropy production along a cone geometry can be minimized by taking some small values of inclination cone half angle γ.

Entropy number against ξ is plotted through Fig. 7.5 with the variation of wavy amplitude α. Results show that the entropy production is higher for large Ri (natural convection flow) as compared to small Ri (forced convection dominated flow). Large values of Ri indicate the dominance of buoyancy forces where large irreversibility effects are observed as a consequence. Moreover, the fluctuations in N_s layer are more prominent with the augmentation of α. Figure 7.6 explores the impact of inclination half angle γ on entropy generation number. Graphical results show that entropy generation number fluctuates in downstream direction having increasing amplitudes with the increase of cone half angle γ. Entropy generation as a function of wavy amplitude α is plotted for different γ in Fig. 7.7 for two different characters of Ri. Overall, the dependence of N_s upon γ for small values of wavy amplitude α is not much prominent, but for the increasing value of α significant dependence of N_s upon γ is seen. Moreover, it is also observable that N_s increases with the increase in values of α. In Fig. 7.8, N_s is plotted against γ for different values of α. A linear dependence of N_s upon γ is obvious from this figure. N_s is an increasing function of Ri as seen from all its graphs.

To categorize the involvement of the viscosity and the temperature gradient of the fluid towards the production of entropy, Bejan number is depicted through Figs. 7.9-7.12. In Fig. 7.9 Bejan number is plotted against η for various values of cone half angle (γ), Prandtl number (Pr), wavy amplitude (α), and Richardson number (Ri). Results show

that under the influence of these physical parameters Be approaches to 1 in the near wall region which highlights that the irreversibility in the system is dominated due to thermal irreversibility. Bejan number decreases monotonically and approaches to its minimum value (which is 0) as we move away from surface. Consequently, entropy production totally depends upon viscous dissipation. In the main flow region reduction in Be occurs by an increment of Ri, which means that in a natural convection dominated flow, the production of entropy is totally dependent on the viscosity of the fluid. Similar trend can also be seen with the variation of Pr and γ. With the augmentation of wavy amplitude α, Bejan number increases in the main flow region. Bejan number is plotted against ξ in Fig. 7.10. An interesting role of α on Be is observed from here. The fluctuations in the Bejan number are of very small amplitude in the upstream region which significantly develop at the downstream locations. Similar trend of Be is also depicted through Fig. 7.11 plotted by the alteration of γ. Bejan number is plotted against cone half angle γ with the enhancement of α through Fig. 7.12. It is interesting to note that the variation in Be is more significant with the variation of α in case of small cone half angle and the dependence of Be on α becomes weaker for the large values of γ.

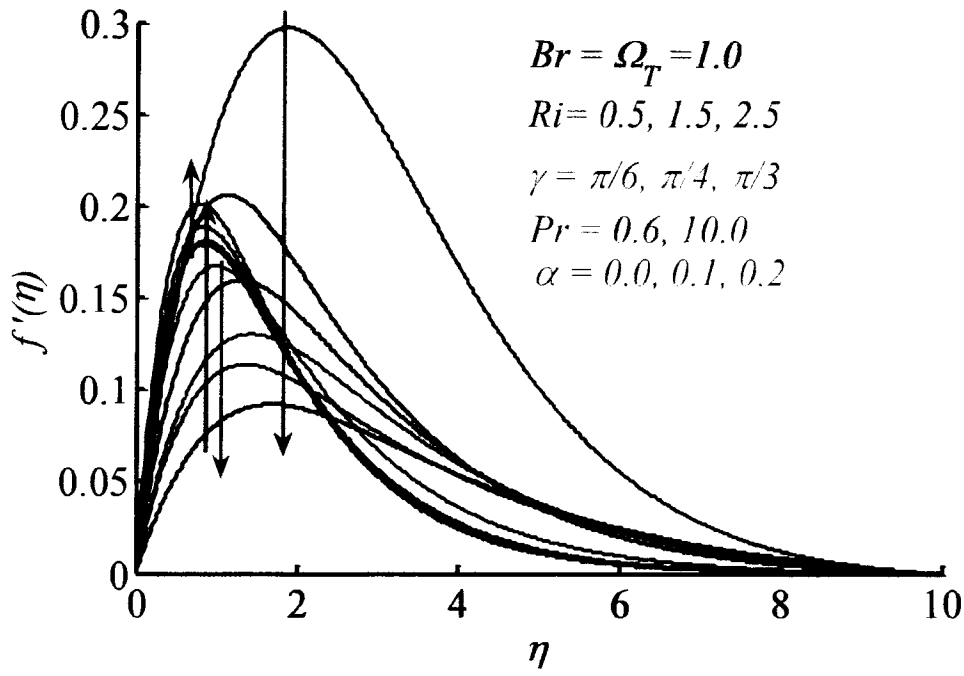

Fig. 7.2: Velocity profile plotted against η.

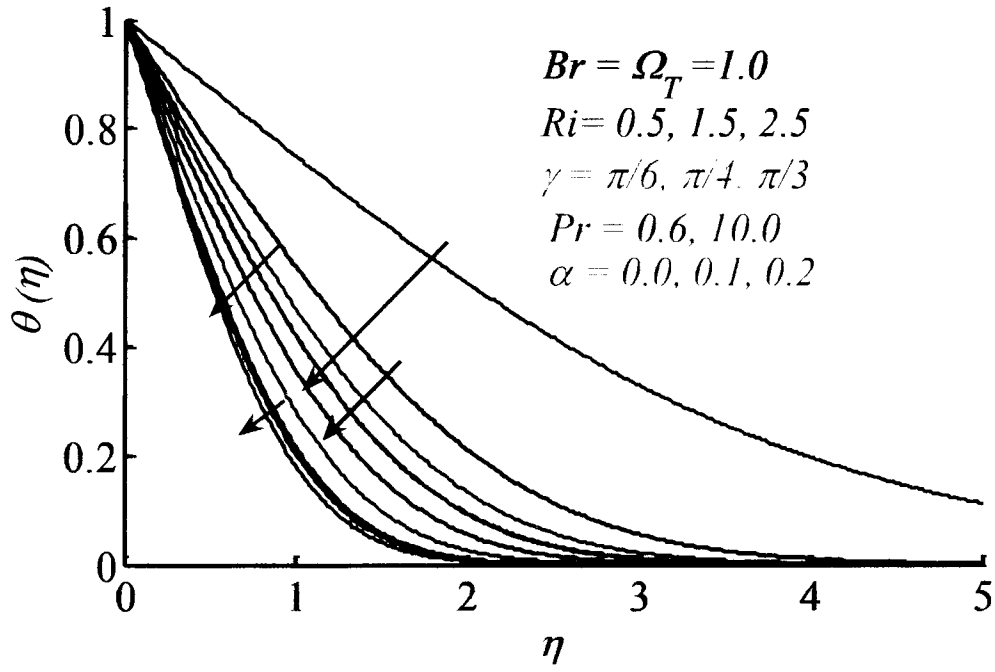

Fig. 7.3: Temperature profile plotted against η.

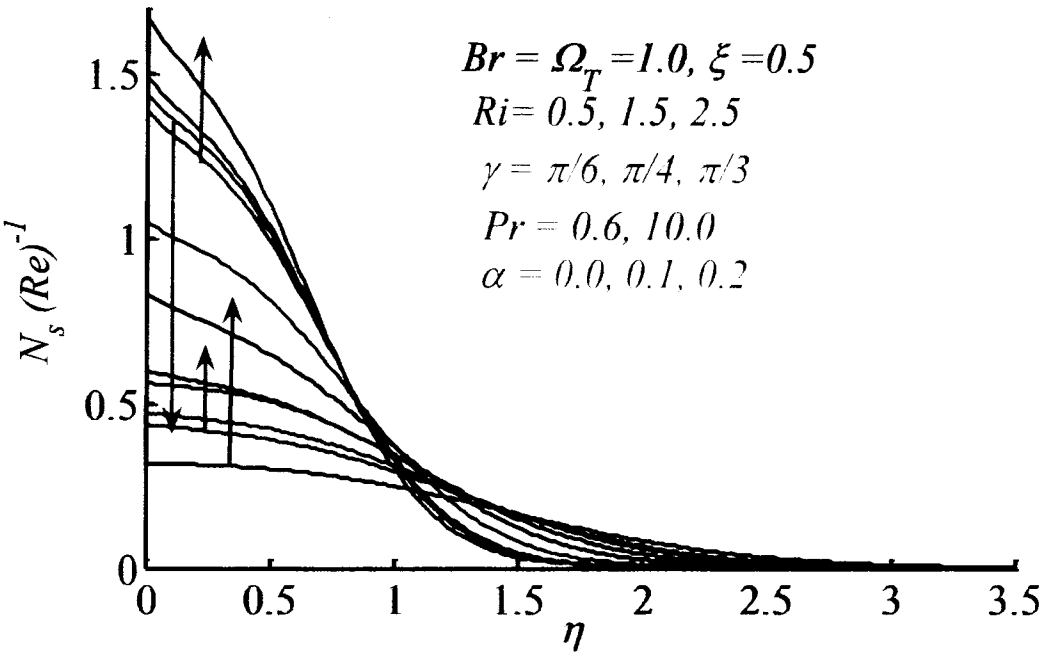

Fig. 7.4: Impact of Ri, α, γ, and Pr on N_s at $\xi = 0.5$.

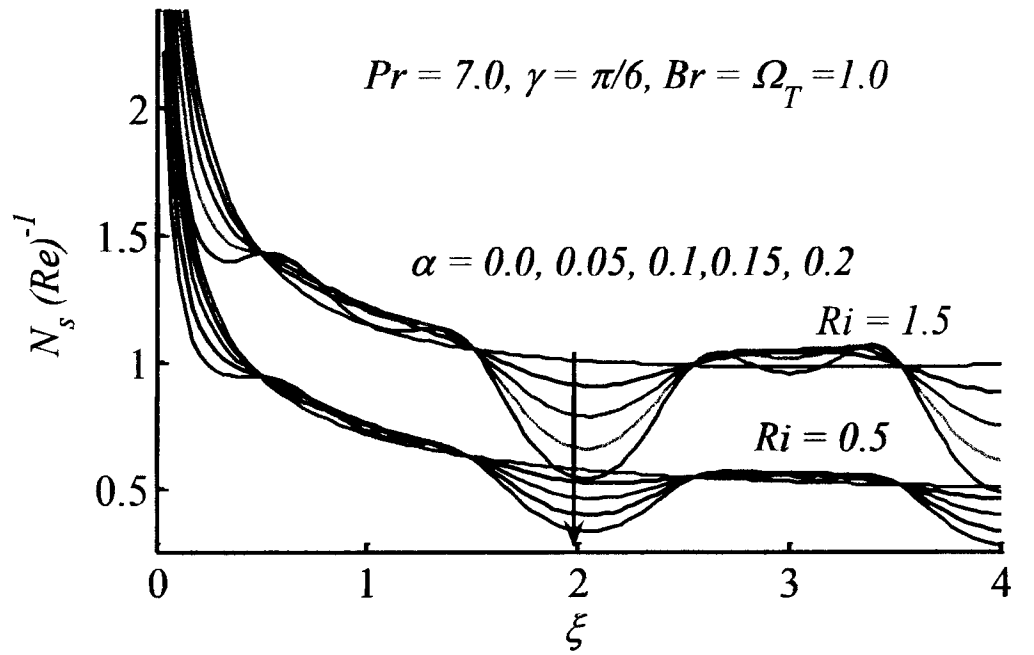

Fig. 7.5: N_s plotted against ξ for selected values of α.

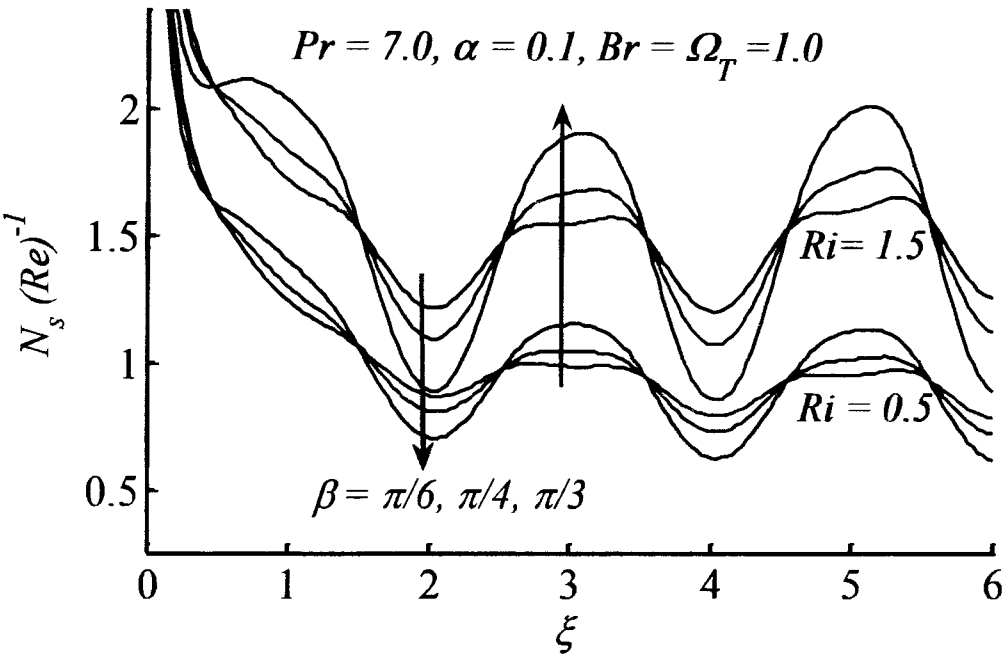

Fig. 7.6: Impact of cone half angle γ on N_s when plotted against ξ.

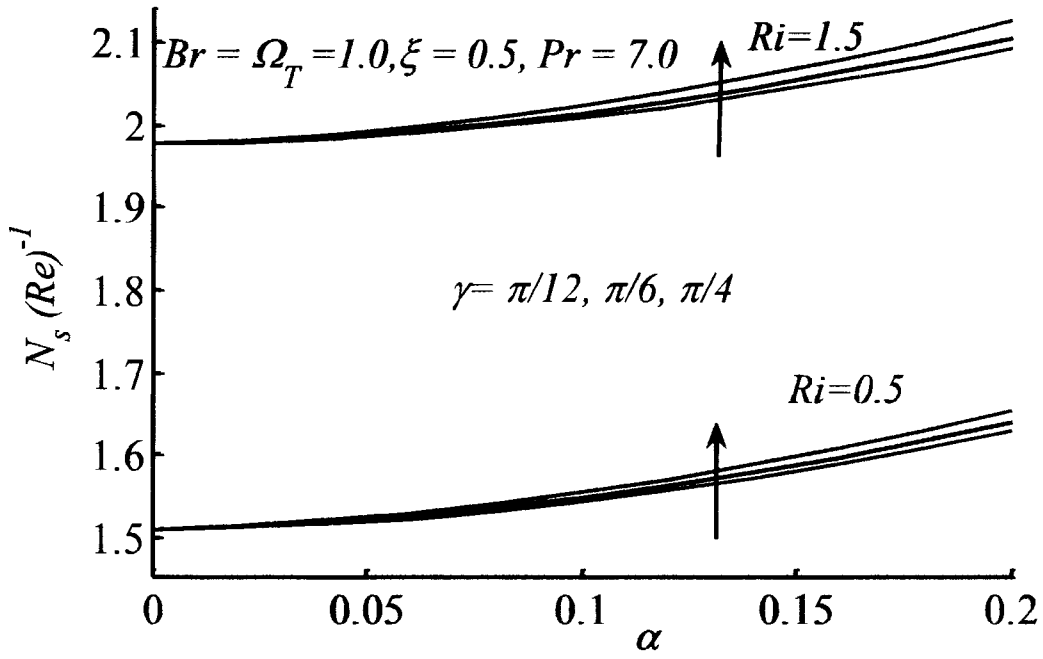

Fig. 7.7: Entropy generation number plotted against α for different γ.

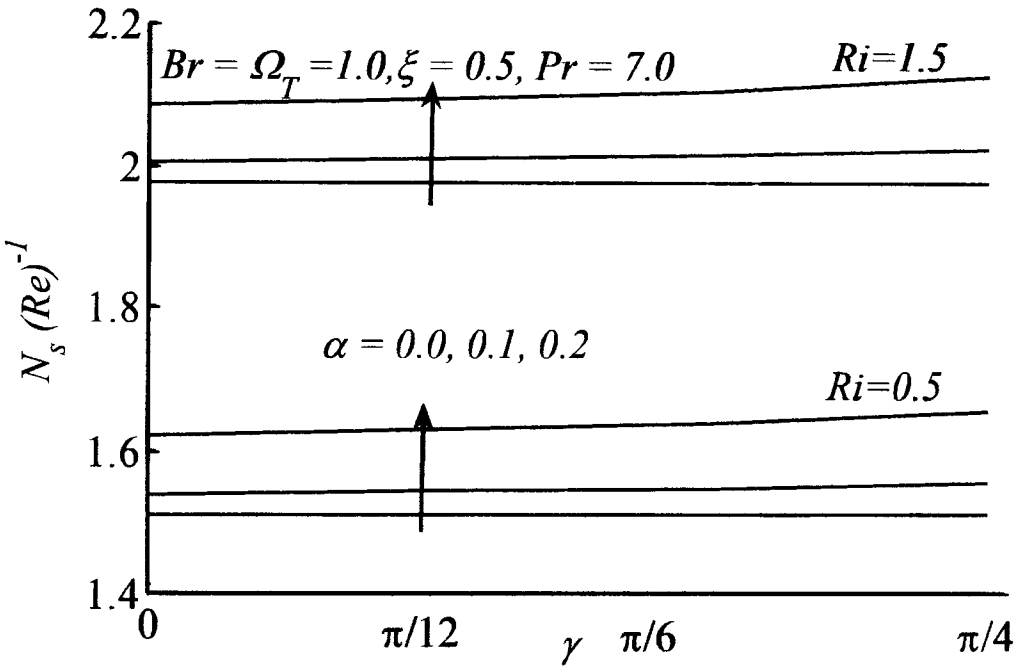

Fig. 7.8: N_s profile against γ for various values of α.

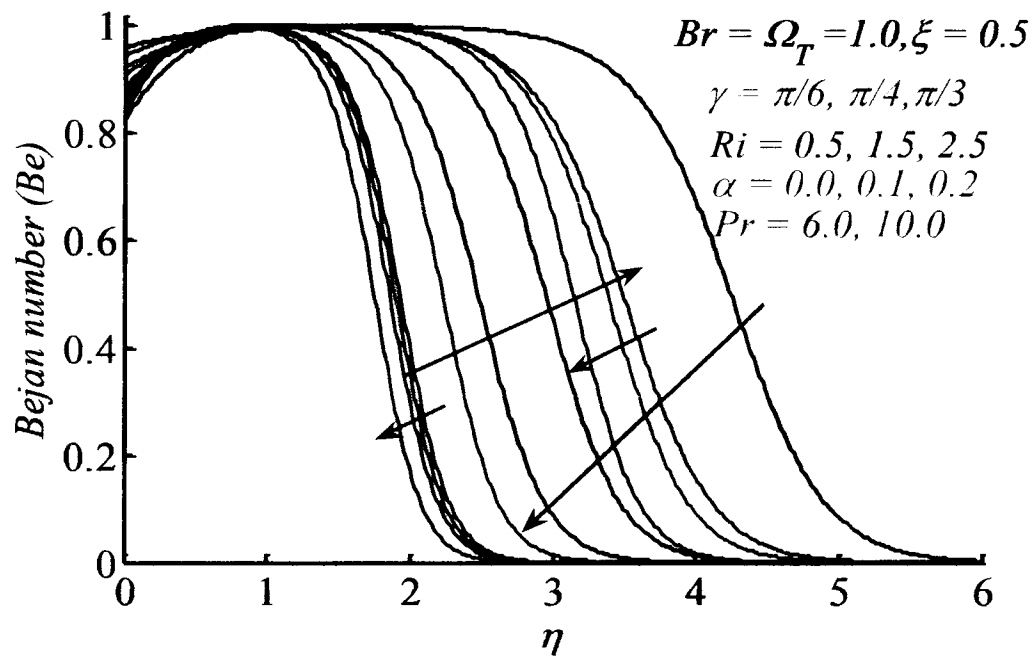

Fig. 7.9: Dependence of local Bejan number on $Ri, \gamma, \alpha,$ and Pr.

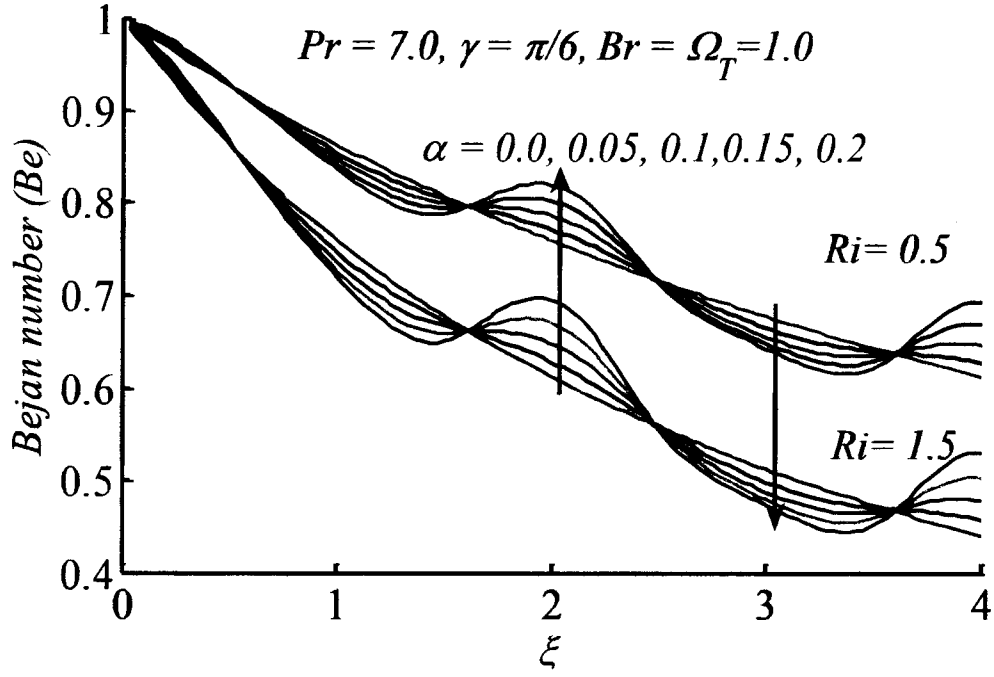

Fig. 7.10: *Be* plotted against ξ with the variation of α.

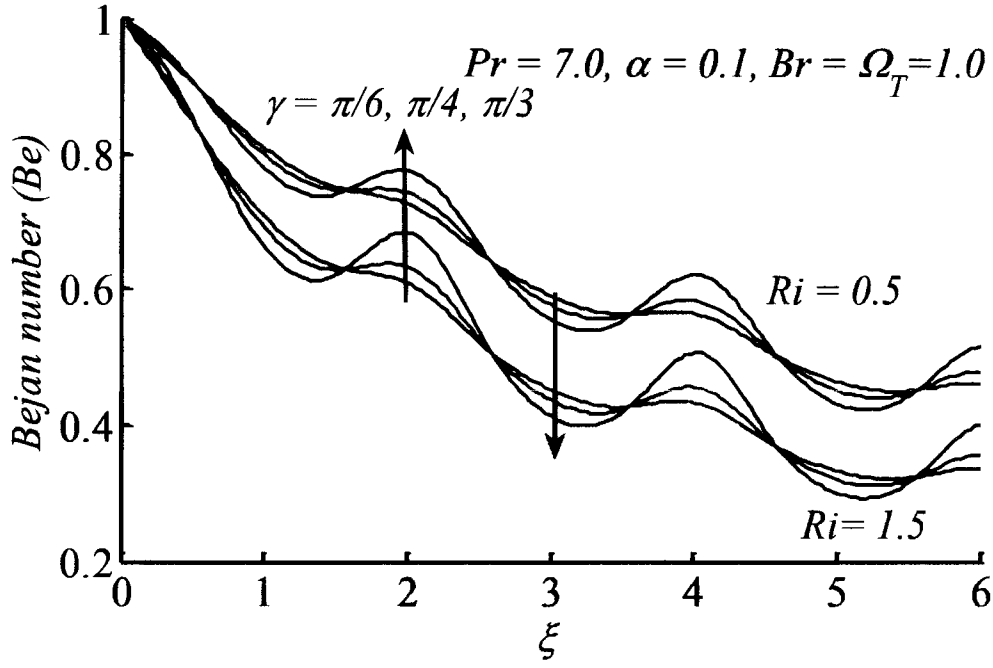

Fig. 7.11: Local Bejan number plotted against ξ for different γ.

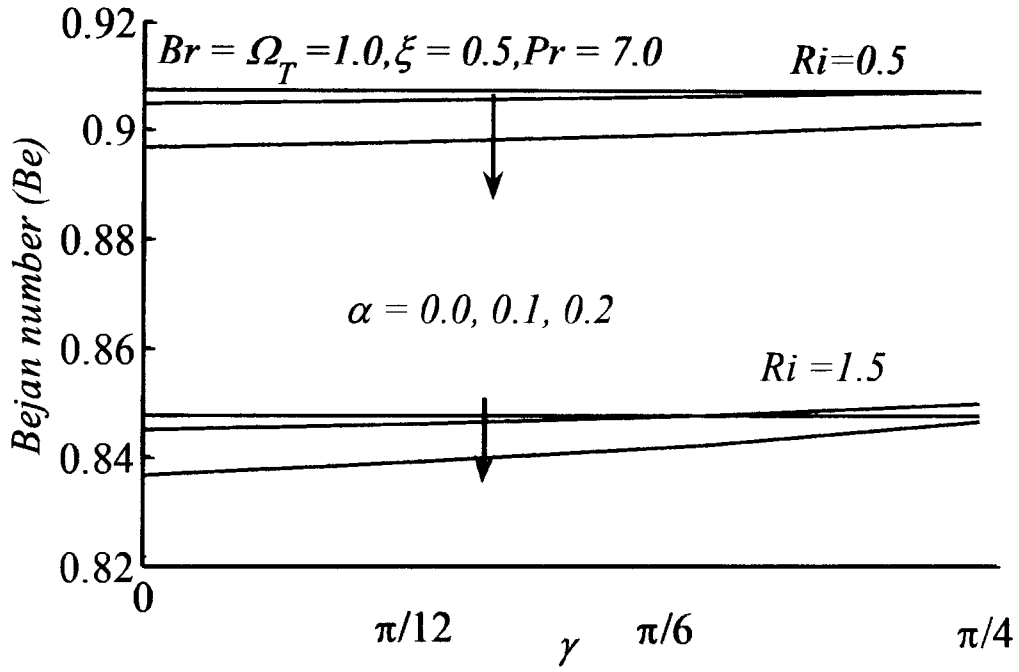

Fig. 7.12: Influence of wavy amplitude on *Be* when plotted against γ.

7.5 Final remarks

In the current analysis, entropy generation in a mixed convection boundary layer flow of viscous fluid over a heated wavy cone is studied. For the solution of the boundary layer equations implicit finite difference scheme has been implemented. The role of physical parameters on the production of entropy is examined. It is noted that the amplitude of the wavy surface contributes a major role in the minimization of the production of entropy. On the other hand, an increase in the cone half angle γ contributes to increase the entropy production. Furthermore, it is worth mentioning that the production of entropy reduces when we consider the small values of Richardson number. Thus, for any physical system of natural convection flow, consideration of forced convection phenomenon is useful. Bejan number assures that in the case of buoyancy driven natural convection flow, the major contributor towards the entropy generation is the viscous dissipation.

Chapter 8

Entropy generation analysis over a disk of sinusoidal wavy texture rotating in a viscous fluid

Entropy generation analysis of the flow and heat transfer over an infinite wavy disk is the objective of the current chapter. The wavy disk rotates about its axis due to which the flow over the disk is axisymmetric. The surface of the disk is taken of sinusoidal shape due to which a significant alteration in the heat transfer rate occurs. Due to such kind of surface texture of the disk, the flow becomes non-similar. The primary objective of the present study is to explore that how does the phenomenon of entropy generation is affected due to a wavy texture of the rotating disk. The disk surface preserves at constant wall temperature (CWT) or constant heat flux (CHF). The involvement of the physical parameters in the entropy generation function has been examined in detail and the findings are deliberated with the help of various graphs. Findings explore that the surface roughness plays a substantial role towards the minimization of entropy production.

8.1 Mathematical formulation

Consider an incompressible viscous fluid over a rotating disk of infinite radius. The disk rotates in a fixed frame with rotation rate Ω^*. The texture of the disk surface is taken of sinusoidal shape and is defined by a differentiable function $z^* = S^*(r^*) = \bar{\alpha}\cos\left(\frac{2\pi r^*}{l}\right)$ as seen in Fig. 8.1 where $\bar{\alpha}$ is the amplitude and l is the wavelength of the wavy texture. The wavelength to amplitude ratio is kept small to make the boundary layer assumption valid and to avoid flow separation.

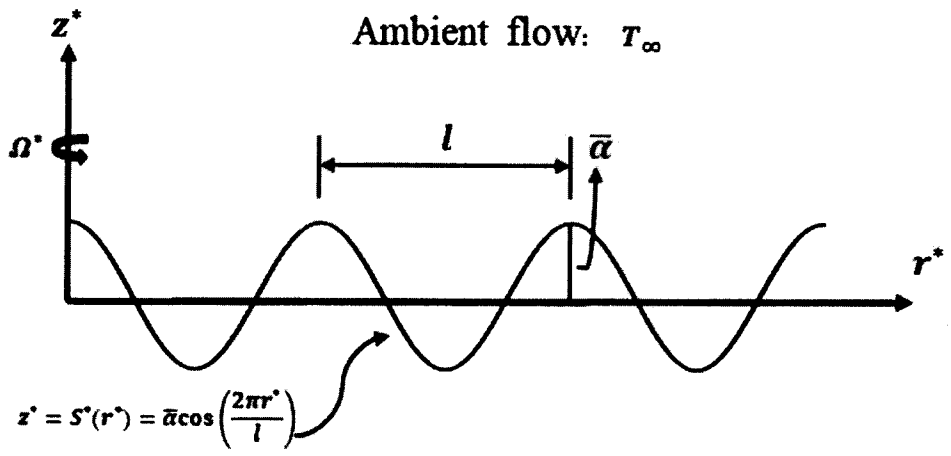

Figure 8.1: Flow geometry and coordinate system.

The governing equations are achieved in cylindrical coordinates (r^*, θ^*, z^*) in which r^* is taken along the surface and z^* is orthogonal to the surface. The governing conservation laws in cylindrical coordinates read as:

Mass

$$\frac{1}{r}\frac{\partial(ru)}{\partial r} + \frac{\partial w}{\partial z} = 0, \tag{8.1}$$

Momentum

$$u\frac{\partial u}{\partial r} - \frac{v^2}{r} + w\frac{\partial u}{\partial z} = -\frac{\partial p}{\partial r} + Re^{-1}\left[\frac{1}{r}\frac{\partial}{\partial r}\left(r\frac{\partial u}{\partial r}\right) + \frac{\partial^2 u}{\partial z^2} - \frac{u}{r^2}\right], \tag{8.2}$$

$$u\frac{\partial v}{\partial r} + \frac{uv}{r} + w\frac{\partial u}{\partial z} = Re^{-1}\left[\frac{1}{r}\frac{\partial}{\partial r}\left(r\frac{\partial v}{\partial r}\right) + \frac{\partial^2 v}{\partial z^2} - \frac{v}{r^2}\right], \tag{8.3}$$

$$u\frac{\partial w}{\partial r} + w\frac{\partial w}{\partial z} = -\frac{\partial p}{\partial z} + Re^{-1}\left[\frac{1}{r}\frac{\partial}{\partial r}\left(r\frac{\partial w}{\partial r}\right) + \frac{\partial^2 w}{\partial z^2}\right], \tag{8.4}$$

Energy

$$u\frac{\partial \theta}{\partial r} + w\frac{\partial \theta}{\partial z} = \frac{k}{\rho C_p}Re^{-1}\left[\frac{1}{r}\frac{\partial}{\partial r}\left(r\frac{\partial \theta}{\partial r}\right) + \frac{\partial^2 \theta}{\partial z^2}\right]. \tag{8.5}$$

The boundary data for the specified flow in the case of constant wall temperature (CWT) are written as

$$\begin{gathered} u = w = 0, \quad v = r, \quad \theta = 1, \quad \text{at} \quad z = \alpha\cos(2\pi r), \\ u = v = \theta = 0 \quad \text{as} \quad z \to \infty. \end{gathered} \tag{8.6a,b}$$

In the case of constant heat flux (CHF) at the boundary, the thermal boundary condition in Eq. (8.6a) is replaced by

$$\frac{\partial \theta}{\partial n} = -l\left(\frac{\Omega^*}{\nu}\right)^{1/2}, \qquad \text{at} \quad z = \alpha\cos(2\pi r). \tag{8.7}$$

In the above dimensionless system, the following dimensionless variables are used:

$$r = \frac{r^*}{l}, z = \frac{z^*}{l}, u = \frac{u^*}{\Omega^* l}, v = \frac{v^*}{\Omega^* l}, w = \frac{w^*}{\Omega^* l}, p = \frac{p^*}{\rho\Omega^{*2} l^2}, \alpha = \frac{\bar{\alpha}}{l}$$

$$\theta(\xi, \eta) = \frac{T - T_\infty}{T_w - T_\infty}, \qquad \text{for CWT} \tag{8.8a}$$

and

$$\theta(\xi, \eta) = \frac{(T - T_\infty)}{q}\left(\frac{\Omega^*}{\nu}\right)^{1/2} K_f, \quad \text{for CHF} \tag{8.8b}$$

with regard to the numerical computation, one may use the transformation $\xi = r$, $\eta = z - s(r)$ where $s(r) = \alpha\cos(2\pi r)$. In the current analysis, attention is focused upon boundary layer flow close to the surface of the disk. For thin boundary layer, the variables are re-scaled:

$$w = W + s'u, \qquad \zeta = Re^{1/2}\eta, \qquad \tilde{w} = Re^{1/2}W, \tag{8.9}$$

where $Re = \Omega^* l^2/\nu$. Moreover, due to small surface undulations, the pressure-gradient in the radial direction may be ignored and, on this basis, we eliminate $\partial p/\partial z$ between Eqs. (8.3) and (8.5). By substituting Eq. (8.9) into the transformed system and omitting the higher order terms, the boundary-layer equations are achieved, given by

$$\frac{u}{r} + \frac{\partial u}{\partial r} + \frac{\partial \tilde{w}}{\partial \zeta} = 0, \tag{8.10}$$

$$u\frac{\partial u}{\partial r} + \tilde{w}\frac{\partial u}{\partial \zeta} = -\frac{s's''}{1 + s'^2}u^2 + \left(1 + s'^2\right)\frac{\partial^2 u}{\partial \zeta^2} + \frac{1}{1 + s'^2}\frac{v^2}{r}, \tag{8.11}$$

$$u\frac{\partial v}{\partial r} + \tilde{w}\frac{\partial v}{\partial \zeta} = \left(1 + s'^2\right)\frac{\partial^2 v}{\partial \zeta^2} - \frac{uv}{r}, \tag{8.12}$$

$$u\frac{\partial\theta}{\partial r}+\tilde{w}\frac{\partial\theta}{\partial\zeta}=\frac{\left(1+s'^{2}\right)}{Pr}\frac{\partial^{2}\theta}{\partial\zeta^{2}}. \tag{8.13}$$

In order to acquire the more convenient form of the above system, implement the following transformations

$$\psi=r^{2}f(r,\zeta),\qquad ur=\frac{\partial\psi}{\partial\zeta},\qquad r\tilde{w}=-\frac{\partial\psi}{\partial r},v=rg'. \tag{8.14}$$

The continuity equation (8.9) is identically satisfied due to the introduction of stream-function ψ. In this way the governing equations read as

$$\begin{aligned}(1+s'^{2})f'''+\frac{1}{1+s'^{2}}g'^{2}-\left(1+\frac{s's''r}{1+s'^{2}}\right)f'^{2}+2ff''\\ =r\left(f'\frac{\partial f'}{\partial r}-f''\frac{\partial f}{\partial r}\right),\end{aligned} \tag{8.15}$$

$$(1+s'^{2})g'''-2f'g'+2fg''=r\left(f'\frac{\partial g'}{\partial r}-g''\frac{\partial f}{\partial r}\right), \tag{8.16}$$

$$\frac{(1+s'^{2})}{Pr}\theta''+2\theta'f=r\left(f'\frac{\partial\theta}{\partial r}-\theta'\frac{\partial f}{\partial r}\right). \tag{8.17}$$

The respective boundary condition in the case of CWT is read as

$$\begin{aligned}f=f'=0,\qquad g'=1,\qquad \theta=1,\quad \text{at}\quad \zeta=0,\\ f'=g'=0,\qquad \theta=0,\quad \text{as}\quad \zeta\to\infty,\end{aligned} \tag{8.18a,b}$$

while the thermal boundary condition (8.18a) is replaced by the following condition in case of CHF

$$\frac{\partial\theta}{\partial\zeta}=-\frac{1}{(1+s'^{2})^{1/2}}\ \text{at}\ \zeta=0, \tag{8.19}$$

where s' and s'' are calculated as $\frac{dS^{*}}{dr^{*}}$ and $\frac{d^{2}S^{*}}{dr^{*2}}$, respectively.

8.2 Entropy analysis

The local entropy generation phenomenon for an incompressible viscous fluid flow in convection heat transfer process is the subject of this investigation. Since the fluid is viscous and obeys Fourier's law of heat conduction, the expression for entropy production is read as (see for instance Arikoglu et al, [131]):

$$S_G = \frac{\kappa}{T_\infty^2}\left[\left(\frac{\partial T}{\partial r^*}\right)^2 + \left(\frac{\partial T}{\partial z^*}\right)^2\right] + \frac{\mu}{T_\infty}\left[2\left[\left(\frac{\partial u^*}{\partial r^*}\right)^2 + \frac{u^{*2}}{r^2} + \left(\frac{\partial w^*}{\partial z^*}\right)^2\right] + \left(\frac{\partial v^*}{\partial z^*}\right)^2 + \left(\frac{\partial w^*}{\partial r^*} + \frac{\partial u^*}{\partial z^*}\right)^2 + \left[r^* \frac{\partial}{\partial r^*}\left(\frac{v^*}{r^*}\right)\right]^2\right]. \quad (8.20)$$

Utilize Eqs. (8.8) and (8.9) in above equation, we have the following entropy generation expression for constant wall temperature and constant heat flux cases, respectively:

$$(S_G)_{CST} = \frac{k\Delta T^2}{T_\infty{}^2}\frac{Re}{l^2}\left(1 + s'^2\right)\theta'^2 + \frac{\mu Re\Omega^{*2}}{T_\infty}\left[\left(1 + s'^2\right)^2\left(\frac{\partial u}{\partial \zeta}\right)^2 + \left(1 + s'^2\right)\left(\frac{\partial v}{\partial \zeta}\right)^2\right], \quad (8.21)$$

$$(S_G)_{CHF} = \frac{q^2}{kT_\infty{}^2}\frac{\nu Re}{\Omega^* l^2}\left(1 + s'^2\right)\theta'^2 + \frac{\mu Re\Omega^{*2}}{T_\infty}\left[\left(1 + s'^2\right)^2\left(\frac{\partial u}{\partial \zeta}\right)^2 + \left(1 + s'^2\right)\left(\frac{\partial v}{\partial \zeta}\right)^2\right]. \quad (8.22)$$

Using Eq. (8.14) in Eqs. (8.21) the dimensionless entropy generation function in case of constant wall temperature is obtained as

$$N_s = \frac{(S_G)_{CST}}{S^*_{G_0}} = (1 + s'^2)\theta'^2 + \frac{Br^*}{\Omega_T} r^2[(1 + s'^2)^2 f''^2 + (1 + s'^2) g''^2], \quad (8.23)$$

where $S^*_{G_0} = \frac{k\Omega^*\Delta T^2}{\nu T_\infty^2}$ is the characteristic entropy generation, and $Br^* = \frac{\mu\Omega^{*2} l^2}{k\Delta T}$ is the rotational Brinkman number. Bejan number (Be) effectively handles the above-

mentioned problem and easily characterizes the dominance of thermal irreversibility or the viscous irreversibility during the process of entropy generation. The Bejan number (Be) takes the following form for the current study (in CST case):

$$Be = \frac{(1+s'^2)\theta'^2}{(1+s'^2)\theta'^2 + \frac{Br^*}{\Omega_T} r^2[(1+s'^2)^2 f''^2 + (1+s'^2)g''^2]}. \tag{8.24}$$

Similarly for constant heat flux case, use of Eq. (8.14) in Eq. (8.22) gives the dimensionless entropy generation number of the form

$$N_s = \frac{(S_G)_{CHF}}{S_{G_0}^{**}} = (1+s'^2)\theta'^2 + \frac{Br^{**}}{\Lambda} r^2[(1+s'^2)^2 f''^2 + (1+s'^2)g''^2], \tag{8.25}$$

where $S_{G_0}^{**} = \frac{q^2}{kT_\infty^2}$ is the characteristic entropy generation, $Br^{**} = \frac{\mu\Omega^{*5/2}l^2}{\sqrt{\nu}q}$ is the rotational Brinkman number and $\Lambda = \frac{q}{\sqrt{\frac{\Omega^*}{\nu}}kT_\infty}$ is the dimensionless heat flux. Since the Bejan number captures the dominance of thermal irreversibility or the viscous irreversibility during the process of entropy production. Bejan number (Be) takes the following form for the current case of constant heat flux (CHF):

$$Be = \frac{(1+s'^2)\theta'^2}{(1+s'^2)\theta'^2 + \frac{Br^{**}}{\Lambda} r^2[(1+s'^2)^2 f''^2 + (1+s'^2)g''^2]}. \tag{8.26}$$

8.3 Results and discussion

In the current section the entropy generation phenomenon is deliberated with the help of Eqs. (8.23)-(8.26). For doing so, Keller-Box method [137, 139] is implemented for the numerical solution of non-linear system (8.15)-(8.17) with the boundary condition (8.18) and (8.19) for both cases (CWT & CHF). The impact of surface undulations (α) upon dimensionless entropy generation number (N_s) is illustrated for Figs. 8.2-8.3 with

CWT and CHF cases, respectively. It is seen that, N_s is large at the surface for both cases (CWT & CHF) and decreases monotonically from the boundary to the ambient region. It is observed that entropy generation decreases in the vicinity of the surface with the increment of δ which means that in any thermal system, entropy generation can be minimized by the consideration of rough surface as compared to flat boundary. The involvement of thermal irreversibility and viscous irreversibility towards the production of entropy are categorized with the help of Bejan number. The influence of amplitude to wavelength ratio (α) upon Bejan number for CWT and CHF is shown in Figs. 8.4-8.5. It is noted that Be reduces due to the increment of α. This impact highlights that the viscous irreversibility become dominant with the surface undulations particularly in a case of CWT. Moreover, from the Bejan profile it is clear that at the surface, viscous irreversibility is dominant while in the ambient location the irreversibility is totally controlled by the heat transfer. Dependence of N_s upon Brinkman number (Br) for CWT and CHF are depicted through Figs. 8.6-8.7. In both cases (CWT and CHF) entropy production increases due to the increment of Br and this augmentation is quite obvious because enhancement in Br means viscosity of the fluid increases. Figures 8.8-8.9 represent the influence of Br upon Bejan number. It is noted that, Be reduces due to the increasing value of Br. Moreover, these variations in Be can be seen in the main flow region and at the surface there is no such variation in Be because at the boundary fluid friction irreversibility is dominant for any value of Br.

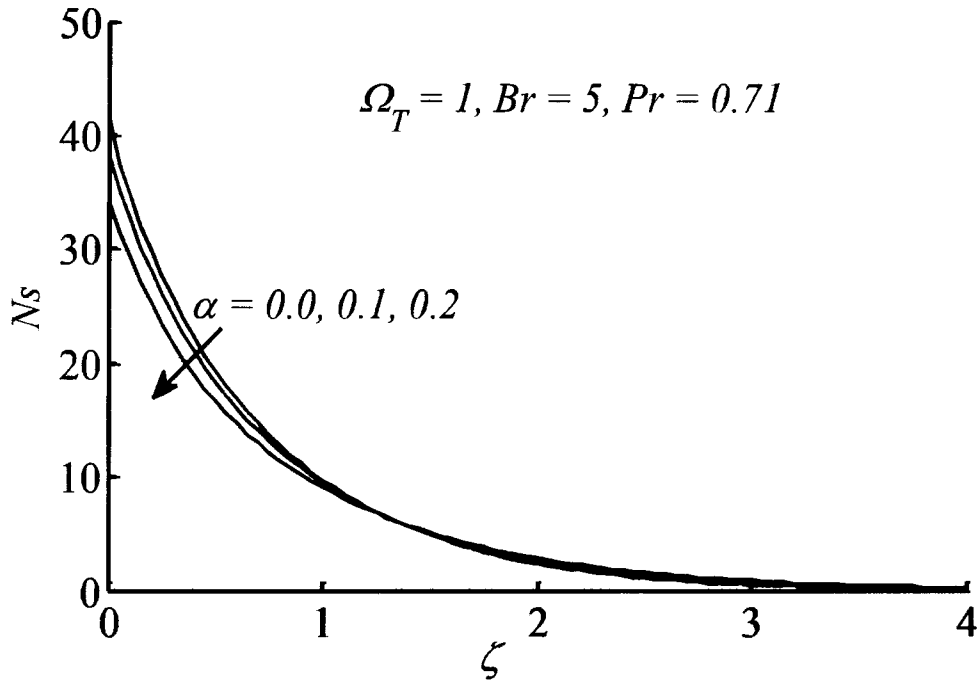

Fig. 8.2: Entropy generation profile for different α (CWT).

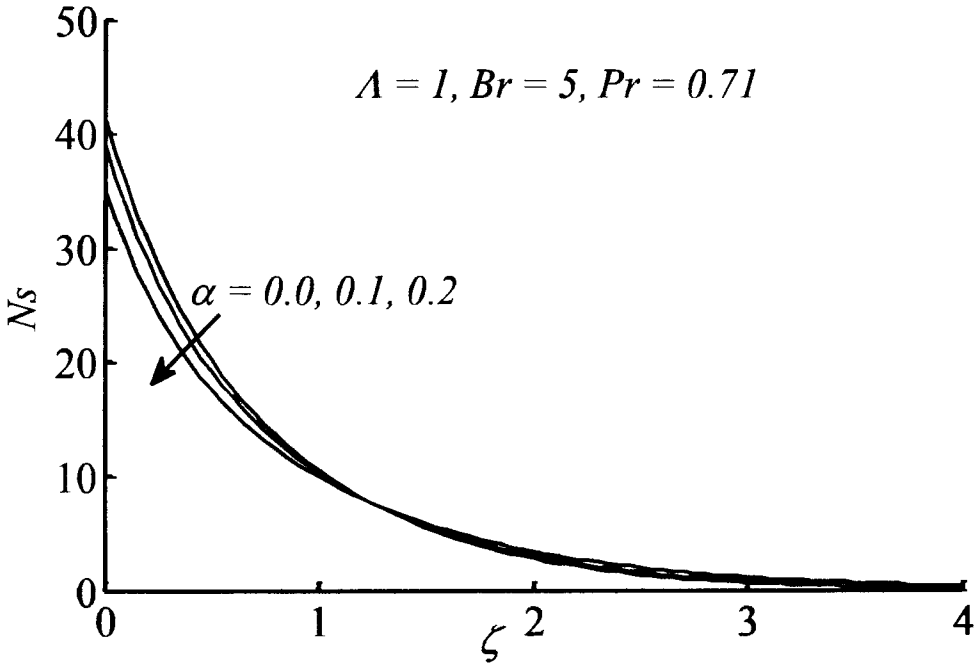

Fig. 8.3: Entropy generation profile for different α (CHF).

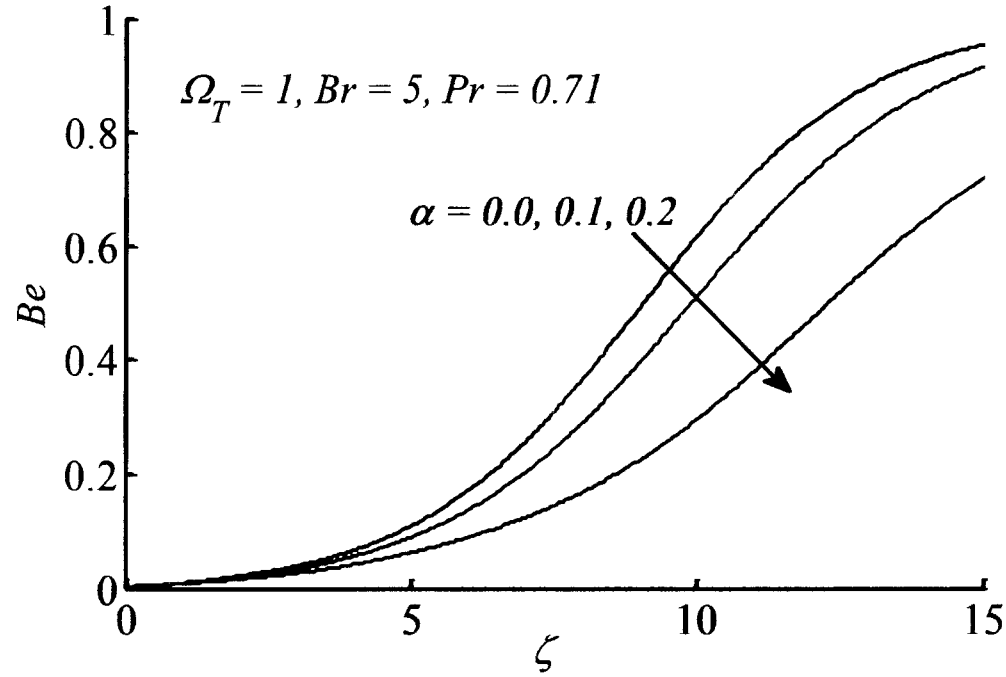

Fig. 8.4: Impact of α on Bejan number (CWT).

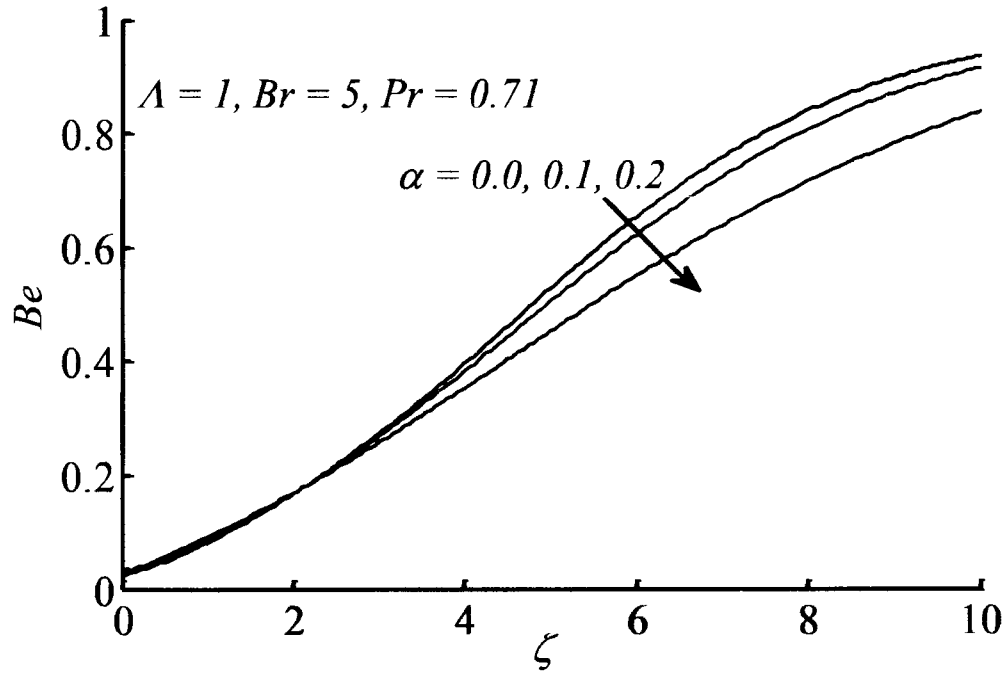

Fig. 8.5: Effects of α on Bejan number (CHF).

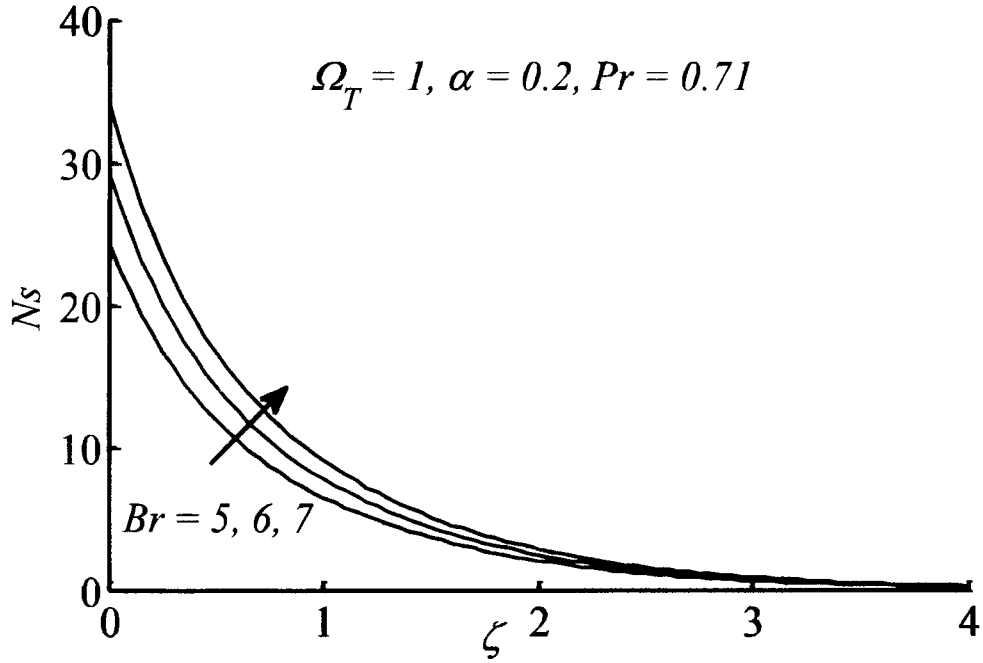

Fig. 8.6: Dependence of entropy generation number on *Br* (CWT).

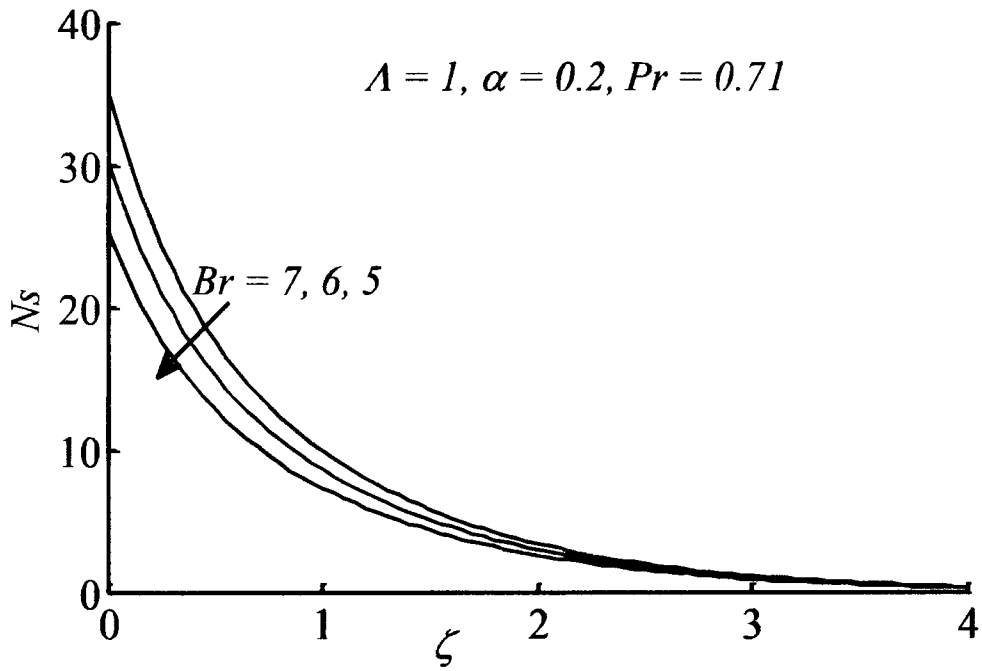

Fig. 8.7: Variations in entropy generation due to Brinkman number (CHF).

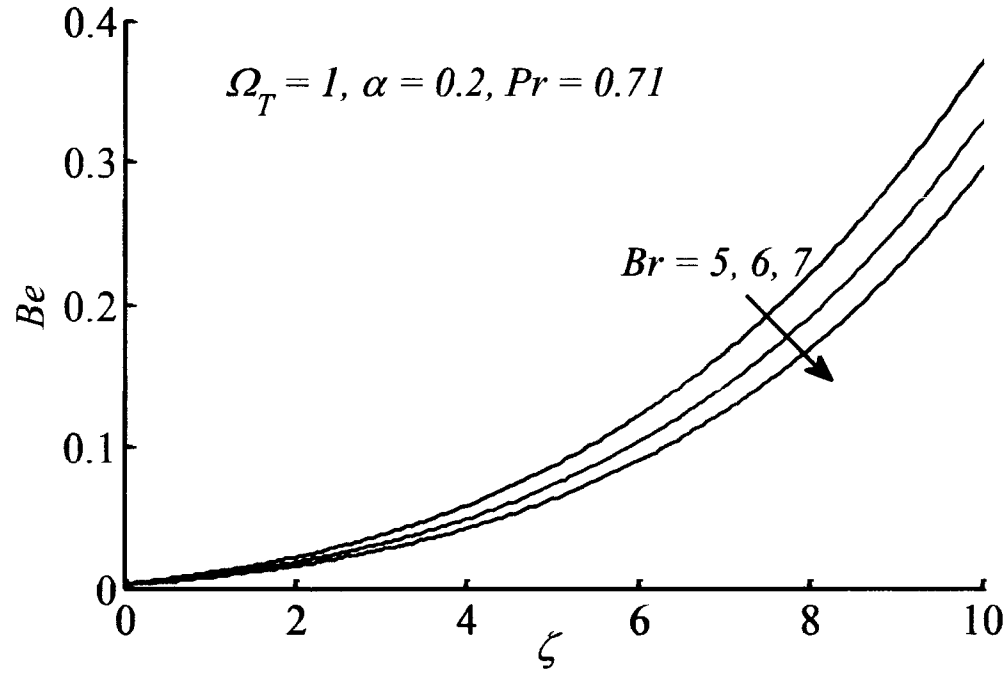

Fig. 8.8: Effects of Br on Bejan number (CWT).

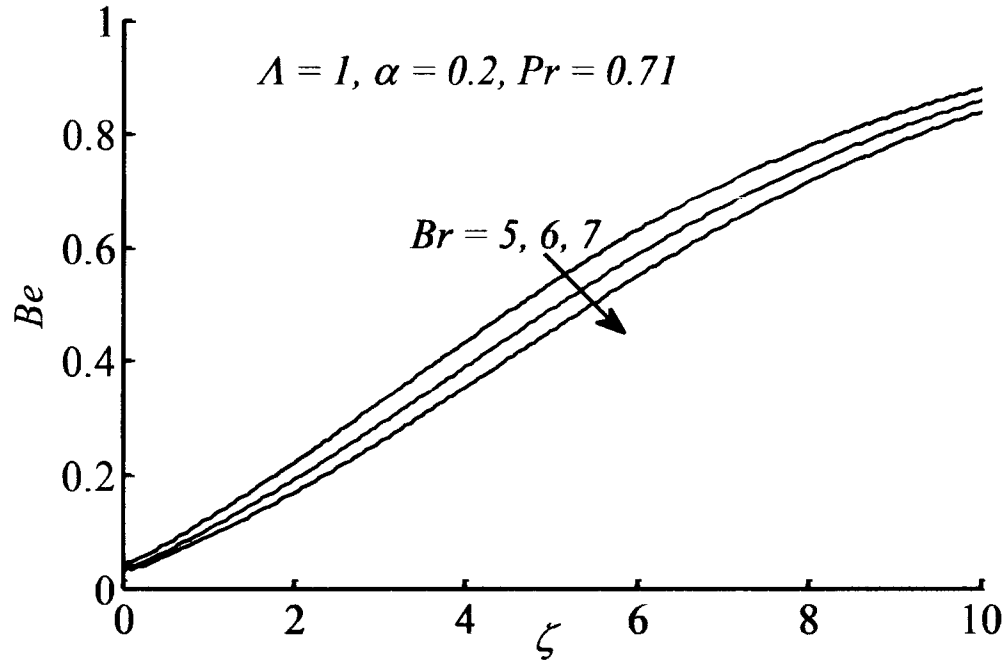

Fig. 8.9: Bejan number profile for various values of Br (CHF).

8.4 Conclusions

Entropy generation phenomenon for the flow induced due to the rotation of an infinite sinusoidal wavy disk with the rotation rate Ω^* has been investigated numerically. Keller-Box method is executed for the solution of the governing non-linear system. The analysis has been performed for the constant wall temperature and constant heat flux cases. The obtained solution declares that, the presence of surface undulations contributes significantly in the minimization of entropy production. Furthermore, it is observed that the amplitude to wave length ratio significantly alters the Bejan number in the case of constant wall temperature as compared to constant heat flux case.

Chapter 9

Conclusions

In this dissertation, attention has been given to the entropy analysis of non-similar flows of viscous fluid over non-flat surfaces. In this regard, second law of thermodynamics has been applied to examine the irreversibility of the system through entropy generation rate. It is an established fact that the heat transfer rate of any thermal system can be improved by introducing a certain type of irregularities on the bounding surface. In this regard the sinusoidal wavy shaped surfaces have already been considered in literature and a significant alteration in the heat transfer rate has been reported. Therefore, it was desirable to perform the entropy generation analysis in such flows to overall estimate the thermal performance of such systems. Interestingly due to such a periodic surface texture of the boundary the flow becomes non-similar in nature. Therefore, neither the rate of heat transfer nor the rate of entropy generation remains alike on the whole longitudinal domain. Various types of flow geometries including horizontal, vertical, and inclined wavy surfaces, vertical wavy cone, and rotating wavy disk have been taken into consideration during this study. In all these situations the primary objective is the analysis is to sort out the impact of surface texture upon entropy generation phenomenon.

Entropy generation rate in the boundary layer flow along a horizontal moving wavy surface has been investigated where the findings explore that due to the surface undulations the entropy production decreases. It has been shown that entropy number is high at the upstream locations due to large temperature and velocity gradients. Moreover, high entropy generation rate is observed in the fluids having large Prandtl

number. In addition to this, the increasing amplitude of the fluctuating entropy profile is also observed downstream due to the increase of group parameter (ω) which is a consequence of high fluid friction irreversibility.

The enhancement in heat transfer rate has been reported by many researchers due to the consideration of nanofluid instead of pure fluid. For mathematical representation of nanofluids various models have been utilized. In all such studies the obtained results reflect a significant enhancement in heat transfer rate due to the inclusion of nanoparticles. On the basis of available scrutiny, we have used Tiwari and Das model, and Buongiorno model for the analysis of combined effect of surface texture and nanoparticles upon entropy generation in the boundary layer flow. Two types of nanoparticles, namely, Fe_3O_4 and Cu have been considered for the analysis of entropy production in these flows. Although, the heat transfer rate augments significantly due to the increase of nanoparticles concentration but the irreversibility of the system increases which is a serious concern. Thus, the volume concentration of nanoparticles is observed to be kept up to a certain range. It is revealed that the Fe_3O_4 based nanofluid is more effective in order to minimize the entropy production in comparison to the Cu based nanofluid.

Consideration has also been given to the Buongiorno model which includes the effects of Brownian motion and thermophoresis phenomena of nanoparticles to examine the entropy generation in nanofluid flow. It is reminded that the Tiwari and Das does not include the effects of Brownian motion and thermophoresis. Due to these physical parameters, entropy generation reduces in the neighborhood of wavy surface and an opposite behavior is obtained in faraway region. Enhancement of Brownian and thermophoresis parameters reduces Bejan number in the upstream locations and no such prominent effects were seen in the downstream region. Moreover, graphical results

explore that in the longitudinal direction of the wavy plate, entropy profile due to thermal irreversibility is prominent for various physical parameters. The impact of Brinkman number upon entropy profile is more prominent in comparison of mass transfer parameter.

Irreversibility analysis of mixed convection boundary layer flow along a vertical wavy plate has also been reported. The results show that the entropy production increases due to the strength of mixed convection flow and consequently entropy is high in the case of natural convection flow. However, in a physical situation of natural convection flow, entropy generation can be minimized with the aid of forced convection phenomenon. Moreover, dependence of entropy production upon surface undulations is more significant in the case of free convection flow. Bejan number decreases with the enhancement of Eckert number in both situations (natural convection and forced convection), however this trend is more significant in the downstream region.

Entropy generation phenomenon of mixed convection along an inclined non-flat boundary has been studied numerically. It was found that for large values of the inclination angle ($\gamma = \pi/2$) entropy generation is high while less entropy produces due to zero value of inclination angle (absence of gravity). Due to wavy amplitude, it is noted that the entropy generation decreases. Bejan number fluctuates significantly for large value of wavy amplitude. Considerable enhancement in entropy number is observed near to the wavy plate with the enhancement of Brinkman number and this variation is more significant for the natural convection flow. So, in order to control the entropy production of any natural convection flow, it is very useful to include the forced convection phenomenon there.

Consideration has been given to the wavy cone geometry for the mixed convection flow to examine the entropy production. It is found that the entropy generation augments due to increase of cone half angle and mixed convection parameter. Thus, entropy generation over a cone geometry can be reduced due to the consideration of smaller values of cone half angle. Moreover, N_s layer fluctuates with increasing amplitude in the downstream direction with the enhancement of cone half angle. Impact of surface undulations of wavy cone upon entropy production is similar as the impact of surface texture in previously considered flow geometries. Due to influence of involved physical parameters, Bejan number reaches to 1 in the vicinity of the cone which signifies that the irreversibility in the system is dominated due to thermal irreversibility while it decreases monotonically and approaches to 0 as one moves away from the boundary. Consequently, entropy production is totally controlled by viscous dissipation. Moreover, Bejan number elaborates that viscous dissipation is a major contributor towards the production of entropy in the case of natural convection flow.

Continuing with the axisymmetric flow, a rotating wavy disk subjected to a constant wall temperature and a constant heat flux has also been investigated numerically for the analysis of entropy generation phenomenon over it. The amplitude to wavelength ratio of the disk surface reduces the production of entropy which is a similar finding as in the other flow geometries The results reveal that the Bejan number decreases with the enhancement of Brinkman number in both cases (CWT & CHF). Moreover, close to the surface, the value of Be was near about 0 which reflects that the irreversibility is totally controlled by the viscous dissipation.

In this dissertation two-dimensional flow corresponding to planner geometries and axisymmetric (cone) geometry, and an axisymmetric three-dimensional rotating disk geometry have been considered. In all such geometries the corresponding flat surfaces

have been considered of non-flat (wavy) nature. The study also includes the influence of natural convection and the consideration of nanofluid. Overall, it is concluded that the surface undulations play an important role to reduce the entropy generation, quite significantly, in the thermal transport process from the surfaces of non-flat texture. Increased entropy generation phenomenon is observed in the case of nanofluid and natural convection. However, it is observed that the entropy production, in a natural convection flow, can be minimized to some extent by introducing a forced flow there.

References

[1] A. Bejan, Study of entropy generation in fundamental convective heat transfer, Trans. ASME J. Heat Transf., 101 (1979) 718–725.

[2] A.Bejan, Second-law analysis in heat transfer and thermal design, Adv. Heat Transf.,15 (1982) 1-58.

[3] A. Bejan, *Entropy generation through heat and fluid flow*, Wiley New York 1994.

[4] A. Bejan, *Entropy Generation Minimization*, CRC Press New York 1996.

[5] J. San, Z. Laven, Entropy generation in convective heat transfer and isothermal mass transfer, J. Heat Transf., 109 (1987) 647–52.

[6] V.S. Arpaci, A. Selamet, Entropy production in boundary layers, J. Thermophys. Heat Transf., 4 (1990) 404–407.

[7] C.G. Carrington, Z.F. Sun, Second law analysis of combined heat and mass transfer in internal flow and external flows, Int. J. Heat Fluid Flow,132(1) (1992) 65–70.

[8] S. Mahmud, R.A. Fraser, The second law analysis in fundamental convective heat transfer problems, Int. J. Therm. Sci., 42 (2003) 177–186.

[9] M.Q.A. Odat, R.A. Damseh, M.A.A. Nimr, Effect of magnetic field on entropy generation due to laminar forced convection past a horizontal flat plate, Entropy, 4 (2004) 293-303.

[10] O.D. Makinde, Second law analysis for variable viscosity hydromagnetic boundary layer flow with thermal radiation and Newtonian heating, Entropy, 13 (2011) 1446–1464.

[11] A.S. Butt, A.Ali, Effects of magnetic field on entropy generation in flow and heat transfer due to radially stretching surface, Chin. Phys. Lett., 30 (2013) 24701– 24704.

[12] M.M. Rashidi, F. Mohammadi, S. Abbasbandy, M.S. Alhuthali, Entropy generation analysis for stagnation point flow in a porous medium over a permeable stretching surface, J. Appl. Fluid Mech., 8 (2015) 753-765.

[13] J.A. Falade, S.O. Adesanya, J.C. Ukaegbu, M.O. Osinowo, Entropy generation analysis for variable viscous couple stress fluid flow through a channel with non-uniform wall temperature, Alexandria Eng. J., 55 (2016) 69–75.

[14] A.S. Butt, S. Munawar, A. Ali, A. Mehmood, Entropy generation in the Blasius flow under thermal radiation, Phys. Scr., 85(3) (2012) 035008.

[15] L.S. Yao, Natural convection along a vertical wavy surface, Trans. ASME J. Heat Transf., 105 (1983) 465 – 468.

[16] L.S. Yao, S.G. Moulic, Natural convection along a wavy surface with uniform heat flux, ASME J. Heat Transf. 111 (1989) 1106-1108.

[17] D.A.S. Rees, I. Pop, Free convection induced by a horizontal wavy surface in a porous medium, Fluid Dyn. Res., 14 (1994) 151-166.

[18] D.A.S. Rees, I. Pop, Boundary layer flow and heat transfer on a continuous moving wavy surface, Acta Mech., 112 (1995) 149-158.

[19] M.A. Hossain, I. Pop, Magneto-hydrodynamic boundary layer flow and heat transfer on a continuous moving wavy surface, Acta Mech., 48(5) (1996) 813-283.

[20] M. Molla, M.A. Hossain, L.S. Yao, Natural convection flow along a vertical wavy surface with uniform surface temperature in presence of heat generation/absorption, Int. J. Therm. Sci., 43 (2004) 157-163.

[21] M. Molla, M.A. Hossain, L.S. Yao, Natural convection flow along a vertical complex wavy surface with uniform heat flux, Int. J. Heat Transfer, 129 (2007) 1403-1407.

[22] M.A. Alim, M.R. Karim, M.M. Akand, Heat generation effects on MHD natural convection flow along a vertical wavy surface with variable thermal conductivity, Am. J. Comput. Math., 2 (2012) 42-50.

[23] M. Narayana, P. Sibanda, S.S. Motsa, P.G. Siddheshwar, On double-diffusive convection and cross diffusion effects on a horizontal wavy surface in a porous medium, Bound. Val. Prob., 88 (2012) 1–22.

[24] S.U.S. Choi, Enhancing thermal conductivity of fluids with nanoparticles, Trans. ASME, F.E.D., 231 (1995) 99-105.

[25] R.K. Tiwari, M.K. Das, Heat transfer augmentation in a two-sided lid-driven differentially heated square cavity utilizing nanofluids, Int. J. Heat Mass Transf., 50 (2007) 2002-18.

[26] J. Buongiorno, Convective transport in nano-fluids, Trans. ASME J. Heat Transfer, 128 (2006) 240-250.

[27] M. Chopkar, P.K. Das, I. Manna, Synthesis and characterization of nanofluid for advanced heat transfer applications, Scr. Mater., 55 (2006) 549–552.

[28] K. Khanafer, K. Vafai, A critical synthesis of thermophysical characteristics of nanofluids, Int. J. Heat Mass Transf., 54 (2011) 4410–4428.

[29] S. Kakac, A. Pramuanjaroenkij, Review of convective heat transfer enhancement with nanofluids, Int. J. Heat Mass Transf. 52 (2009) 3187–3196.

[30] H.F. Oztop, E. Abu-Nada, Numerical study of natural convection in partially heated rectangular enclosures filled with nano-fluids, Int. J. Heat Fluid Flow, 29 (2009) 1326-1336.

[31] S. Ozerinc, S. Kakac, A. Yazıcıoglu, Enhanced thermal conductivity of nanofluids: a state-of- the-art review, Microfluid. Nanofluid., 8 (2010) 145–170.

[32] L.S. Sundar, K.V. Sharma, M.T. Naik, M.K. Singh, Empirical and theoretical Correlations on viscosity of nanofluids: a review, Renew. Sustain. Energy Rev., 25 (2013) 670–686.

[33] X.Q. Wang, A.S. Mujumdar, Heat transfer characteristics of nanofluids: a review, Int. J. Therm. Sci., 46 (2007) 1–19.

[34] M. Hassani, M.M. Tabar, H. Nemati, G. Domairry, F. Noori, An analytical solution for boundary layer flow of a nano-fluid past a stretching sheet, Int. J. Therm. Sci., 50 (2011) 2256–2263.

[35] P. Rana, R. Bhargava, Flow and heat transfer of a nano-fluid over a nonlinearly stretching sheet: a numerical study. Commun. Nonlinear Sci. Numer. Simul., 17 (2012) 212–226.

[36] S. Kakac, A. Pramuanjaroenkij, Review of convective heat transfer enhancement with nano-fluids, Int. J. Heat Mass Transf., 52 (2009) 3187–3196.

[37] O.D. Makinde, A. Aziz, Boundary layer flow of a nano-fluid past a stretching sheet with a convective boundary condition, Int. J. Therm. Sci., 50, (2011) 1326–1332.

[38] R.S.R. Gorla, M. Kumari, Free convection along a vertical wavy surface in a nanofluid, J. Nano Eng. Nano Sys., 225(3) (2011) 133-142.

[39] S.E. Ahmed, M.A. El-Aziz, Effect of local thermal non-equilibrium on unsteady heat transfer by natural convection of a nanofluid over a vertical wavy surface, Meccanica, 48(1) (2013) 33-43.

[40] A. Mehmood, M.S. Iqbal, I. Mustafa, Cooling of moving wavy surface through MHD nano-fluid, Zeitschrift für Naturforschung A, 71 (7) (2016) 583–593.

[41] A. Mehmood, M.S. Iqbal, Heat transfer analysis in natural convection flow of nanofluid past a wavy cone, J. Mol. Liq., 223 (2016) 1178-1184.

[42] A. Mehmood, M.S. Iqbal, Effect of heat absorption in natural convection nanofluid flow along a vertical wavy surface, J. Mol. Liq., 224 (2016) 1326-1331.

[43] I. Mustafa, T. Javed, A. Ghaffari, Hydromagnetic natural convection flow of water-based nanofluid along a vertical wavy surface with heat generation, J. Mol. Liq., 229 (2017) 246-254.

[44] I. Mustafa, T. Javed, Heat transfer in natural convection flow of nanofluid along a vertical wavy plate with variable heat flux, Therm. Sci., 23 (2019) 179-190.

[45] P.K. Singh, K.B. Anoop, T. Sundararajan, S.K. Das, Entropy generation due to flow and heat transfer in nanofluids, Int. J. Heat Mass Transf., 53 (2010) 4757–4767.

[46] J. Li, C. Kleinstreuer, Entropy generation analysis for nanofluid flow in microchannels, Trans. ASME J. Heat Transf. 132 (2010) 122401.1–122401.8.

[47] V. Bianco, S. Nardini, O. Manca, Enhancement of heat transfer and entropy generation analysis of nanofluids turbulent convection flow in square section tubes, Nanoscale Res. Lett. 6 (2011) 252.

[48] M. Karami, E. Shirani, A. Avara, Analysis of entropy generation, pumping power, and tube wall temperature in aqueous suspensions of alumina particles, Heat Transf. Res. 43 (4) (2012) 327–342.

[49] A. Falahat, A. Vosough, Effect of nanofluid on entropy generation and pumping power in coiled tube, J. Thermophys. Heat Transf., 26 (1) (2012) 141–146.

[50] M.M. Rashidi, S. Abelman, N. Freidoonimehr, Entropy generation in steady MHD flow due to a rotating porous disk in a nanofluid, Int. J. Heat Mass Transf., 62 (2013) 515–525.

[51] A.H. Mahmoudi, M. Shahi, F. Talebi, Entropy generation due to natural convection in a partially open cavity with a thin heat source subjected to a nanofluid, Numer. Heat Transf. Part A, 61 (2012) 283–305.

[52] A. Malvandi, D.D. Ganji, F. Hedayati, E. Yousefi-Rad, An analytical study on entropy generation of nanofluids over a flat plate, Alex. Eng. J., 52, 595–604 (2013)

[53] A. Noghrehabadi, M.R. Saffarian, R. Pourrajab, M. Ghalambaz, Entropy analysis for nano-fluid flow over a stretching sheet in the presence of heat generation/absorption and partial slip, J. Mech. Sci. Technol., 27 (2013) 927–937.

[54] M.H. Abolbashari, N. Freidoonimehr, F. Nazari, M.M. Rashidi, Entropy analysis for an unsteady MHD flow past a stretching permeable surface in nano-fluid. Powder Technol., 267 (2014) 256–267.

[55] S. Das, S. Chakraborty, R.N. Jana, O.D. Makinde, Entropy analysis of unsteady magneto- nano-fluid flow past accelerating stretching sheet with convective boundary condition, Appl. Math. Mech. Engl. Ed., 36 (2015) 1593-1610.

[56] E.M. Sparrow, R. Eichorn, J.L. Gregg, Combined forced and free convection in boundary layer flow, Phys. Fluids, 2 (1959) 319–328.

[57] J.H. Merkin, The effects of buoyancy forces on the boundary layer flow over semi-infinite vertical flat plate in a uniform free stream, J. Fluid Mech., 35 (1969) 439–450.

[58] J.R. Lloyd, E.M. Sparrow, Combined forced and free convection flow on vertical surfaces, Int. J. Heat Mass Transf., 13 (1970) 434–438.

[59] G. Wilks, Combined forced and free convective flow on vertical surfaces, Int. J. Heat Mass Transf., 16 (1973) 1958–1964.

[60] L.S. Yao, S.G. Moulic, Mixed convection along a wavy surface, Trans. ASME J. Heat Transf., 111 (1989) 974-979.

[61] M.A. Hossain, H.S. Takhar, Radiation effect on mixed convection along a vertical plate with uniform surface temperature, Heat Mass Transf., 31 (1996) 243-248.

[62] F.M. Hady, A.Y. Bakier, R.S.R. Gorla, Mixed convection boundary layer flow on a continuous flat plate with variable viscosity, Heat Mass Transf., 31 (1996) 169-172.

[63] M.A. Hossain, D.A.S. Rees, Combined heat and mass transfer in natural convection flow from a vertical wavy surface, Acta Mech., 136 (1999) 113-141.

[64] J.H. Jang, W.M. Yan, Mixed convection heat and mass transfer along a vertical wavy surface, Int. J. Heat Mass Transf., 47 (2004) 419–428.

[65] M.M. Molla, M.A. Hossain, Radiation effect on mixed convection laminar flow along a vertical wavy surface, Int. J. Therm. Sci., 46 (2007) 926–935.

[66] S. Siddiqa, M.A. Hossain, Mixed convection boundary layer flow over a vertical flat plate with radiative heat transfer, Appl. Math., 3 (2012) 705-716.

[67] S. Siddiqa, M.A. Hossain, S.C. Saha, Natural convection flow with surface radiation along a vertical wavy surface, Numer. Heat Transf. A: Appl., 64 (2013) 400-415.

[68] N. Parveen, S. Nath, M.A. Alim, Viscous dissipation effect on natural convection flow along a vertical wavy surface, Procedia Eng., 90 (2014) 294-300.

[69] S. Siddiqa, M.A. Hossain, R.S.R Gorla, Natural convection flow of viscous fluid over triangular wavy horizontal surface, Comput. Fluids, (2014), doi: http://dx.doi.org/10.1016/j.compfluid.2014.10.001

[70] D. Srinivasacharya, B. Mallikarjuna, R. Bhuvanavijaya, Radiation effect on mixed convection over a vertical wavy surface in Darcy porous medium with variable properties, J. Appl. Sci. Eng., 18(3) (2015) 265-274.

[71] A. Selamet, V.S. Arpaci, Entropy production in boundary layers, J. Therm. Heat Transf., 4 (1990) 404–407.

[72] B. Abu-Hijleh, W. Heilen, Entropy generation due to laminar natural convection over a heated rotating cylinder, Int. J. Heat Mass Transf., 42 (1999) 4225–4233.

[73] O.M. Haddad, M. Abu-Qudais, B.A. Abu-Hijleh, A.M. Maqableh, Entropy generation due to laminar forced convection flow past a parabolic cylinder, Int. J. Numer. Methods Heat Fluid Flow, 10 (2000) 770-779.

[74] U. Narusawa, The second-law analysis of mixed convection in rectangular ducts, Heat Mass Transf., 37 (2001) 197–203.

[75] S.H. Tasnim, S. Mahmud, Mixed convection and entropy generation in a vertical annular space, Int. J. Exergy, 2 (2002) 373-379.

[76] S. Mahmud, R.A. Fraser, Analysis of mixed convection radiation interaction in a vertical channel: Entropy generation, Int. J. Exergy, 2 (2002) 330–339.

[77] M.Q. Al-Odat, R.A. Damseh, M.A. Al-Nimr, Effect of magnetic field on entropy generation due to laminar forced convection past a horizontal flat plate, Entropy, 4 (2004) 293–303.

[78] O.M. Haddad, M.K. Alkam, M.T. Khasawneh, Entropy generation due to laminar forced convection in the entrance region of a concentric annulus, Energy, 29 (2004) 35-55.

[79] O. Haddad, M. Abuzaid, M. Al-Nimr, Entropy generation due to laminar incompressible forced convection flow through parallel-plates microchannel, Entropy, 6 (2004) 413-426.

[80] C.K. Chen, Y.T. Yang, K.H. Chang, Entropy generation of a radiation effect on a laminar mixed convection along a wavy surface, Heat Mass Transf., 47(2011) 385-395.

[81] A.S. Butt, S. Munawar, A. Mehmood, A. Ali, Entropy analysis of mixed convective magnetohydrodynamic flow of a viscoelastic fluid over a stretching sheet, Z. Naturforsch. A - J. Phys. Sci., 67 (2012) 451–459.

[82] A.S. Butt, S. Munawar, A. Ali, Entropy effects in hydromagnetic free convection flow past a vertical plate embedded in a porous medium in the presence of thermal radiation, Eur. Phys. J. Plus, 128(5) (2013) 1-15.

[83] S. Morsli, A. Sabeur-Bendehina, Entropy generation and natural convection in square cavities with wavy walls, J. Appl. Mech. Tech. Phys. 54 (6) (2013) 913–920.

[84] W.T. Kierkus, An analysis of laminar free convection flow and heat transfer about an inclined isothermal plate, Int. J. Heat Mass Transf., 11 (1968) 241-253.

[85] L. Pera, B. Gebhart, Natural convection boundary layer flow over horizontal and slightly inclined surfaces, Int. J. Heat Mass Transf., 16 (1973) 1131-1136.

[86] G. Wickern, Mixed convection from an arbitrarily inclined semi-infinite flat plate-I. The influence of the inclination angle, Int. J. Heat Mass Transf., 34 (1991) 1935-1945.

[87] M.H. Lin, C.T. Chen, Numerical study of thermal instability in mixed convection flow over horizontal and inclined surfaces, Int. J. Heat Mass Transf., 45 (2002) 1595-1603.

[88] C.C. Wang, C.K. Chen, Mixed convection boundary layer flow on inclined wavy plates including the magnetic field effect, Int. J. Therm. Sci., 44 (2005) 577–586.

[89] Y. Varol, H.F. Oztop, A comparative numerical study on natural convection in inclined wavy and flat-plate solar collectors, Build. Environ., 43 (2008) 1535–1544.

[90] M.M. Rashidi, N. Laraqi, S.M. Sadri, A novel analytical solution of mixed convection about an inclined flat plate embedded in a porous medium using the DTM-Padé, Int. J. Therm. Sci., 49 (2010) 2405-2412.

[91] M.N. Uddin, M.A. Alim, M.M.K. Chowdhury, Effects of mass transfer on MHD mixed convective flow along inclined porous plate, Procedia Eng., 90 (2014) 491 – 496.

[92] C. Tian, J. Wang, X. Cao, C. Yan, A.A. Ala, Experimental study on mixed convection in an asymmetrically heated, inclined, narrow, rectangular channel, Int. J. Heat Mass Transf., 116 (2018) 1074–1084.

[93] N.C. Roy, Natural convection flow of a combustible along inclined hot plates, Therm. Sci. Eng. Prog., 11 (2019) 409–416.

[94] A.C. Baytas, Entropy generation for natural convection in an inclined porous cavity, Int. J. Heat Mass Transf., 43 (2000) 4225–4233.

[95] O.D. Makinde, E. Osalusi, Entropy generation in a liquid film falling along an inclined porous heated plate, Mech. Res. Commun., 33 (2006) 692-698.

[96] O.D. Makinde, Irreversibility analysis for a gravity driven non-Newtonian liquid film along an inclined isothermal plate, Phys. Scr., 74 (2006) 642-645.

[97] S. Taghizadeh, A. Asaditaheri, Heat transfer and entropy generation of laminar mixed convection in an inclined lid driven enclosure with a circular porous cylinder, Int. J. Therm. Sci., 134 (2018) 242–257.

[98] S.O. Adesanya, A.C. Egere, R.S. Lebelo, Entropy generation analysis for a thin couple stress film flow over an inclined surface with Newtonian cooling, Physica A, 528 (2019) 121260.

[99] H.J. Merk, J.A. Prins, Thermal convection in laminar boundary layer-I, Int. Appl. Sci. Res., A4 (1953) 11–24.

[100] H.J. Merk, J.A. Prins, Thermal convection in laminar boundary layer-II, Int. Appl. Sci. Res., A4 (1954) 195–206.

[101] R.G. Hering, R.J. Grosh, Laminar free convection from a non-isothermal cone, Int. J. Heat Mass Transf., 5 (1962) 1059–1068.

[102] R.G. Hering, R.J. Grosh, Laminar combined convection from a rotating cone, Trans. ASME J. Heat Transf., 2 (1963) 29–34.

[103] M. Alamgir, Overall heat transfer from vertical cones in laminar free convection an approximate method, Trans. ASME J. Heat Transf., 101 (1) (1979) 174–176.

[104] P. Singh, V. Radhakrishnan, K.A. Narayan, Non-similar solutions of free convection flow over a frustum of a cone for constant wall temperature, Ingen. Arch., 59 (1989) 382–389.

[105] M. Kumari, I. Pop, G. Nath, Mixed convection along a vertical cone, Int. Commun. Heat Mass Transf., 16 (1989) 247-255.

[106] P. Singh. V. Radhakrishnan, K.A. Narayan, Natural convection flow over a vertical frustum of a cone for constant wall heat flux, Appl. Sci. Res., 46 (1989) 335-345.

[107] T.Y. Wang, C. Kleinstreuer, H. Chiang, Mixed convection from a rotating cone with variable surface temperature, Numer. Heat Transf. Part A, 25 (1994) 75-83.

[108] K.A. Yih, Mixed convection about a cone in a porous medium: the entire regime, Int. Commun. Heat Mass Transf., 26 (1999) 1041–1050.

[109] K.A. Yih, Radiation effect on mixed convection over an isothermal cone in porous media, Heat Mass Transf., 37 (2001) 53–57.

[110] I. Pop, T. Grosan, M. Kumari, Mixed convection along a vertical cone for fluids of any Prandtl number: case of constant wall temperature, Int. J. Numer. Meth. Heat Fluid Flow, 13 (2003) 815-829.

[111] I. Pop, T.Y. Na, Natural convection from a wavy cone, Appl. Sci. Res., 54 (1995) 125– 136.

[112] I. Pop, T.Y. Na, Natural convection of a Darcian fluid about a wavy cone, Int. Comm. Heat Mass Transf., 21 (1994) 891–899.

[113] I. Pop, T.Y. Na, Natural convection over a frustum of a wavy cone in a porous medium, Mech. Res. Commun., 22 (1) (1995) 81–190.

[114] M.A. Hossain, M.S. Munir, I. Pop, Natural convection of a viscous fluid with variable viscosity and thermal conductivity from a vertical wavy cone, Int. J. Therm. Sci., 40 (2001) 437–443.

[115] T. Von Kármán, Uber laminare und turbulente Reibung, Z. Angew. Math. Mech. 1 (1921) 233–252.

[116] W.G. Cochran, The flow due to a rotating disk, Math. Proc. Camb. Phil. Soc., 30 (1934) 365–375.

[117] U.T. Bodewadt, Die Drehströmmung uber festem Grund, Z. Angew. Math. Mech. 20 (1940) 241–253.

[118] G.K. Batchelor, Note on a class of solutions of the Navier–Stokes equations representing steady non-rotationally symmetric flow, Quart. J. Mech. Appl. Math. 4 (1951) 29–41.

[119] J.T. Stuart, On the effects of uniform suction on the steady flow due to a rotating disk, Q. J. Mech. Appl. Maths. 7 (1954) 446-457.

[120] M.H. Rogers, G. N. Lance, The rotationally symmetric flow of a viscous fluid in the presence of an infinite rotating disk, J. Fluid Mech. 7 (1960) 617-631.

[121] N. Kelson, A. Desseaux, Note on porous rotating disk flow, Aust. N. Z. Ind. Appl. Math. J. 42 (2000) 837–855.

[122] M. Turkyilmazoglu, Purely analytic solutions of magnetohydrodynamic swirling boundary layer flow over a porous rotating disk, Comput. Fluids 39 (2010) 793–799.

[123] A. Das, Analytical solution to the flow between two coaxial rotating disks using HAM, Procedia Eng., 127 (2015) 377 – 382.

[124] M. Ibrahim, Numerical analysis of time-dependent flow of viscous fluid due to a stretchable rotating disk with heat and mass transfer, Results Phys., 18 (2020) 103242.

[125] G. Le Palec, Numerical study of convective heat transfer over a rotating rough disk with uniform wall temperature, Int. Commun. Heat Mass Transf., 16 (1989) 107-113.

[126] G. Le Palec, P. Nardin, D. Rondot, Study of laminar heat transfer over a sinusoidal-shaped rotating disk, Int. J. Heat Mass Transf., 33 (1990) 1183–1192.

[127] M.S. Yoon, J.M. Hyun, J.S. Park, Flow and heat transfer over a rotating disk with surface roughness, Int. J. Heat Fluid Flow, 28 (2007) 262–267.

[128] M.S. Yoon, J.S. Park, J.M. Hyun, Magnetohydrodynamics flow over a rapidly rotating axisymmetric wavy disk, Fluid Dyn. Res., 43 (2011) 1–16.

[129] A. Mehmood, M. Usman, B. Weigand, Heat and mass transfer phenomena due to a rotating non-isothermal wavy disk, Int. J. Heat Mass Transf., 129 (2019) 96–102.

[130] M. Usman, A. Mehmood, B. Weigand, Heat transfer from a non-isothermal rotating rough disk subjected to forced flow, Int. Commun. Heat Mass Transf., 110 (2020) 104395.

[131] A. Arikoglu, I Ozkol, G. Komurgoz, Effect of slip on entropy generation in a single rotating disk in MHD flow, Appl. Energy, 85 (2008) 1225–1236.

[132] S. Chen, Entropy generation inside disk driven rotating convectional flow, Int. J. Therm. Sci., 50 (2011) 626-638.

[133] M.M. Rashidi, M. Ali, N. Freidoonimehr, F. Nazari, Parametric analysis and optimization of entropy generation in unsteady MHD flow over a stretching rotating disk using artificial neural network and particle swarm optimization algorithm, Energy, 55 (2013) 497-510.

[134] A.S. Butt, A. Ali, Analysis of entropy generation effects in unsteady squeezing flow in a rotating channel with lower stretching permeable wall, J. Taiwan Inst. Chem. Eng., 48 (2015) 8-17.

[135] J.C. Maxwell, *A Treatise on Electricity and Magnetism*, Vol. 1. 2nd Ed. Oxford Clarendon Press London, 1881.

[136] H.B. Keller, Numerical methods in boundary layer theory, Ann. Rev. Fluid Mech., 10 (1988) 793-796.

[137] T. Cebeci, P. Bradshaw, *Momentum Transfer in Boundary layers*, Hemisphere Publishing Corporation, New York, 1977.

[138] T. Y. Na, *Computational Methods in Engineering Boundary Value Problems*, Academic Press Inc London, 1979.

[139] T. Cebeci, P. Bradshaw, *Physical and computational aspects of convective heat transfer*, Springer New York, 1988.

[140] A. Einstein, A new determination of the molecular dimensions, Ann. Phys., 19(2) (1906) 289-306.

[141] A. Einstein, The theory of the Brownian motion, Ann. Phys., 19(2) (1906) 371-381.

[142] A. Einstein, Correction of my work: A new determination of the molecular dimensions, Ann. Phys., 34(3) (1911) 591-592.

[143] H.C. Brinkman, The viscosity of concentrated suspensions and solution, J. Chem. Phys., 20 (1952) 571-581.

[144] S. Roy, Free convection from a vertical cone at high Prandtl numbers, Trans. ASME, J. Heat Transf., 96 (1974) 115-117.

[145] K.Y. Yih, The effect of uniform lateral mass flux on free convection about a vertical cone embedded in porous media, Int Commun. Heat Mass Transf., 24 (1997) 1195-1205.